Improved Methods and Reagents for Pretargeted Radioimmunotherapy of Cancer

By Stefan C. Zajic

B.S.E., University of Pennsylvania, 2001

Submitted to the Department of Chemical Engineering in Partial Fulfillment of the Requirements for the Degree of

DOCTOR OF PHILOSOPHY
in Chemical Engineering

at the

Massachusetts Institute of Technology
October 2006
[February 2007]

Signature of Author _____
Department of Chemical Engineering
October 2006

Certified by _____
K. Dane Wittrup
J.R. Mares Professor of Chemical Engineering and Bioengineering
Thesis Advisor

Accepted by _____
William M. Deen
Professor of Chemical Engineering
Chairman, Committee for Graduate Students

Improved Methods and Reagents for Pretargeted Radioimmunotherapy of Cancer

By Stefan C. Zajic

Submitted to the Department of Chemical Engineering on
October 24, 2006 in Partial Fulfillment of the Requirements
for the Degree of Doctor of Philosophy in Chemical Engineering

ABSTRACT

Pretargeted radioimmunotherapy (PRIT) of cancer improves upon conventional radioimmunotherapy (RIT) by decoupling the pharmacokinetics of the targeting agent and the radioisotope. In order to improve upon PRIT, we have considered variables such as treatment setting and methodology, the transport and clearance characteristics of targeting agents, and the radionuclides used for therapy. PRIT has been modeled with the aim of examining the theoretical potential of PRIT under optimal conditions to kill every cell in malignant, avascular micrometastases. A mathematical model of PRIT was developed that combined a two-compartment pharmacokinetic model, antibody binding kinetics, diffusion and catabolism in tumor spheroids, and radiation dosimetry models for alpha- and beta-emitting radionuclides. This model demonstrated that it is theoretically possible to kill every cell in 100 μm radius micrometastases using ^{90}Y- or ^{213}Bi-based PRIT with acceptable toxicity as described. The therapeutic window for dosing radionuclide-carrying hapten was found to be strongly dependent on cell-specific parameters such as antigen concentration, void fraction, and the radiosensitivity parameter α, as well as on targeting agent molecular parameters such as the diffusivity and antigen-binding association rate. Surprisingly, the therapeutic window was insensitive to the radiosensitivity metric α/β, the targeting agent antigen-binding dissociation rate, and all pharmacokinetic parameters. Overall, ^{213}Bi-based PRIT significantly outperformed ^{90}Y-based PRIT in terms of the safe therapeutic time window for radiometal dosing and the degree of cell overkill that could be achieved.

An attempt was made to isolate high-affinity scFv or linear peptide binders against the loaded metal chelate Ga-DOTA-biotin. Unfortunately, several different approaches led only to scFvs and linear peptides with at best micromolar affinity for Ga-DOTA-biotin. It is possible that Ga-DOTA-biotin is a difficult target against which to engineer high affinity binders due to the chelate's six-coordinate binding of the gallium ion, which may result in rapid exchange of the carboxyl arms of the chelate in solution. As an alternative approach to targeting agent design, an anti-CEA, anti-fluorescein single-chain bispecific diabody was designed, produced in *S. cerevisiae* and characterized. The full-length diabody (55 kDa) binds CEA expressed on the surface of colorectal cancer-derived SW1222 cells with a K_d of 4.3 ± 2.5 nM, and also binds fluorescein while bound to CEA on the cell surface.

Lastly, in order to assist in protein engineering via directed evolution, asymptotically optimal probability estimation was combined with numerical bootstrapping and non-linear curve fitting to make accurate predictions of the actual underlying diversities of populations based on small samples of data.

To my parents, my first and best teachers.

Acknowledgements

This work could not have been completed without the help, guidance and kindness of countless people. First and foremost, I'd like to thank my advisor, Dane Wittrup, for his endless encouragement, engagement and ideas. The hours that Dane and I spent sitting across a table from each other, talking about my successes, failures and new paths forward were the foundation of my graduate research. I'm incredibly grateful for his help, advice and wisdom. Dane also deserves immense credit for building and sustaining a fantastic group of students. In addition, I'd like to thank the members of my thesis committee – William Deen, Jeffrey Coderre and Amy Keating – for their time, thoughtfulness, suggestions and advice.

The members of the Wittrup Lab have been an invaluable resource. Andy Yeung provided me with my first introduction to working in the lab, and was always there to answer questions. Katarina Midelfort helped me find my way around the lab and showed me how to use nearly every instrument when I was just getting started. Andy Rakestraw has been a good friend and officemate throughout my time with the group, and was always willing to talk about difficulties I encountered during my research. Ginger Chao and I shared adjacent benches in our old lab, and adjacent desks in our new office – I think I must have asked her a thousand questions, and she always seemed to have the answers. Shaun Lippow has been a good friend over the years, and was always happy to take time to talk about my research. Members of the tumor targeting group within the lab – Greg Thurber, Mike Schmidt, Margie Ackerman and Kelly Davis – were particularly important to my research. Greg's skills at model programming were invaluable, Mike taught me the finer points of protein purification, Margie lent her time and expertise in mammalian cell culture, and Kelly spurred my research forward with insightful, stimulating questions. Three undergraduate researchers made material contributions to my research: Karen Hunter studied the metal specificity of anti-metal-chelate antibodies, Prashant Dilwali examined the binding of linear peptides to metal chelates, and Zhitong Zhang implemented software for use in diversity estimation. Other members of the group, past and present – Brenda Kellogg, Christilyn Graff, Dave Colby, Jeff Swers, Bala Rao, Jennifer Cochran, Mark Olsen, Yong-Sung Kim, Andrea Piatesi, Dasa Lipovsek, Wai Lau, Letha Sooter, Steve Sazinsky, Shanshan Wu Howland, Annie Gai, Ben Hackel, David Liu, and Pankaj Karande – have been wonderful colleagues who were always willing to help, and who deeply enriched my experience as part of the group. The people in the Wittrup Lab are the finest group I have worked with, and they have my lasting gratitude.

On a personal note, I simply could not have done this without Jessica Brooks, my companion and partner for six years. I don't know how I could have navigated the trials and tribulations of graduate school without her. She has my love and thanks, every day. I'd like to thank my family – Diana, Gregg and Lara Zajic – for a lifetime of love, support and encouragement, and for making me who I am today. I'd like to thank my grandfather, Stuart Churchill, for his support and advice, for urging me to study chemical engineering, and for showing me parts of the world I wouldn't have experienced without him. I'd also like to thank Eduardo Glandt, who was the best mentor an undergraduate could have, and who urged me to pursue the biology-related fields of study within chemical engineering.

Finally, I'd like to thank all of my friends for the support, encouragement, love and good times they've given me these past five years. Molly Brooks and Peter Lesser were my first friends in Boston, and they remain very close to my heart. They were always there for me – to listen, to offer advice, and to celebrate – and I think of them as family. Nick McCarthy, Lisa Smith, Kyle Bittinger and Tara Bledsoe have been the best friends a person could hope for. Lastly, I'd like to thank WMBR – 88.1 FM, MIT's campus radio station, where I met Nick, Kyle, and Lisa, and which served as a "home away from the lab" during my time here. To everyone who helped me along the way, including those I've neglected to mention: thank you.

This work was supported by the MIT/NIGMS Biotechnology Training Program, and by NCI CA101830.

Table of Contents

Chapter 1: Introduction and Background

Pretargeted radioimmunotherapy (PRIT) of cancer improves upon conventional radioimmunotherapy (RIT) by decoupling the pharmacokinetics of the targeting agent and the radioisotope. In order to optimize PRIT, we must consider variables such as treatment setting and methodology, the transport and clearance characteristics of the targeting agents, and the radionuclides used for therapy. Protein and peptide engineering via directed evolution can be used to isolate improved reagents for PRIT. Asymptotically optimal probability estimation can be adapted in order for protein engineers to better estimate the underlying diversity of populations enriched for improved clones.

1.1 Origins and development of radioimmunotherapy

The idea of using antibodies to deliver radiation to cancer cells was proposed immediately following the development of monoclonal antibody technology [1]. The simplest form of radioimmunotherapy (RIT) is the direct conjugation of a radioisotope to an antibody that binds specifically to cancer cells. Antibodies have *in vivo* biological half-lives of days to weeks; radiolabeled antibodies in a patient's circulation result in high doses of radiation to healthy tissues. A high dose to healthy tissues limits the amount of antibody that can be administered, which in turn limits the success of the therapy. Only extremely radiosensitive cancers can be effectively treated using this conventional form of RIT [2].

1.2 Pretargeted radioimmunotherapy

Pretargeted radioimmunotherapy (PRIT) was proposed as an alternative to conventional RIT in which the pharmacokinetics of the antibody and the radioactivity are decoupled. In all PRIT treatments, a bispecific protein (hereafter refered to as the targeting agent or bispecific) with specificities to both a cancer cell-surface antigen and the radioisotope-carrying small molecule (hereafter referred to as the hapten) is administered to the patient. The bispecific circulates throughout the patient's body, where it will bind to accessible cancer cells. After remaining bispecific has cleared from the patient's body, the hapten is administered. Because the hapten is typically a small molecule, it will rapidly perfuse throughout the body and then clear quickly, binding only to the hapten-specific part of the bispecific that is prelocalized to cancer cells. The subsequent radioactive decay leads to cancer cell cytotoxicity and death, while the patient's healthy tissues are spared. In three-step variants of PRIT, a clearance step in added in which the targeting agent in the blood is removed from the body by the administration of another molecule. This additional step does not, however, change the fundamental idea behind the treatment – it simply speeds the clearance of the targeting agent from the body.

The concept behind pretargeting has been in existence for more than two decades [3, 4], yet to date has failed to realized its full potential. While it has had encouraging successes in mouse xenograft models [5-7], PRIT has had marginal therapeutic success in clinical trials [8, 9]. Next, we examine the different design decisions that need to be considered in order to improve upon current methods and molecules employed in PRIT.

1.2.1 Treatment setting

Antibody-based cancer therapies, including PRIT, have been developed primarily to target vascularized, heterogeneous solid tumors, as treating these tumors is an urgent clinical need. However, there are many obstacles and disadvantages to using antibodies for the treatment of solid tumors. First, there is the significant problem of delivering the antibody to the tumor. Poor transport in tumors can place severe pharmacokinetic restrictions on anti-tumor antibodies, and their large molecular mass exacerbates these effects [10]. Second, the heterogeneous nature of these tumors makes them very difficult to competely neutralize with a "magic bullet" therapy such as PRIT, as there are often significant regions of non-antigen-presenting cells. Finally, the cells in the hypoxic and necrotic regions of these tumors are often highly radioresistent. Notable exceptions – such as Zevalin and Bexxar – have been successful only in the treatment of pharmacokinetically accessible, radiosensitive cancers [2]. These issues also present significant barrier to successful PRIT of solid tumors that may be minimized or reduced in mouse models, but will remain problematic in treating human patients. For these reasons, rather than targeting solid tumors, we believe that PRIT is better suited for use as an adjuvent therapy targeting avascular micrometastases, and have investigated the use of PRIT in that setting in this work. For the purposes of this work, we define micrometastases to be cancer cell clusters which have not initiated angiogenesis, and are typically 100-300 μm in radius.

1.2.2 Targeting agent selection

An extremely wide variety of antibody-based targeting molecules have been proposed for or used in pretargeting studies, including: IgG-streptavidin [5], IgG-biotin [11], bispecific mAbs, other bispecific antibody-based molecules, and antibody-DNA

fusions [12]. The streptavidin-biotin interaction was originally utilized in PRIT because very high affinity interactions between proteins and small molecules were otherwise hard to come by. There are two main problems, however, with using streptavidin and biotin to link the targeting agent and the hapten. First and most important is the problem of streptavidin's large size (53 kDa). When fused to an IgG, the resulting fusion protein is quite large and faces significant transport limitations; streptavidin also makes a poor hapten as it will not clear very rapidly from the circulation. The second limitation of using the streptavidin-biotin linkage in PRIT is the problem of endogenous biotin, which can compete with the biotin present on either the targeting agent or hapten. Although this problem is fairly manageable in humans, endogenous levels of biotin are much higher in mice, making murine to human comparisons of PRIT protocols more difficult. While innovative solutions have been found to the endogenous biotin problem [13, 14], the large size of streptavidin alone is reason enough to seek other molecules out as targeting agents. The great advances in protein engineering that have been made during the development of streptavidin-biotin-based PRIT now allow for the engineering of extremely high affinity interactions in antibody-based molecules significantly smaller than streptavidin.

1.2.3 Radionuclide selection

While the scope of this project did not include working with hot radiolabeled hapten, it was necessary to select potential radionuclides of therapeutic interest so that appropriate hapten molecules could be selected and designed. The choice of which radionuclide to use for PRIT (or, more generally, for any type of radioimmunotherapy) hinges on the following variables: particle type (alpha or beta), linear energy density

(LED) of radiation, radioactive half-life, and mean path length of the radiated particles. Alpha particles tend to have shorter path-lengths (50-70 μm) than the electrons emitted by beta-emitting radionuclides commonly used in radiotherapy, which may make them better suited for targeting cell spheroids sized 100-300 μm, as the bulk of the energy released by localized radionuclides will be deposited in the targeted cells, rather than in the healthy tissues surrounding the spheroids [15]. Due to their much higher linear energy density, alpha particles are also far more radiotoxic than beta particles, with only a few alpha particle passes through a cell nucleus required to kill a cell under certain circumstances [16]. However, alpha-emitting radionuclides are limited by a variety of factors, including generally short half-lives (^{213}Bi has a half-life of just 45 minutes), the problem of radioactive daughter nuclide release from the site of localization [17], and to date very low achievable specific activities in radiometal haptens, as compared to beta-emitting radionuclides [18].

Most radionuclides used in RIT and PRIT today have relatively long path lengths (for example, ^{131}I and ^{90}Y have mean path lengths of 0.5-0.9mm and 5mm in tissue [19, 20]). This is to be expected, as they are used primarly in the treatment of solid tumors, where their long path lengths can hit neighboring cells to which radioisotope has not been localized. These long path lengths, however, are not ideal for treating micrometastases. The ideal sizes of tumors for treatment with ^{90}Y and ^{131}I have been calculated to be 2 cm and 3 mm, respectively [21, 22]; micrometastases are at least a full order of magnitude smaller. As a result, beta-emitters with shorter path-lengths (such as ^{67}Ga, with a mean path length of 100 μm [23]) may be better suited for PRIT [24].

1.3 Protein engineering

When PRIT was first proposed as a method for treating cancer, the protein engineering field was still in its infancy. Since that time, protein engineering has developed to the point at which it is straightforward to develop extremely high affinity antibodies against most antigens. Methodological advances in protein engineering such as the introduction of directed evolution have been coupled with technological innovations, such as the development of flow cytometry and fluorescent activated cell sorting (FACS), to allow researchers to engineer higher-affinity, smaller, more specific and more stable proteins than ever before.

1.3.1 Protein engineering via directed evolution

Perhaps the most powerful idea introduced to the field of protein engineering in its history has been engineering via directed evolution [25]. In this method, a large library of protein molecules is created using molecular biology techniques. This library is then screened in a high-throughput manner that allows the selection of desirable clones within the library. These clones are then subjected to rounds of mutation to create new libraries, and the process is repeated until clones with the desired properties – i.e. enzymatic activity, binding affinity, fluorescence or stability – have been isolated. In all of the commonly-used variants of protein engineering via directed evolution, the genotype and phenotype of the protein are physically linked, so that the retrieval of an improved protein clone also yields its sequence information. The three primary technological platforms for protein engineering via directed evolution are phage display [26], yeast surface display [27] and ribosome/RNA display [28].

Phage display is the oldest and at present most commonly used platform for the directed evolution of proteins. In phage display, one or more copies of the protein of interest is expressed as a fusion on the surface of filamentous phage. A large library of clones can then be panned by incubating the phage on immobilized antigen and washing away non-binding phage. The main advantages of phage display are its ease of use, low cost and the ability to screen extremely large libraries in single pannings. There are several drawbacks, however: first, many proteins of interest are not properly folded when expressed as fusion proteins on phage. Second, fusing the protein to the surface of the phage changes its function significantly, and so clones of interest must be subcloned and secreted solubly in order to be accurately evaluated. Finally, the screening process is not quantitative, in that it can be difficult to tune the panning conditions in order to obtain clones with specific properties.

In yeast surface display, proteins of interest are displayed on the surface of the yeast *Sacchromyces cervisiae* by fusion to the Aga1 and Aga2 mating proteins. Because proteins are processed by the yeast's eukaryotic secretory pathway, many proteins that cannot be displayed on the surface of phage can be functionally expressed on the surface of yeast. Screening clones displayed on the surface of yeast is typically done via fluorescent activated cell sorting (FACS), rather than by panning. Large libraries of yeast displaying many different protein mutants are created and fluorescently labeled under conditions such that desirable mutants have a brighter fluorescent signal than the rest of the library. Because the selection process is controlled by a computer and based on the fluorescence of individual cells, yeast surface display selections can be performed in a high quantitative manner [29]. The only drawback of yeast surface display is that library

sizes are limited by the throughput of cell sorters, which at present can sort approximately 10^8 cells per hour, making libraries larger than 10^9 impractical to screen via FACS. However, larger yeast libraries can also be sorted using magnetic activated cell sorting (MACS), which is physically analogous to phage panning [30]. Recently, Feldhaus and colleagues constructed a human non-immune library of single-chain variable fragments (scFvs) displayed on the surface of yeast [31] from which antibodies of therapeutic interest have been isolated [32].

In ribosome display and closely-related mRNA display, the RNA coding for a protein and the expressed protein itself are physically linked. This RNA-protein fusion can then be panned directly against target molecules. The advantages of ribosome display include the lack of a transformation step, which drastically increases the sizes of libraries that can be constructed, and very rapid selection cycling. Disadvantages include the problems with protein folding and expression that might be expected in the absence of an organism's secretory pathway [33].

1.3.2 Peptide engineering

The display and screening methods discussed above can also be used to isolate short peptides against targets of interest. Constrained peptide libraries are commonly displayed on the surface of phage and screened against various small molecule [34] and protein targets [35-37], but linear peptide libraries have also been displayed on the surface of yeast and screened for binding to patterned material surfaces [38, 39]. Mutagenesis is often performed in between selections rounds when doing protein engineering, but this is not the case for peptide engineering. Because of the short length of peptides, peptide libraries are typically only screened once, and then resynthesized

with conserved residues held constant. Libraries can be easily synthesized using commercially available oligonucleotides.

1.4 Asymptotically optimal probability estimation

In the late stages of successful protein engineering efforts, a population of improved clones is isolated. These improved clones have often been generated and isolated at great expense, time and effort of the individual or company doing the protein engineering. It is in the interest of that individual to examine each and every improved clone, since some clones will be better than others in terms of the characteristic being selected for, while others will be desirable in other unintended ways (for example, they might happen to be easily secreted, or very stable, etc). The question then arises: how many unique clones are present in the enriched population? This is a surprisingly difficult question to answer because the investigator typically has at his or her disposal only an incomplete sample set of the total number of clones in the population. For example, one might sequence 50 improved single clones, and discover that 30 are unique. How many total unique clones are present in the population, and how many clones must be sequenced in order to come across every clone? These questions are of both scientific and practical importance – rare clones could possess novel biochemical or biophysical properties, but the benefit of isolating them must be balanced against the cost and time spent sequencing and characterizing individual proteins.

Orlitsky and colleages have developed an improved algorithm for asymptotically optimal probability estimation that can be used to directly address the common problem in protein engineering discussed above [40].

1.5 Thesis Overview

This document presents the work accomplished towards the goal of optimizing PRIT treatment methods and therapeutic reagents. In Chapter 2, a comprehensive model of PRIT is developed in which it is shown that PRIT can be successfully used to kill every cell in avascular micrometastases embedded in normal tissue. In Chapter 3, efforts directed at isolating gallium-DOTA(1,4,7,10-tetraazacyclododecane-1,4,7,10-tetraacetic acid)-biotin-binding scFvs and linear and constrained peptides for use as part of a bispecific targeting agent are described. Chapter 4 presents the application of asymptotically optimal probability estimation to the problem of diversity estimation in protein or peptide engineering. Finally, in Chapter 5, an alternative targeting agent is developed in which the targeting agent binds to both carcinoembryonic antigen (CEA) and fluorescein; radioactive payloads of almost any type can then be conjugated to fluorescein to create the hapten reagent. This targeting agent was constructed at the DNA level, secreted from *S. cerevisiae*, and characterized in solution and on the surface of CEA-expressing mammalian cells.

1.6 Works Cited

1. Kohler, G. and C. Milstein, *Continuous cultures of fused cells secreting antibody of predefined specificity*. Nature, 1975. **256**(5517): p. 495-7.
2. Dillman, R.O., *Radioimmunotherapy of B-cell lymphoma with radiolabelled anti-CD20 monoclonal antibodies*. Clin Exp Med, 2006. **6**(1): p. 1-12.
3. Goodwin, D., et al., *Use of specific antibody for rapid clearance of circulating blood background from radiolabeled tumor imaging proteins*. Eur J Nucl Med, 1984. **9**(5): p. 209-15.
4. Goodwin, D.A., et al., *Monoclonal antibody hapten radiopharmaceutical delivery*. Nucl Med Commun, 1986. **7**(8): p. 569-80.
5. Zhang, M., et al., *Pretargeting radioimmunotherapy of a murine model of adult T-cell leukemia with the alpha-emitting radionuclide, bismuth 213*. Blood, 2002. **100**(1): p. 208-16.

6. Pagel, J.M., et al., *Comparison of anti-CD20 and anti-CD45 antibodies for conventional and pretargeted radioimmunotherapy of B-cell lymphomas.* Blood, 2003. **101**(6): p. 2340-8.
7. Subbiah, K., et al., *Comparison of immunoscintigraphy, efficacy, and toxicity of conventional and pretargeted radioimmunotherapy in CD20-expressing human lymphoma xenografts.* J Nucl Med, 2003. **44**(3): p. 437-45.
8. Grana, C., et al., *Pretargeted adjuvant radioimmunotherapy with yttrium-90-biotin in malignant glioma patients: a pilot study.* Br J Cancer, 2002. **86**(2): p. 207-12.
9. Knox, S.J., et al., *Phase II trial of yttrium-90-DOTA-biotin pretargeted by NR-LU-10 antibody/streptavidin in patients with metastatic colon cancer.* Clin Cancer Res, 2000. **6**(2): p. 406-14.
10. Jain, R.K., *Transport of molecules, particles, and cells in solid tumors.* Annu Rev Biomed Eng, 1999. **1**: p. 241-63.
11. Sung, C. and W.W. van Osdol, *Pharmacokinetic comparison of direct antibody targeting with pretargeting protocols based on streptavidin-biotin binding.* J Nucl Med, 1995. **36**(5): p. 867-76.
12. Chang, C.H., et al., *Molecular advances in pretargeting radioimunotherapy with bispecific antibodies.* Mol Cancer Ther, 2002. **1**(7): p. 553-63.
13. Hamblett, K.J., et al., *A streptavidin-biotin binding system that minimizes blocking by endogenous biotin.* Bioconjug Chem, 2002. **13**(3): p. 588-98.
14. Hamblett, K.J., et al., *Role of biotin-binding affinity in streptavidin-based pretargeted radioimmunotherapy of lymphoma.* Bioconjug Chem, 2005. **16**(1): p. 131-8.
15. Behr, T.M., et al., *High-linear energy transfer (LET) alpha versus low-LET beta emitters in radioimmunotherapy of solid tumors: therapeutic efficacy and dose-limiting toxicity of 213Bi- versus 90Y-labeled CO17-1A Fab' fragments in a human colonic cancer model.* Cancer Res, 1999. **59**(11): p. 2635-43.
16. Charlton, D.E., *Radiation effects in spheroids of cells exposed to alpha emitters.* Int J Radiat Biol, 2000. **76**(11): p. 1555-64.
17. McDevitt, M.R., et al., *Tumor therapy with targeted atomic nanogenerators.* Science, 2001. **294**(5546): p. 1537-40.
18. McDevitt, M.R., et al., *An alpha-particle emitting antibody ([213Bi]J591) for radioimmunotherapy of prostate cancer.* Cancer Res, 2000. **60**(21): p. 6095-100.
19. Behr, T.M., et al., *Cure of metastatic human colonic cancer in mice with radiolabeled monoclonal antibody fragments.* Clin Cancer Res, 2000. **6**(12): p. 4900-7.
20. Witzig, T.E., et al., *Randomized controlled trial of yttrium-90-labeled ibritumomab tiuxetan radioimmunotherapy versus rituximab immunotherapy for patients with relapsed or refractory low-grade, follicular, or transformed B-cell non-Hodgkin's lymphoma.* J Clin Oncol, 2002. **20**(10): p. 2453-63.
21. Perkins, A., *In vivo molecular targeted radiotherapy.* Biomed imaging interv J, 2005. **1**(2): p. e9.
22. Wheldon, T.E., et al., *Modelling the enhancement of fractionated radiotherapy by gene transfer to sensitize tumour cells to radiation.* Radiother Oncol, 1998. **48**(1): p. 5-13.

23. Howell, R.W., *Radiation spectra for Auger-electron emitting radionuclides: report No. 2 of AAPM Nuclear Medicine Task Group No. 6.* Med Phys, 1992. **19**(6): p. 1371-83.
24. Michel, R.B., M.W. Brechbiel, and M.J. Mattes, *A comparison of 4 radionuclides conjugated to antibodies for single-cell kill.* J Nucl Med, 2003. **44**(4): p. 632-40.
25. Wittrup, K.D., *Protein engineering by cell-surface display.* Curr Opin Biotechnol, 2001. **12**(4): p. 395-9.
26. Paschke, M., *Phage display systems and their applications.* Appl Microbiol Biotechnol, 2006. **70**(1): p. 2-11.
27. Boder, E.T. and K.D. Wittrup, *Yeast surface display for screening combinatorial polypeptide libraries.* Nat Biotechnol, 1997. **15**(6): p. 553-7.
28. Rothe, A., R.J. Hosse, and B.E. Power, *Ribosome display for improved biotherapeutic molecules.* Expert Opin Biol Ther, 2006. **6**(2): p. 177-87.
29. Boder, E.T. and K.D. Wittrup, *Optimal screening of surface-displayed polypeptide libraries.* Biotechnol Prog, 1998. **14**(1): p. 55-62.
30. Siegel, R.W., et al., *High efficiency recovery and epitope-specific sorting of an scFv yeast display library.* J Immunol Methods, 2004. **286**(1-2): p. 141-53.
31. Feldhaus, M.J., et al., *Flow-cytometric isolation of human antibodies from a nonimmune Saccharomyces cerevisiae surface display library.* Nat Biotechnol, 2003. **21**(2): p. 163-70.
32. Colby, D.W., et al., *Development of a human light chain variable domain (V(L)) intracellular antibody specific for the amino terminus of huntingtin via yeast surface display.* J Mol Biol, 2004. **342**(3): p. 901-12.
33. Lipovsek, D. and A. Pluckthun, *In-vitro protein evolution by ribosome display and mRNA display.* J Immunol Methods, 2004. **290**(1-2): p. 51-67.
34. Marks, K.M., M. Rosinov, and G.P. Nolan, *In vivo targeting of organic calcium sensors via genetically selected peptides.* Chem Biol, 2004. **11**(3): p. 347-56.
35. Meyer, S.C., T. Gaj, and I. Ghosh, *Highly Selective Cyclic Peptide Ligands for NeutrAvidin and Avidin Identified by Phage Display.* Chem Biol Drug Des, 2006. **68**(1): p. 3-10.
36. Morita, Y., et al., *Selection and properties for the recognition of P19 embryonic carcinoma stem cells.* Biotechnol Prog, 2006. **22**(4): p. 974-8.
37. Sharma, A., et al., *Specific and randomly derived immunoactive peptide mimotopes of mycobacterial antigens.* Clin Vaccine Immunol, 2006.
38. Peelle, B.R., et al., *Probing the interface between biomolecules and inorganic materials using yeast surface display and genetic engineering.* Acta Biomater, 2005. **1**(2): p. 145-54.
39. Peelle, B.R., et al., *Design criteria for engineering inorganic material-specific peptides.* Langmuir, 2005. **21**(15): p. 6929-33.
40. Orlitsky, A., N.P. Santhanam, and J. Zhang, *Always Good Turing: asymptotically optimal probability estimation.* Science, 2003. **302**(5644): p. 427-31.

Chapter 2: Theoretical Limitations for Two-step Pretargeted Radioimmunotherapy of Avascular Micrometastases

We examine here the theoretical potential of pretargeted radioimmunotherapy (PRIT) under optimal conditions to kill every cell in malignant avascular micrometastases. A mathematical model of PRIT was developed that combined a two-compartment pharmacokinetic model, antibody binding kinetics, diffusion and catabolism in tumor spheroids, and radiation dosimetry models for alpha- and beta-emitting radionuclides. An infusion dosing scenario was developed in which the patient is infused with targeting agent at the beginning of the therapy to ensure complete saturation of antigen in the micrometastasis with targeting agent. Therapy was modeled using a 55 kDa bispecific molecule and ^{90}Y and ^{213}Bi radionuclides. A sensitivity analysis was performed to determine the parameters with greatest influence on therapeutic success. It is theoretically possible to kill every cell in 100 μm radius micrometastases using ^{90}Y- or ^{213}Bi-based PRIT with acceptable toxicity, as described herein. The model is quite sensitive to certain cell parameters: antigen concentration within the micrometastasis, void fraction and the radiation dosimetry parameter α. The model is also sensitive to certain molecular parameters of the targeting agent: the diffusivity and the targeting agent-antigen association rate. Notably, the model was insensitive to α/β (a common measure of radiosensitivity), the targeting agent-antigen dissociation rate, and all pharmacokinetic parameters. While the qualitative results for ^{90}Y and ^{213}Bi were similar, ^{213}Bi performed better overall, with a significantly larger safe therapeutic time window for dosing radioisotope-carrying hapten. The model results presented here predict that optimized PRIT protocols and reagents can be used to successfully treat clinically

undetectable micrometastases. In addition, these results indicate that PRIT may represent an advantageous use for alpha-emitting radioisotopes in radioimmunotherapy, due to the short residence time of the radionuclide. The sensitivity analysis identifies key parameters that should guide the development and use of improved PRIT reagents and protocols.

2.1 Introduction

Tumor metastasis is the primary cause of mortality for breast cancer patients, but only a minority of patients have clinically detectable metastases at diagnosis, indicating that a large fraction of patients have small, undetectable micrometastases at the time of presentation [1]. Thus, an adjuvant, specific therapy such as pretargeted radioimmunotherapy (PRIT) would have broad clinical relevance, and could be used in conjunction with surgery, chemotherapy or localized radiation therapy to eliminate both the primary tumor burden and dispersed micrometastases.

While antibody-based therapies such as PRIT face significant obstacles in the treatment of solid tumors, they are attractive options for neutralizing avascular micrometastases. Transport to micrometastases is significantly more efficient than in solid tumors [2]; micrometastases are more homogenous, so that cells are more uniformly susceptible to anti-tumor antibodies; lastly, micrometastases that have no developed hypoxic cores may not exhibit increased radioresistance.

Several different modeling approaches have been synthesized in order to theoretically examine PRIT in avascular micrometastases. Sung and colleagues developed an initial framework for modeling PRIT, which they used to examine both

streptavidin-antibody-fusion-based and antibody-biotin-based pretargeting systems in an open, two-compartment pharmacokinetic model [3]. That model was combined here with a model of antibody binding, diffusion and catabolism in tumor spheroids developed by Graff [4] and Thurber [2], and with radiation dosimetry models for alpha- and beta-emitting radionuclides developed by Charlton [5] and Leichner [6], respectively.

Presented here is a theoretical examination of the limits of pretargeted radioimmunotherapy. It is shown that it is possible to use PRIT to kill every cell in an avascular micrometastasis, using either ^{90}Y and ^{213}Bi, without undue systematic cytotoxicity. The therapeutic window for dosing radiometal chelate hapten that will lead to complete cell killing has been calculated, and a single-variable sensitivity analysis has been performed to determine the key parameters within the model, in the context of generating accurate modeling results, and in terms of using this approach successfully in the clinic, where parameters will vary significantly from patient to patient. While there is currently little appropriate data in the literature against which to test the model, this model provides a framework for future analysis of PRIT approaches and provides several experimentally testable hypotheses, the testing of which should significantly advance understanding of PRIT.

2.2 Modeling Methods

For bispecific pharmacokinetics, a two-compartment model is used in which the plasma and normal tissues can exchange material via transcapillary transport and lymphatic drainage [3]. The micrometastasis is embedded within and in close contact with the normal tissue. For the purposes of this model, only one micrometastasis is

considered, but the introduction of additional micrometastases does not change the analysis significantly, as the amount of bispecific material interacting with the micrometastasis is small compared to the total amount of bispecific in the body. In previous PRIT modeling and experimental efforts, the antibody-based targeting agent was almost always delivered as an intravenous bolus dose. In order for bolus-dosed bispecific to saturate the micrometastasis, it must be transported into the normal tissue and completely penetrate into the center of the micrometastases. As detailed by Thurber [2], the problem of delivering an antibody-based agent can be reduced to two comparisons: first, the bispecific must reach the center of the micrometastasis before it is cleared from the plasma (the clearance modulus Γ, defined by Thurber, must be less than 1); second, the rate of bispecific diffusion into the spheroid must be greater than the rate of bispecific-antigen complex catabolism, or achieving complete saturation will not be possible (the Thiele modulus Φ^2 must be less than 1). For an avascular micrometastasis and two-compartment pharmacokinetics, these two moduli are:

$$\Gamma = \frac{R^2\left([Ag]/\varepsilon\right)}{6D\left(AUC_{Ab,normal}\right)} = \frac{R^2\left([Ag]/\varepsilon\right)}{6D\left(\frac{Ab_{n0}}{\lambda} + \frac{\kappa Ab_{p0}}{\lambda}\left(\frac{A}{\alpha} + \frac{B}{\beta}\right)\right)} \quad (1)$$

$$\Phi^2 = \frac{R^2[Ag]_t/\varepsilon\, k_e}{D[Ab]_{p0}} \quad (2)$$

where R is the radius of the micrometastasis, [Ag] is the antigen concentration in the micrometastasis, ε is the void fraction, k_e is the rate of antigen and antigen-antibody complex catabolism, D is the diffusivity of the bispecific in the micrometastasis, Ab_{n0} is the initial bispecific concentration in the normal tissue (i.e. the steady-state concentration during the infusion phase), Ab_{p0} is the initial bispecific concentration in the plasma, A, B, α, and β are biphasic pharmacokinetic clearance parameters, κ is the transcapillary transport rate constant, and λ is the lymphatic clearance rate constant. Base-case values for the constant parameters are provided in Table 2.1.

The bispecific pharmacokinetics in the plasma and normal tissue are:

$$Ab_p(t) = Ab_{p0}\left(Ae^{-\alpha t} + Be^{-\beta t}\right) \quad (3)$$

$$Ab_n(t) = \left\{\kappa Ab_{p0}\left(\frac{Ae^{-(\alpha-\lambda)t}}{\lambda-\alpha} + \frac{Be^{-(\beta-\lambda)t}}{\lambda-\beta}\right) + Ab_{n0} - \kappa Ab_{p0}\left(\frac{A}{\lambda-\alpha} + \frac{B}{\lambda-\beta}\right)\right\}e^{-\lambda t} \quad (4)$$

where $Ab_p(t)$ is the concentration of bispecific in the plasma as a function of time, and $Ab_n(t)$ is the concentration of bispecific in the normal tissue as a function of time. The base-case values of the constant parameters are specified in Table 2.1. The pharmacokinetic parameters (A, B, α and β) were estimated using scaling arguments from a wide range of pre-clinical animal and clinical human data, as little PK data is available on 60 kDa antibody-based bispecific molecules in the literature.

Parameter	Base-case value	Sensitivity range	Citation
A	0.9	0.7-0.9	[7-16]
B	0.1	0.1-0.3	
α ($t_{1/2\alpha}$)	5.8×10^{-4} s^{-1} (0.33 h)	$3.9 - 11.3 \times 10^{-4}$ s^{-1} (0.17 – 0.5 h)	
β ($t_{1/2\beta}$)	1.83×10^{-5} s^{-1} (10.5 h)	$1.38 - 2.75 \times 10^{-5}$ s^{-1} (7 – 14)	
κ	1×10^{-4} s^{-1}	$0.5 - 2 \times 10^{-4}$ s^{-1}	[3]
λ	8.9×10^{-5} s^{-1}	$4.5 - 18 \times 10^{-5}$ s^{-1}	[3]
D	91×10^{-12} m^2/s	$10 - 91 \times 10^{-12}$ m^2/s	[17, 18]
k_{on}	1×10^{5} $M^{-1}s^{-1}$	$1 \times 10^{4} - 1 \times 10^{6}$ $M^{-1}s^{-1}$	[19]
k_{off}	2×10^{-6} s^{-1}	$2 \times 10^{-7} - 100 \times 10^{-6}$ s^{-1}	[20]
R_{syn}	1.15×10^{-10}	not varied	
k_e	38.5×10^{-5} s^{-1}	3.2 ... 77×10^{-5} s^{-1}	[21]
R	100 μm	not varied	[22]
Ag_{vol}	3×10^{-7} M	$1 - 5 \times 10^{-7}$ M	[23]
ε	0.3	0.1 – 0.3	[2]
α (radio.)	0.2 Gy^{-1}	0.05 – 0.4 Gy^{-1}	[24]
α/β	6 Gy^{-2}	1 – 12 Gy^{-2}	[24]
λ' (^{90}Y)	3.00×10^{-6} s^{-1}	not varied	

Table 2.1. Model parameter values, range used for single-variable sensitivity analysis, and literature sources.

The concentrations of bispecific, antigen and complex within the micrometastasis are calculated by numerically solving a system of partial differential equations describing the diffusion, binding and catabolism in a tumor spheroid. The diffusion and binding of bispecific and the synthesis and degradation of antigen in a spherical micrometastasis are governed by the following partial differential equations [20]:

$$\frac{\partial Ab_t}{\partial t} = D\frac{1}{r^2}\frac{\partial}{\partial r}\left(r^2\frac{\partial Ab_t}{\partial r}\right) - k_{on}Ab_tAg + k_{off}B$$

$$\frac{\partial Ag}{\partial t} = R_{syn} - k_{on}Ab_tAg + k_{off}B - k_eAg \qquad (5, 6 \text{ and } 7)$$

$$\frac{\partial B}{\partial t} = k_{on}Ab_tAg - k_{off}B - k_eB$$

where Ab_t, Ag and B are concentrations of bispecific, antigen and complex, k_{on} is the association rate of the bispecific for the antigen, k_{off} is the dissociation rate of the bispecific from the antigen, and R_{syn} is the rate of antigen synthesis. Base-case values of the constant parameters are given in Table 2.1. Boundary and initial conditions for the three partial differential equations given above are required. A Neumann boundary condition is applied at the center of the micrometastasis, specifying zero gradient at r = 0. A Dirichlet boundary condition is used at the edge of the micrometastasis, requiring continuity with normal tissue. Initial states for free bispecific, antigen and complex are also specified.

$$\frac{\partial Ab_t}{\partial r}(0,t) = 0 \quad (8)$$

$$Ab_t(r = R,t) = \varepsilon Ab_n(t) \quad (9)$$

$$\begin{aligned} Ab_t(r,0) &= Ab_{n0} \\ Ag(r,0) &= 0 \\ B(r,0) &= Ag_0 \end{aligned} \quad (10, 11 \text{ and } 12)$$

This system of partial differential equations was solved analytically using a Matlab program that implements the method of lines.

Antigen shedding and down-regulation are not explicitly treated in the model, but could have small effects on the model results. Shedding is primarily dealt with by using an appropriate antigen concentration in the micrometastasis – since internalization of the radionuclide is not required for successful cell-killing, it does not make a great deal of difference whether the bound antigen is on the surface of the cancer cells or has been

shed into the extracellular matrix. Antigen down-regulation could significantly change the results of the therapy, as bound complex on the surface of cells in the micrometastasis is a prerequisite for cell killing. Cancer-specific antigens that are strongly down-regulated by their complementary antibody-based bispecific would make poor candidates for PRIT. Conversely, if an antigen existed that was up-regulated by its bispecific, then that antigen/bispecific pairing would be ideally suited for PRIT, as the increased cell-surface concentration of antigen would allow increased amounts of localized radionuclide. For this modeling effort, it is assumed that the antigen is neither down- nor up-regulated by the binding of the bispecific molecule.

For beta- and low-energy-electron emitters, if the radiometal is evenly distributed throughout the spheroid then the following analytical expression can be used to calculate the dose-rate absorbed by the cells in the spheroid:

$$\dot{D}_\beta(r) = C\Delta\phi_\beta(r) \quad (13)$$

where C is the mean activity per unit mass (Bq/kg), $\Delta = n_\beta E_{av}$ (n_β is the number of beta particles per nuclear transformation and E_{av} is the weighted average beta particle energy), and $\phi_\beta(r)$ is the absorbed fraction for beta particles, defined as [6]:

$$\phi_\beta = G_0 \int \frac{e^{-\mu' r}}{4\pi r^2}\left\{1 + \left[d_1(\mu' r) + d_2(\mu' r)^2 + d_3(\mu' r)^3\right]e^{-(d_4-1)\mu' r}\right\}dV \quad (14)$$

where G_0 can be calculated from Berger's tables [25], and d_1, d_2, d_3, d_4 and μ' are radionuclide-specific constants. $d_{1\text{-}4}$ are fitting coefficients, and μ' is the apparent

absorptions coefficient for beta particles. The constant parameters for ^{90}Y are provided in Table 2.2. Leichner demonstrates that μ' can be accurately estimated for any given radionuclide by:

$$\mu' = 0.474 E_{av}^{-2.0} + 5.80 E_{av}^{-0.82} \quad (15)$$

Leichner's analysis has been validated theoretically and experimentally [26].

Parameter	Value
n_β	1.000
E_{av}	0.9367 MeV
d_1	0.684
d_2	0.114
d_3	1.38
d_4	1.59
μ'	6.6 cm^2/g

Table 2.2. Dosimetry parameters for ^{90}Y.

In order to evaluate the absorbed fraction, the integral may be written as

$$\phi_\beta = G_0 \sum_{k=0}^{3} \phi_\beta^{(k)} \quad (16)$$

with

$$\phi_\beta^{(0)} = \int \frac{e^{-\mu' r}}{4\pi r^2} dV \quad (17)$$

$$\phi_\beta^{(1)} = \int \frac{e^{-d_4 \mu' r}}{4\pi r^2} d_1(\mu' r) dV \quad (18)$$

$$\phi_\beta^{(2)} = \int \frac{e^{-d_4 \mu' r}}{4\pi r^2} d_2(\mu' r)^2 dV \quad (19)$$

$$\phi_\beta^{(3)} = \int \frac{e^{-d_4 \mu' r}}{4\pi r^2} d_3(\mu' r)^3 dV \quad (20)$$

These integrals can be evaluated at any point inside or outside of the sphere, allowing us to calculate an absorbed dose rate at any point desired. Expressions for the above terms at the center of the sphere are provided below; this analysis is taken directly from Leichner. As an example, for 90Y, in a 100 μm radius sphere, $\phi_\beta(cent) = 0.0436$.

$$\phi_0(cent) = \frac{1}{\mu'}\left(1 - e^{-\mu' a}\right) \quad (21)$$

$$\phi_1(cent) = \frac{d_1}{d_4^{\,2}\mu'}\left[1 - (1 + d_4\mu' a)e^{-d_4\mu' a}\right] \quad (22)$$

$$\phi_2(cent) = \frac{d_2}{d_4^{\,3}\mu'}\left\{2 - \left[(d_4\mu' a)^2 + 2(d_4\mu' a + 1)\right]e^{-d_4\mu' a}\right\} \quad (23)$$

$$\phi_3(cent) = \frac{d_3}{d_4^{\,4}\mu'}\left\{6 - \left[6 + d_4\mu' a\left(d_4^{\,2}\mu'^2 a^2 + 3d_4\mu' a + 6\right)\right]e^{-d_4\mu' a}\right\} \quad (24)$$

Alpha-particles differ from beta-particles in that they have a shorter path lengths (50-80 μm), higher energies (5-8 MeV), and higher rates of linear energy transfer (LET) (~100 keV/μm, compared to 0.2 keV/μm for a beta-particle) [27]. Alpha particles must traverse through the nucleus of a cell, as opposed to the cytoplasm, to lead to cell death [28]. Alpha-particle dosimetry for avascular spheroids can be calculated as follows: a radial distribution of radionuclide (either calculated, experimentally determined, or arbitrarily chosen) is converted into a spatial distribution of alpha-particle decays by integrating the radioactivity concentration profiles over time [29]. Absorbed dose and/or cell-killing can be calculated from this decay distribution via Monte Carlo methods [5]. For a radially uniform distribution of ^{213}Bi, Charlton's results are summarized in the following table.

# ^{213}Bi atoms / cell	1	5	8	9	10
spheroid radius (μm)					
25	8.20E-01	3.71E-01	2.04E-01	1.68E-01	1.37E-01
37.5	6.70E-01	1.35E-01	4.06E-02	2.72E-02	1.82E-02
50	5.60E-01	5.51E-02	9.67E-03	5.42E-03	3.03E-03
67.5	4.70E-01	2.29E-02	2.38E-03	1.12E-03	5.26E-04
75	4.30E-01	1.47E-02	1.17E-03	5.03E-04	2.16E-04
87.5	3.90E-01	9.02E-03	5.35E-04	2.09E-04	8.14E-05
100	3.70E-01	6.93E-03	3.51E-04	1.30E-04	4.81E-05
112.5	3.40E-01	4.54E-03	1.79E-04	6.07E-05	2.06E-05

Table 2.3. Surviving cell fraction as a function of spheroid radius and average number of ^{213}Bi atoms per cell (adapted from [5]).

The data in the table above were calculated based on a 50% packing fraction of cells in the spheroid, and an average radius of 5.88μm. The number of cells in each spheroid ranges from 38 (25μm radius spheroid) to 3502 (112.5μm radius spheroid). For each spheroid radius, we can calculate the minimum number of ^{213}Bi atoms per cell required to kill every cell in the spheroid, as shown in the table below.

Spheroid radius (μm)	Cells in spheroid (50% packing)	Maximum surviving fraction for complete killing	Minimum ^{213}Bi atoms per cell for complete killing
25	38	2.63E-02	18.3
37.5	130	7.69E-03	12.2
50	307	3.26E-03	9.9
67.5	600	1.67E-03	8.5
75	1038	9.63E-04	8.2
87.5	1648	6.07E-04	7.9
200	2459	4.07E-04	7.9
112.5	3502	2.86E-04	7.6

Table 2.4. Requirements for complete cell killing.

Note that due to the very high radiotoxicity of ^{213}Bi, only a few atoms of ^{213}Bi per cell are required for complete killing. If each cancer cell has approximately 100,000 copies of the cancer-specific antigen on its surface, and the radiolabeled fraction of metal

chelate is 0.0025 (both of these estimates are conservative), then saturating the cell surface antigen with radiometal chelate would deliver at least 250 ^{213}Bi atoms to the micrometastasis, suggesting that substantial overkill is possible in an optimized PRIT therapy setting. Note also that although Charlton's data only extends to spheroids of radii 112.5um, the number of radionuclide atoms required for complete killing decreases with increasing radius.

The specific activity (decays per second per mass or mole) of the radiometal chelate is an extremely important variable in therapeutic pretargeting, since it directly determines the amount of radioactivity that can be localized on the surface or within a cancer cell. The chart below presents published specific activities for radioisotopes of interest. Note that to date, while the specific activities are similar, the radiolabeled fraction of ^{213}Bi conjugates is far lower than for ^{90}Y, indicating that there is substantial room for improvement.

Isotope	Context	Specific Activity	Fraction Labeled	Citation
^{90}Y	DPTA-protein	111 MBq/mg	~0.1	[30]
^{213}Bi	chelate-mAb	236 MBq/mg	~0.00274	[31]

Table 2.5. Attainable specific activities for radionuclides of interest.

To calculate t_{kill}, the following steps are followed: at each time t, the concentration of bound bispecific at the center of the micrometastasis is calculated; the bispecific concentration is lowest at the center of the spheroid, since antigen-bispecific is being consumed throughout the spheroid but only being replenished via diffusion from the boundary with the normal tissue. However, until very late times bispecific-antigen complex concentration actually varies very little with radius; radial complex concentration profiles as a function of time are shown in Figure 2.1.

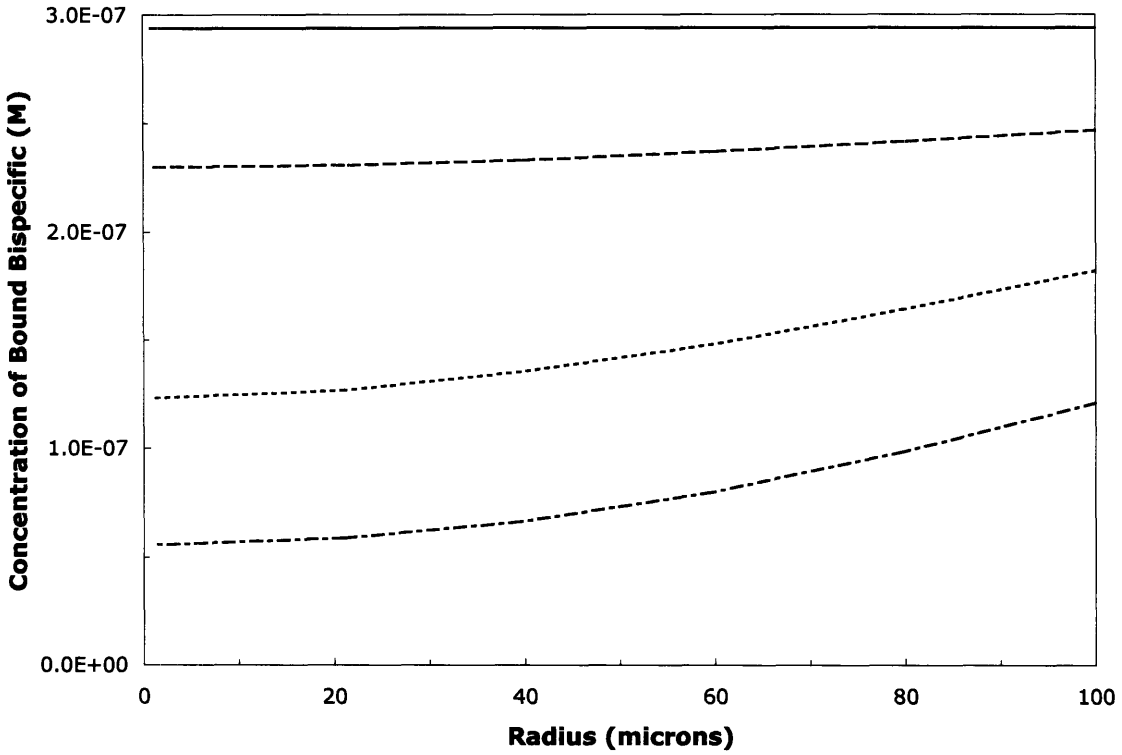

Figure 2.1. Radial concentration profiles of bound bispecific in the tumor micrometastasis as a function of time. Solid line, 1 hr. Dashed line, 12 hrs. Dotted line, 24 hrs. Dash-dotted line, 36 hrs.

Making the conservative assumption that the concentration of bispecific-antigen complex throughout the spheroid is the same as at the center, it is then determined if the resulting dose from radiometal-bispecific-antigen complex is sufficient to kill every cell in the spheroid. For beta particles, the absorbed dose is explicitly calculated as detailed above, and a modified dose-effect relationship is used to determine the surviving fraction [32]:

$$S = e^{-\alpha \dot{D}_{\beta,0}(t)\frac{1}{\lambda'}e^{-\lambda' t}\left[1+\frac{\dot{D}_{\beta,0}(t)}{\mu+\lambda'}\left(\frac{\beta'}{\alpha'}\right)\right]} \qquad (25)$$

where dosimetry parameters are defined as above, S is the surviving fraction, λ' is the radioactive decay constant of the radionuclide of interest, and α' and β' are cell-line specific radiosensitivity parameters.

For beta particle-emitters, t_{kill} is the first time at which the surviving fraction is greater than 1 divided by the number of cells in the spheroid. For alpha-particle emitters, t_{kill} can be simply calculated as the first time at which the concentration of bispecific at the center of the micrometastasis drops below the concentration corresponding to the required number of radionuclide atoms per cell, as set forth in Table 2.4. Charlton shows that such predictions are not particularly sensitive to the spatial distribution of radionuclide – rather, it is the overall average concentration that is important. As a result, small stochastic cell-to-cell variations in the number of localized radionuclides need not be of great concern.

Finally, a single-variable sensitivity analysis was performed by varying each of the model parameters across its greatest reasonable range, and calculating the size of the therapeutic window Δt to determine how it varied as a function of the parameter of interest.

2.3 Results

The goal of this modeling effort is to determine if it is theoretically possible to kill every cell in an avascular micrometastasis using PRIT with ^{90}Y and ^{213}Bi with acceptable systemic toxicity. In order to determine this endpoint, the following steps must be performed: calculating the concentration of the bispecific as a function of time in the plasma and normal tissues; calculating the concentration of free bispecific, free antigen

and bispecific-antigen bound complex in the micrometastasis as functions of time and radius; calculating the time (t_{MTD}) after bispecific administration that radiometal-carrying hapten can first safely be administered, and the time (t_{kill}) after bispecific administration before which the hapten must be dosed in order to ensure that every cell in the micrometastasis is neutralized. The duration $\Delta t = t_{kill} - t_{MTD}$ determines the size of the therapeutic time window for radiometal hapten dosing. If Δt is positive, then the therapy can theoretically be successful; if Δt is negative, then it is not possible to kill every cell in the spheroid under the specified conditions without exceeding the maximum tolerated dose (MTD). As a practical matter, Δt should be maximized, in order to provide reduced uncertainty for patient safety and ensure complete cell killing via predicted overkill.

These two requirements (MTD and minimum effective dose) for delivering bispecific to a micrometastasis set strict limits on how much bispecific must be dosed if saturation is to be achieved, to the point that improbably large bolus antibody doses can be required to completely saturate the antigen in the tumor with antibody. To address this problem, and to maximize the potential of PRIT, we propose to use infusion dosing of bispecific to saturate the micrometastasis. In an infusion dosing scenario, the patient is infused with bispecific for a sufficient period of time to ensure than all antigen in the micrometastasis is bound with antibody, circumventing the clearance modulus requirement. While this may require large amounts of bispecific, the production of such amounts is certainly achievable, and the steady-state plasma concentration of bispecific is not unreasonably high (in the hundreds of nanomolar). At the point of complete saturation (or sometime after), the bispecific infusion is stopped (time $t = 0$). Bispecific will clear rapidly from the plasma, less rapidly from the normal tissues, and still less

rapidly from the micrometastasis. Under the right conditions, this will lead to a therapeutic window in which radiometal hapten can be dosed safely and still lead to complete killing in the micrometastasis.

A base-case set of modeling parameters was developed using the best available parameter values from the literature (Table 2.1). The initial bispecific concentration in the plasma was set at 200 n*M*, which corresponds to $\Phi^2 = 0.212$. According to Thurber's analysis of antibody penetration into tumor spheroids and our numerical calculations [2], this concentration is sufficient to ensure near-complete saturation of antigen in the micrometastasis. Given this initial bispecific concentration, equations 3 and 4 above were used to calculate the resulting pharmacokinetic profiles, which are presented in Fig. 2.2. As illustrated in Fig. 2.2, the concentration of the bispecific in the plasma drops quite rapidly, while the concentration in the normal tissue falls less quickly.

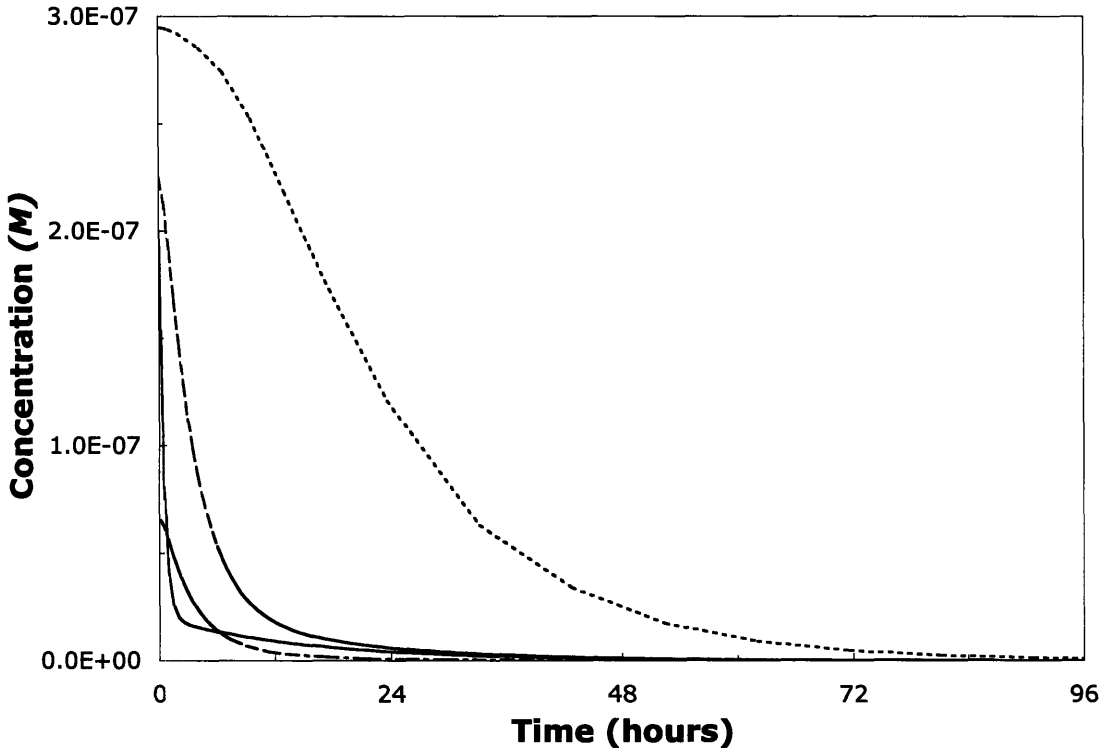

Figure 2.2. Bispecific pharmacokinetics and micrometastasis saturation calculated using base-case parameter set. Concentration of bispecific in plasma, solid line. Concentration of bispecific in normal tissue, dashed line. Concentration of bispecific-antigen complex at center of micrometastasis, dotted line. Concentration of free bispecific at center of micrometastasis, dash-dotted line.

The pharmacokinetic parameters α, β, A and B for a 60 kD protein were difficult to estimate from the literature, as their values vary widely in animal experiments and human trials and defied attempts at allometric scaling. This extreme variation may be due to the fact that a protein of 60 kD is very close to the molecular weight cut-off for glomerular filtration in the kidneys, which could lead to radically different pharmacokinetic outcomes as a result of relatively small variations in the actual cut-off weight in different animals or populations of animals. To determine how important these pharmacokinetic parameters were to the model, three different sets of pharmacokinetic parameters were compiled: base-case, fast and slow. The concentration profiles of the

bispecific as calculated using these different parameter sets are presented in the Figures 2.3 and 2.4.

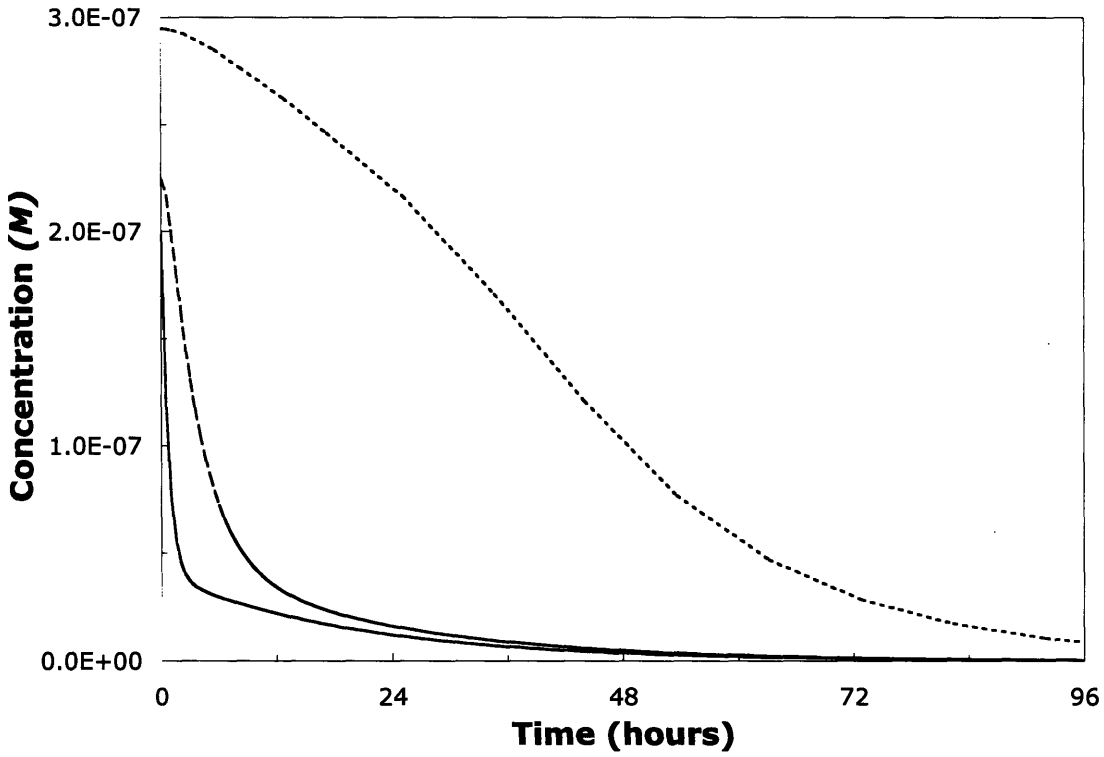

Figure 2.3. Bispecific pharmacokinetics and micrometastasis saturation calculated using slow pharmacokinetic parameter set. Concentration of bispecific in plasma, solid line. Concentration of bispecific in normal tissue, dashed line. Concentration of bispecific-antigen complex at center of micrometastasis, dotted line.

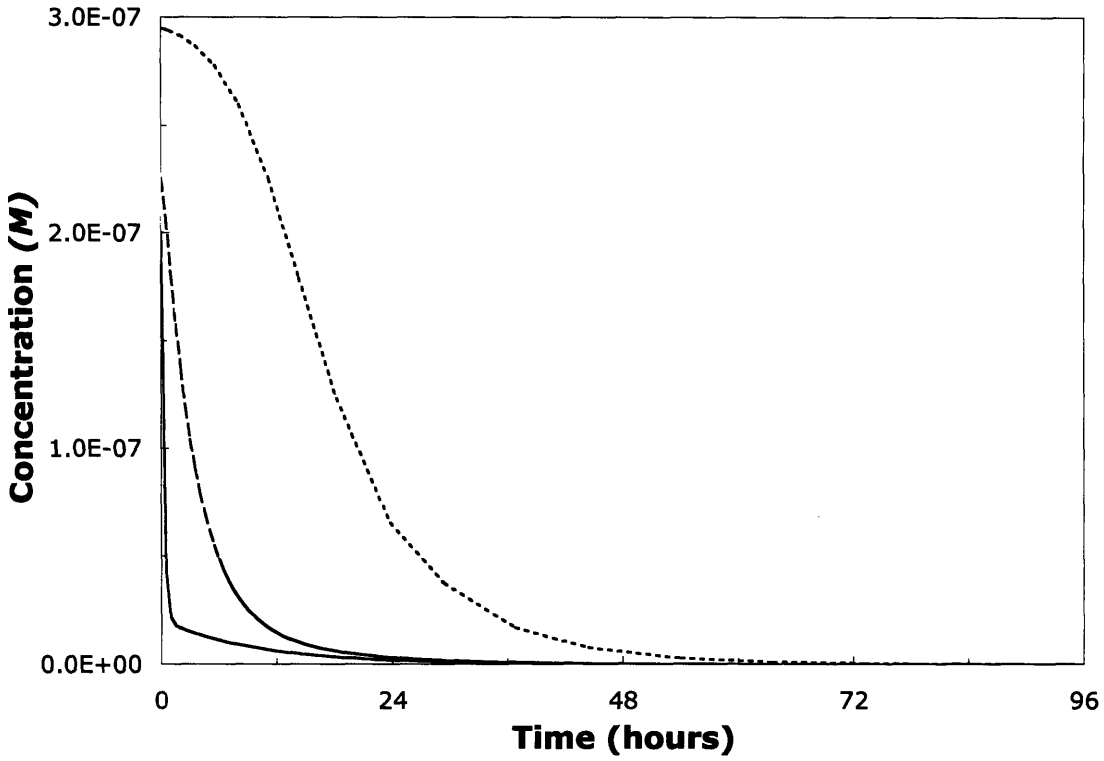

Figure 2.4. Bispecific pharmacokinetics and micrometastasis saturation calculated using fast pharmacokinetic parameter set. Concentration of bispecific in plasma, solid line. Concentration of bispecific in normal tissue, dashed line. Concentration of bispecific-antigen complex at center of micrometastasis, dotted line.

Next, the expression for bispecific concentration in the normal tissue specified by equation 4 was used as a time-varying boundary condition to the system of partial differential equations 5, 6 and 7, in order to calculate the concentrations of free antibody, free antigen and bound complex in the micrometastases as functions of radius and time. The concentrations of free antibody and bound complex at the center (r = 0) of the micrometastasis are also shown in Fig. 2.2. In the micrometastasis, free bispecific diffusing into the spheroid is rapidly bound by newly synthesized antigen, keeping the concentration of free antibody in the micrometastasis extremely low. As a result, only

the concentration of bound complex needs to be considered to accurately calculate radiation dosimetry.

While an antibody-based targeting agent such as a bispecific molecule 50-60 kD in size will encounter significant resistance in passing through the capillary wall, a small molecule radionuclide hapten will rapidly perfuse all tissues of the body [33]. The initial plasma concentration of radiometal hapten required to completely bind all remaining bispecific in the body can be calculated from hapten-bispecific association and dissociation rates, the antigen turnover rate, and the pharmacokinetic constants for the hapten. Given the rapid extravasation times of small molecule haptens, it is reasonable to assume that it is possible to bind every molecule of bispecific in the patient with radiometal hapten.

The earliest time at which radiometal hapten can be dosed will be a function of the maximum tolerated dose absorbed by the patient from hapten-bispecific complex that is located in healthy tissues. The fate of radiometal chelate that binds to circulating (non-localized) bispecific has not been experimentally determined. Metal chelates alone generally pass through the kidneys and are eliminated in the urine, resulting in minimal dose to healthy tissues [33, 34]. On the other hand, directly radiolabeled antibodies, antibody fragments and peptides are taken up by the kidney, which can lead to substantial, even dose-limiting nephrotoxicity [35, 36]. Until there is evidence to the contrary, we should conservatively assume that radiometal chelate bound non-covalently to antibody-based molecules behaves in the same manner as covalently-linked radiometal – that is, it is localized to the kidney. The renal accretion of antibody fragments can be significantly inhibited by administering D-lysine, which can decrease the renal dose by

up to five-fold, increase the maximum tolerated dose, and in some cases change the dose limiting organ from the kidney to the blood [35].

Experimentally, it has been found that in therapeutic radioimmunotherapy, the bone-marrow is almost always the dose-limiting tissue, and we expect this to be the case in PRIT, as well. In a mouse study comparing the efficacy of ^{213}Bi- and ^{90}Y-labeled anti-tumor Fab' fragments, Behr and co-workers found that with lysine protection, the MTD of ^{90}Y-Fab' was 9.25 MBq and the MTD of ^{213}Bi-Fab' was 25.9 MBq, with the blood (the dose-limiting organ) receiving doses of 5-8 Gy. Bone marrow transplantation allowed increases in MTD to 14.8 MBq of ^{90}Y-Fab' and 40.7 MBq of ^{213}Bi-Fab' [37]. In a Phase I/II clinical trial of ^{90}Y-Zevalin, the MTD was 11.1 - 14.3 MBq/kg, with most adverse events being hematologic [38], once again indicating that the bone marrow was the dose-limiting tissue.

Thus, we can determine t_{MTD} directly by simply determining the time at which the concentration of bispecific in the plasma drops below the concentration that correlates to the clinically determined MTD, assuming that all of the bispecific is bound by radiometal chelate with a maximal specific activity. For example, given a MTD of 12.95 MBq/kg for antibody-conjugated ^{90}Y and a body weight of 90 kg, the MTD of antibody-bound ^{90}Y is 1.17 GBq. This corresponds to roughly 7 nmol of ^{90}Y-bispecific labeled at 111 MBq/mg. To calculate t_{MTD}, we simply need to determine at what time 7 nmol of bispecific remains in the body; this is straightforward, and the calculation is similar for ^{213}Bi.

The boundaries of the therapeutic window, t_{MTD} and t_{kill}, were determined from the plasma concentration of the bispecific and the concentration of antigen-bispecific

complex at the center of the micrometastasis, as set forth in the Methods above. For the base case, the ^{90}Y dosimetry calculations led to a t_{MTD} of 9.2, and t_{kill} of 29.4, giving a therapeutic window of 20.2. For ^{213}Bi dosimetry, a t_{MTD} of 17.6 and t_{kill} of 79.3 were calculated, leading the a greater therapeutic window of 61.7. Therapeutic window results for the slow and fast pharmacokinetic data sets are presented below.

Parameter set	^{90}Y			^{213}Bi		
	t_{MTD}	t_{kill}	Δt	t_{MTD}	t_{kill}	Δt
Base-case	9.2	29.4	20.2	17.6	79.3	61.7
Slow PK	34.3	59.5	25.2	45.4	125.8	80.4
Fast PK	6.1	21.7	15.6	11.7	54.5	42.8

Table 2.6. Variation of therapeutic window with fast, slow and base-case pharmacokinetics. All times in hours.

While the pharmacokinetic profiles vary significantly for the different data sets, the therapeutic window is notably insensitive to pharmacokinetic parameters, because both of the window-determining concentration profiles (blood and tumor) shift to approximately the same degree, keeping the window size approximately constant.

Using the base case analysis as a starting point, a single-variable sensitivity analysis was performed, with the therapeutic window Δt being the output. Each parameter was independently varied across all reasonable and/or relevant values. The range of each variable is given in Table 2.1. The results of the sensitivity analysis are presented in Figs. 2.5, 2.6 and 2.7. For the two radionuclides ^{90}Y and ^{213}Bi, the parameters are grouped into three sets – parameters that are cell-type specific, molecular parameters of the bispecific molecule, and pharmacokinetic and patient parameters. The results are presented for each of these three sets.

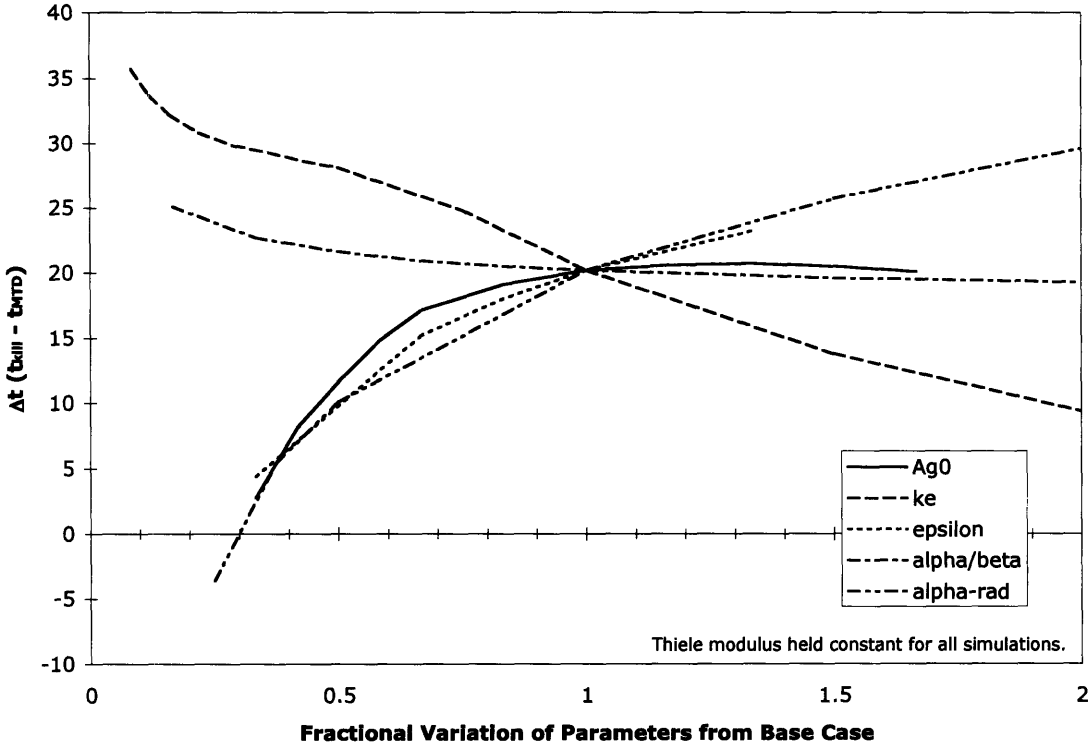

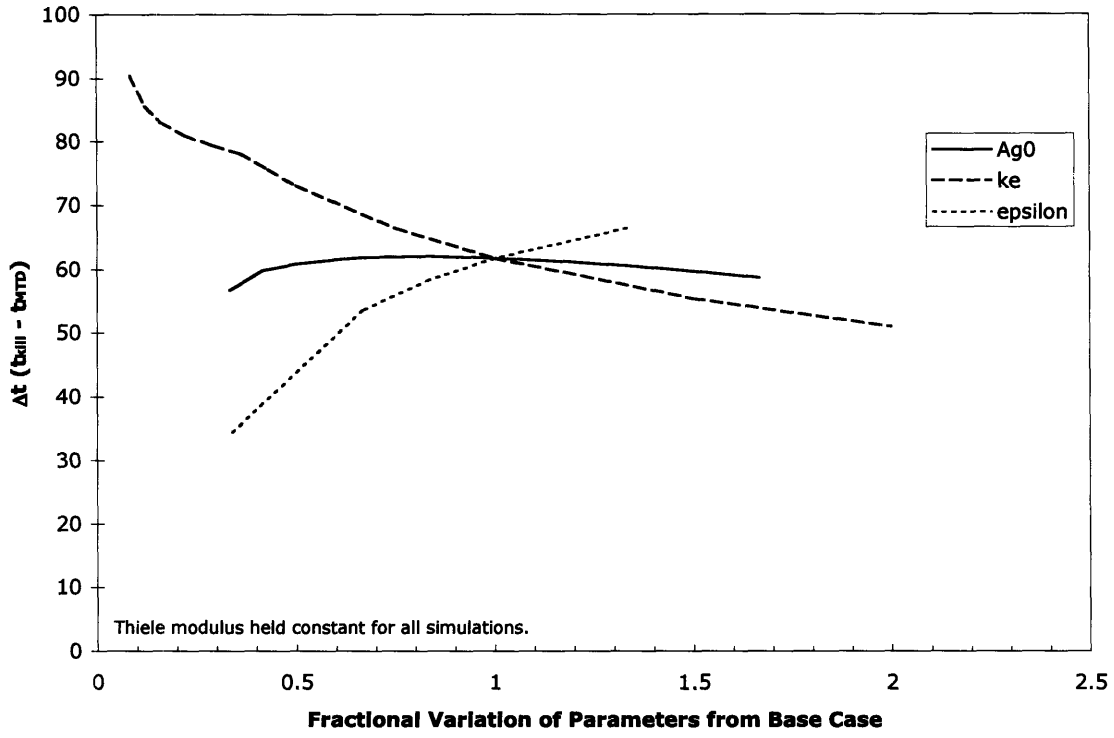

Figure 2.5 a, b. Sensitivity of therapeutic window for ^{90}Y (a) and ^{213}Bi (b) radionuclides to parameters that are cell- or spheroid-specific.

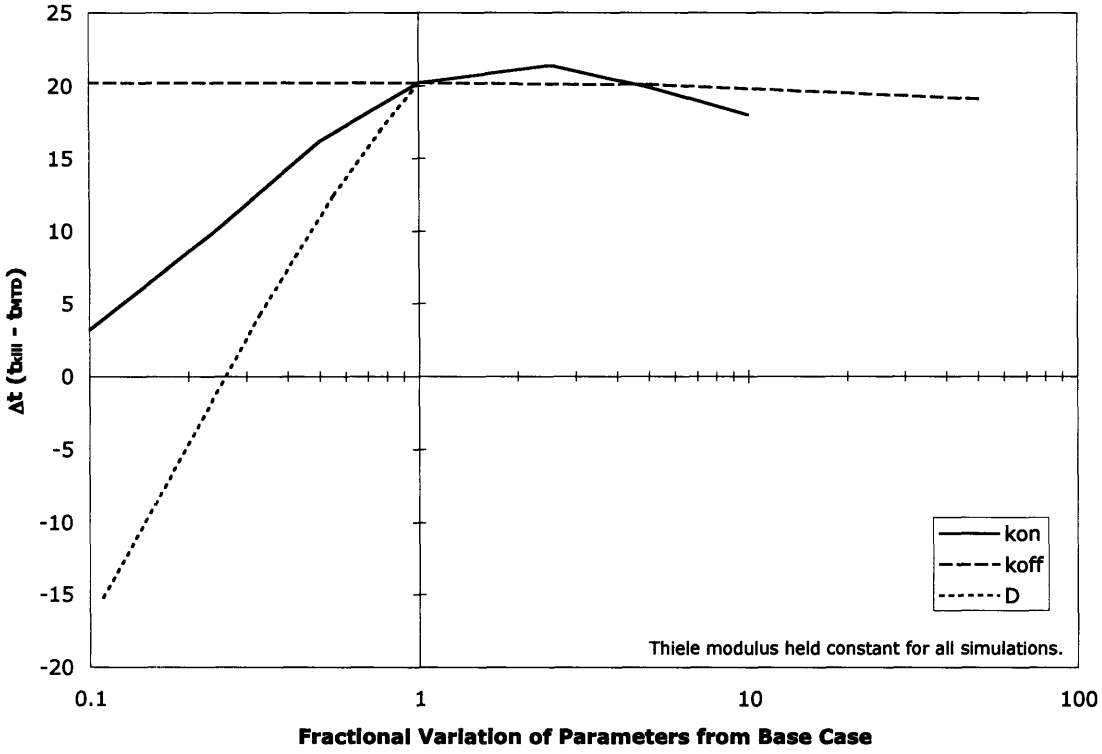
25
20
15
10
5
0
-5
-10
-15
-20
0.1
1
10
100
Δt (tkill - tMTD)
Fractional Variation of Parameters from Base Case
kon
koff
D
Thiele modulus held constant for all simulations.

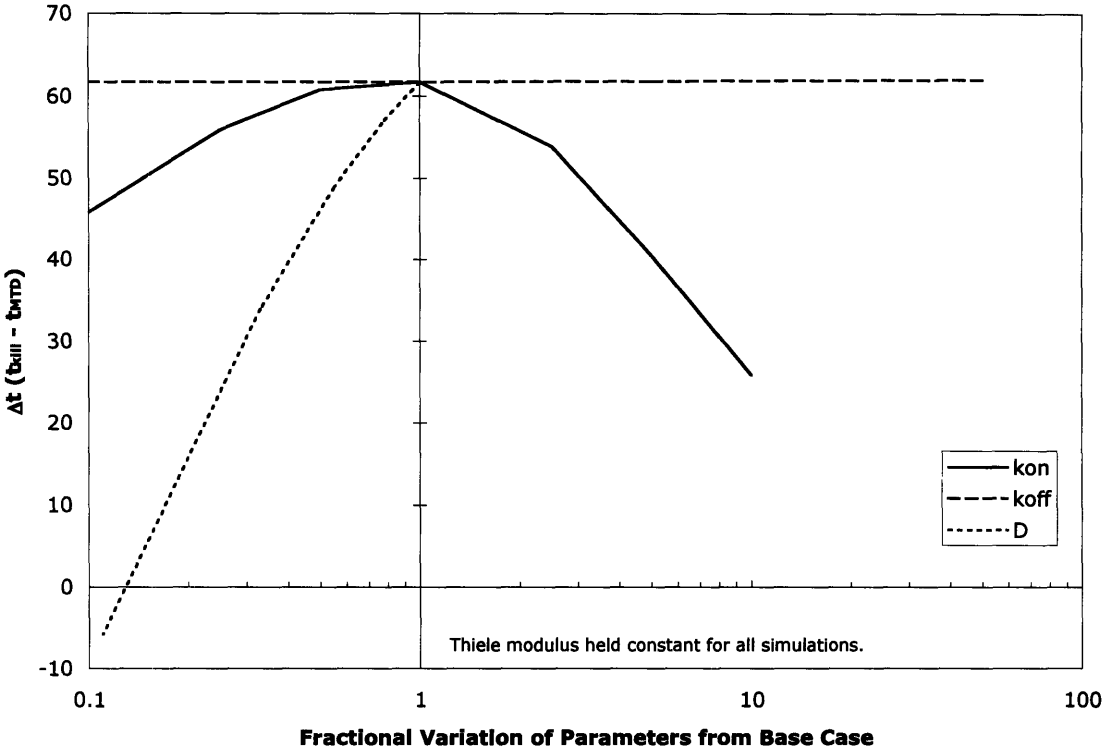

Figure 2.6 a, b. Sensitivity of therapeutic window for ^{90}Y (a) and ^{213}Bi (b) radionuclides, with to molecular parameters of the bispecific molecule.

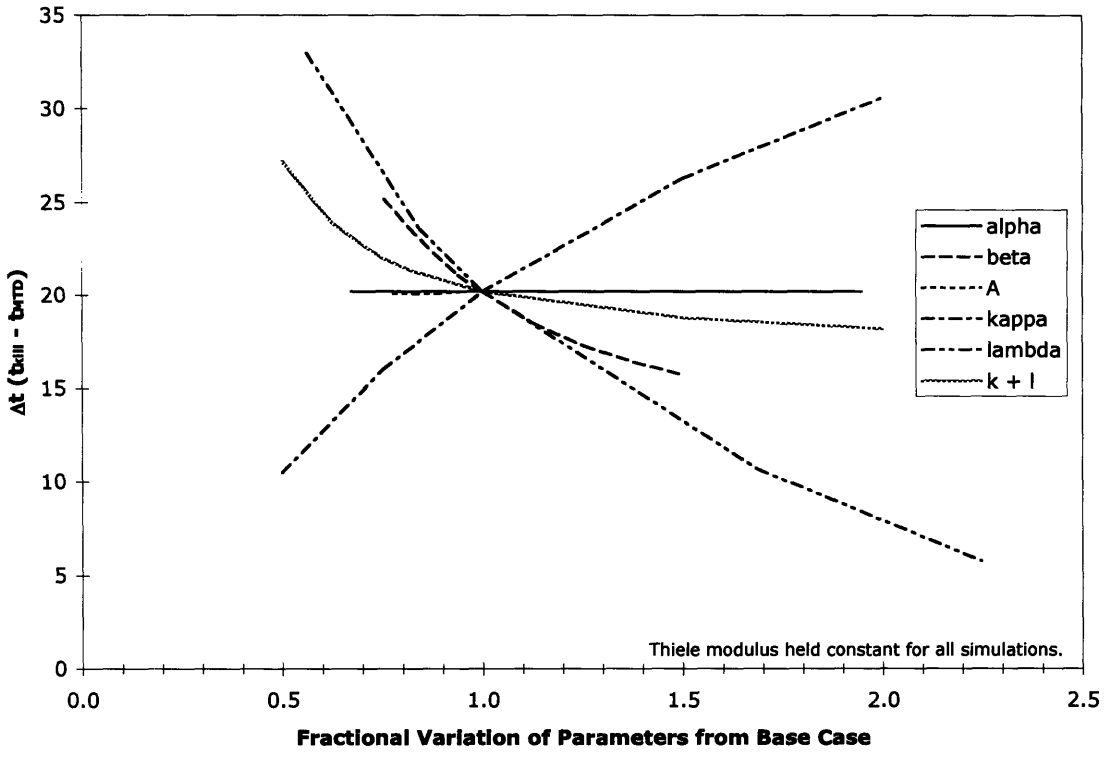

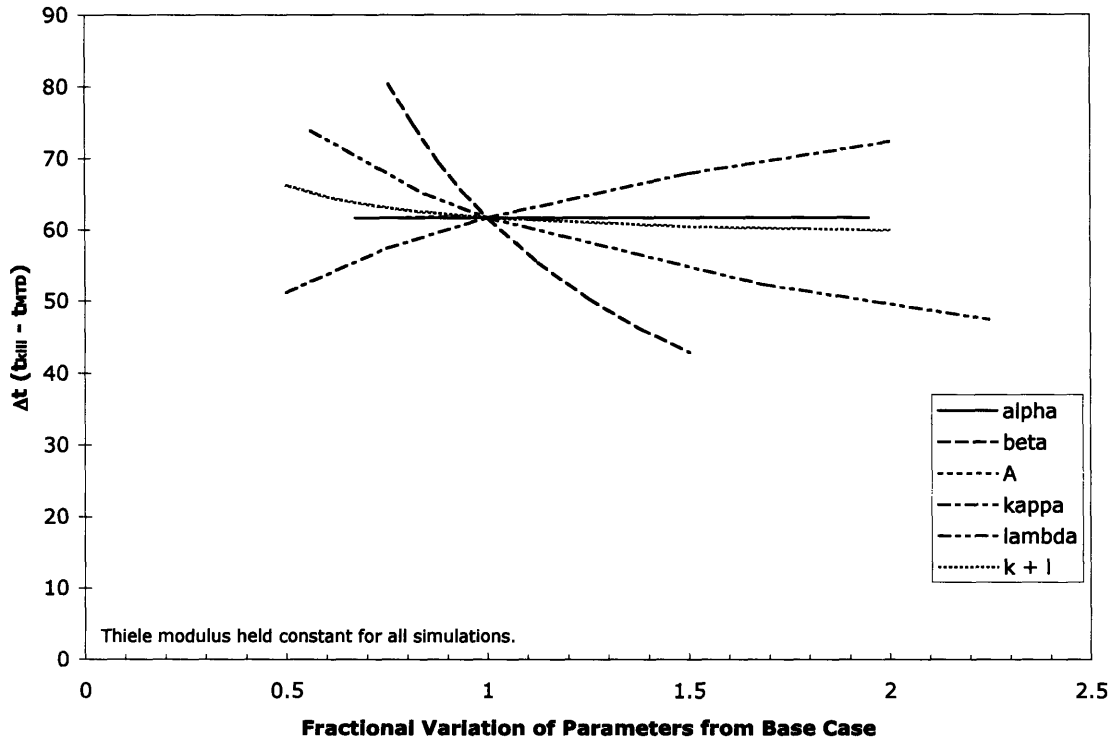

Figure 2.7 a, b. Sensitivity of therapeutic window for ^{90}Y (a) and ^{213}Bi (b) radionuclides to pharmacokinetic and patient-specific parameters.

As illustrated in Fig. 2.5a, the size of the therapeutic window Δt is quite sensitive to certain cell parameters for ^{90}Y-based PRIT. A two-fold change in either antigen concentration, void fraction or the radiation dosimetry parameter α result in substantial decreases in the therapeutic window to near or beyond $\Delta t = 0$, the point at which it is no longer theoretically possible for PRIT to be used to kill every cell in the micrometastasis. Notably, the model is insensitive to α/β, a traditional measure of radiosensitivity, but is quite sensitive to α, the radiosensitivity parameter associated with first-pass cell killing by beta particles. Additionally, as shown in Fig. 2.6a, Δt is quite sensitive to D and k_{on}, but insensitive to changes in k_{off}. Lastly, Δt is remarkably insensitive to variation in pharmacokinetic parameters for ^{90}Y-based PRIT, as shown in Fig. 2.7a. Even very large variations in pharmacokinetics do not lead to situations in which ^{90}Y-based PRIT is theoretically unsuccessful. This is due to the fact that while changing pharmacokinetic parameters affects the concentration of bispecific in the plasma as a function of time, that plasma concentration in turn affects the normal and tumor bispecific concentrations. As a result, the curves that determine t_{MTD} and t_{kill} are shifted in the same direction when pharmacokinetic parameters are changed, resulting in relatively small changes in the therapeutic window.

The results are similar for ^{213}Bi, but the therapeutic window remains further above zero than for ^{90}Y, since Δt for the base-case for ^{213}Bi is much larger than for ^{90}Y. For the cell parameters, the model is fairly sensitive to ε, as shown in Fig. 2.5b. As it is for ^{90}Y, the model is very sensitive to changes in D and k_{on}, and insensitive to both changes in k_{off} and pharmacokinetic parameters for ^{213}Bi, as shown in Figs. 2.6b and 2.7b.

2.4 Discussion & Conclusions

We have shown that it is theoretically possible to use PRIT in an adjuvant setting to kill every cell in an avascular micrometastasis using either a beta-emitting radionuclide (^{90}Y) or an alpha-emitting radionuclide (^{213}Bi) while maintaining safe doses of radiometal. In this analysis, ^{213}Bi performed particularly well, with a very large therapeutic window, indicating both a high degree of confidence in the method since the large therapeutic window reduces concerns about patient-to-patient variability, and also possibility to deliver many times the necessary cell-killing dose to the metastasis. Alpha-emitting radionuclides have been long thought to have great potential in cancer therapy due to their high radiotoxicity, but their use has been limited as a result of the main problem of conventional radioimmunotherapy (a poor dose ratio of tumor to healthy tissue) being exacerbated by the radiotoxicity of an alpha emitter. PRIT may present an ideal setting for alpha emitters to be used, since they would be in the patients' circulatory system for only a short time, yet can be effectively targeted to micrometastases where they can do a great deal of damage.

While the chosen beta-emitter ^{90}Y does not perform quite as well as ^{213}Bi, it does show some promise, both for itself and for other beta-emitting radionuclides. ^{90}Y, with a long path length of 5 mm, is not an ideal radionuclide for adjuvant PRIT, since much of the radiation emitted by the radionuclide will be deposited outside of the micrometastasis. Thus, other beta-emitting radionuclides with more appropriate path lengths (such as Ga-67) may perform even better in this model of PRIT [39].

There are two key features of the approach described here that led to the results presented. First, the reduction of the key rate processes into Thiele and clearance moduli, in addition to enhancing understanding of the tumor targeting process, also led us to employ an infusion, rather than bolus dosing scenario. The infusion dosing scenario, because it ensures complete saturation of the micrometastasis with bispecific at the outset, provides optimal conditions for determining the limits of pretargeting.

The sensitivity analysis performed on the results of the model described herein are the most significant results presented in this work. It revealed the relatively counterintuitive findings that pharmacokinetic parameters are largely unimportant to the overall success of failure of the pretargeted therapy. On the other hand, the model is quite sensitive to cellular parameters, suggesting that molecular-level descriptions of different cancer types and cell-lines may be extremely useful in determining if PRIT can be successful for a particular cancer. Parameters specific to the individual patient could be determined during the imaging dosimetry tests that precede all radioimmunotherapy.

2.5 Works Cited

1. Klauber-DeMore, N., et al., *Biological behavior of human breast cancer micrometastases*. Clin Cancer Res, 2001. **7**(8): p. 2434-9.
2. Thurber, G., Zajic, SC and Wittrup, KD, *Theoretical Criteria for Antibody Saturation of Tumors and Micrometastases*. J Nucl Med. **in press**.
3. Sung, C. and W.W. van Osdol, *Pharmacokinetic comparison of direct antibody targeting with pretargeting protocols based on streptavidin-biotin binding*. J Nucl Med, 1995. **36**(5): p. 867-76.
4. Graff, C.P. and K.D. Wittrup, *Theoretical analysis of antibody targeting of tumor spheroids: importance of dosage for penetration, and affinity for retention.* Cancer Res, 2003. **63**(6): p. 1288-96.
5. Charlton, D.E., *Radiation effects in spheroids of cells exposed to alpha emitters.* Int J Radiat Biol, 2000. **76**(11): p. 1555-64.
6. Leichner, P.K., *A unified approach to photon and beta particle dosimetry*. J Nucl Med, 1994. **35**(10): p. 1721-9.

7. Ferraiolo BL, M.M.a.G.C., *Protein Pharmacokinetics and Metabolism.* 1992, Plenum Press: New York. p. 228-232.
8. Pentel, P.R., et al., *Pharmacokinetics and toxicity of high doses of antibody Fab fragments in rats.* Drug Metab Dispos, 1988. **16**(1): p. 141-5.
9. Lobo, E.D. and J.P. Balthasar, *Application of anti-methotrexate Fab fragments for the optimization of intraperitoneal methotrexate therapy in a murine model of peritoneal cancer.* J Pharm Sci, 2005. **94**(9): p. 1957-64.
10. Gaudreault, J., et al., *Preclinical pharmacokinetics of Ranibizumab (rhuFabV2) after a single intravitreal administration.* Invest Ophthalmol Vis Sci, 2005. **46**(2): p. 726-33.
11. Mager, D.E., et al., *Simultaneous modeling of abciximab plasma concentrations and ex vivo pharmacodynamics in patients undergoing coronary angioplasty.* J Pharmacol Exp Ther, 2003. **307**(3): p. 969-76.
12. Grene-Lerouge, N.A., et al., *Interspecies scaling of clearance and volume of distribution for digoxin-specific Fab.* Toxicol Appl Pharmacol, 1996. **138**(1): p. 84-9.
13. Wu, A.M., et al., *Tumor localization of anti-CEA single-chain Fvs: improved targeting by non-covalent dimers.* Immunotechnology, 1996. **2**(1): p. 21-36.
14. Adams, G.P., et al., *Delivery of the alpha-emitting radioisotope bismuth-213 to solid tumors via single-chain Fv and diabody molecules.* Nucl Med Biol, 2000. **27**(4): p. 339-46.
15. Adams, G.P., et al., *Prolonged in vivo tumour retention of a human diabody targeting the extracellular domain of human HER2/neu.* Br J Cancer, 1998. **77**(9): p. 1405-12.
16. Behr, T.M., et al., *Experimental studies on the role of antibody fragments in cancer radio-immunotherapy: Influence of radiation dose and dose rate on toxicity and anti-tumor efficacy.* Int J Cancer, 1998. **77**(5): p. 787-95.
17. Brown, E.B., et al., *Measurement of macromolecular diffusion coefficients in human tumors.* Microvasc Res, 2004. **67**(3): p. 231-6.
18. Alexandrakis, G., et al., *Two-photon fluorescence correlation microscopy reveals the two-phase nature of transport in tumors.* Nat Med, 2004. **10**(2): p. 203-7.
19. Midelfort, K.S., et al., *Substantial energetic improvement with minimal structural perturbation in a high affinity mutant antibody.* J Mol Biol, 2004. **343**(3): p. 685-701.
20. Graff, C.P., et al., *Directed evolution of an anti-carcinoembryonic antigen scFv with a 4-day monovalent dissociation half-time at 37 degrees C.* Protein Eng Des Sel, 2004. **17**(4): p. 293-304.
21. Nichols, B.J., et al., *Rapid cycling of lipid raft markers between the cell surface and Golgi complex.* J Cell Biol, 2001. **153**(3): p. 529-41.
22. Groebe, K. and W. Mueller-Klieser, *On the relation between size of necrosis and diameter of tumor spheroids.* Int J Radiat Oncol Biol Phys, 1996. **34**(2): p. 395-401.
23. Berk, D.A., et al., *Direct in vivo measurement of targeted binding in a human tumor xenograft.* Proc Natl Acad Sci U S A, 1997. **94**(5): p. 1785-90.
24. Carlson, D.J., et al., *Comparison of in vitro and in vivo alpha/beta ratios for prostate cancer.* Phys Med Biol, 2004. **49**(19): p. 4477-91.

25. Berger, M.J., *Distribution of absorbed dose around point sources of electrons and beta particles in water and other media.* J Nucl Med, 1971: p. Suppl 5:5-23.
26. Sarfaraz, M. and B.W. Wessels, *Validation of an analytical expression for the absorbed dose from a spherical beta source geometry and its application to micrometastatic radionuclide therapy.* Clin Cancer Res, 1999. **5**(10 Suppl): p. 3020s-3023s.
27. Mulford, D.A., D.A. Scheinberg, and J.G. Jurcic, *The promise of targeted {alpha}-particle therapy.* J Nucl Med, 2005. **46 Suppl 1**: p. 199S-204S.
28. Munro, T.R., *The relative radiosensitivity of the nucleus and cytoplasm of Chinese hamster fibroblasts.* Radiat Res, 1970. **42**(3): p. 451-70.
29. Ballangrud, A.M., et al., *Response of LNCaP spheroids after treatment with an alpha-particle emitter (213Bi)-labeled anti-prostate-specific membrane antigen antibody (J591).* Cancer Res, 2001. **61**(5): p. 2008-14.
30. Chinol, M. and D.J. Hnatowich, *Generator-produced yttrium-90 for radioimmunotherapy.* J Nucl Med, 1987. **28**(9): p. 1465-70.
31. McDevitt, M.R., et al., *An alpha-particle emitting antibody ([213Bi]J591) for radioimmunotherapy of prostate cancer.* Cancer Res, 2000. **60**(21): p. 6095-100.
32. Dale, R.G., *The application of the linear-quadratic dose-effect equation to fractionated and protracted radiotherapy.* Br J Radiol, 1985. **58**(690): p. 515-28.
33. Le Mignon, M.M., et al., *Gd-DOTA. Pharmacokinetics and tolerability after intravenous injection into healthy volunteers.* Invest Radiol, 1990. **25**(8): p. 933-7.
34. Tsai, S.W., et al., *Metabolism and renal clearance of 111In-labeled DOTA-conjugated antibody fragments.* Bioconjug Chem, 2001. **12**(2): p. 264-70.
35. Behr, T.M., et al., *Overcoming the nephrotoxicity of radiometal-labeled immunoconjugates: improved cancer therapy administered to a nude mouse model in relation to the internal radiation dosimetry.* Cancer, 1997. **80**(12 Suppl): p. 2591-610.
36. Barone, R., et al., *Patient-specific dosimetry in predicting renal toxicity with (90)Y-DOTATOC: relevance of kidney volume and dose rate in finding a dose-effect relationship.* J Nucl Med, 2005. **46 Suppl 1**: p. 99S-106S.
37. Behr, T.M., et al., *High-linear energy transfer (LET) alpha versus low-LET beta emitters in radioimmunotherapy of solid tumors: therapeutic efficacy and dose-limiting toxicity of 213Bi- versus 90Y-labeled CO17-1A Fab' fragments in a human colonic cancer model.* Cancer Res, 1999. **59**(11): p. 2635-43.
38. Witzig, T.E., et al., *Phase I/II trial of IDEC-Y2B8 radioimmunotherapy for treatment of relapsed or refractory CD20(+) B-cell non-Hodgkin's lymphoma.* J Clin Oncol, 1999. **17**(12): p. 3793-803.
39. Michel, R.B., M.W. Brechbiel, and M.J. Mattes, *A comparison of 4 radionuclides conjugated to antibodies for single-cell kill.* J Nucl Med, 2003. **44**(4): p. 632-40.

Chapter 3: Isolation and characterization of gallium-DOTA-biotin-binding antibodies and peptides

We attempted to isolate high affinity scFv or linear peptide binders against the loaded metal chelate Ga-DOTA-biotin. A nonimmune library of human scFv fragments displayed on the surface of yeast was screened using MACS and FACS, and subsequent yeast-displayed affinity maturation libraries were constructed by V_H domain shuffling and random mutagenesis. These libraries were also screened, but improved scFv mutants were not isolated. The highest affinity obtained for an scFv against Ga-DOTA-biotin was in the low micromolar range, and the clones isolated were difficult to characterize. A linear peptide library displayed on the surface of yeast was also screened for binding to Ga-DOTA-biotin. Several peptides that bound specifically to Ga-DOTA-biotin were isolated, but they were strongly positively charged and bound the metal chelate with only lower micromolar affinity. It is possible that it is difficult to engineer antibody fragments and linear peptides for binding to Ga-DOTA-biotin due to the chelate's six-coordinate binding of the gallium ion, which may result in rapid exchange of the carboxyl arms of the chelate in solution.

3.1 Introduction

An extremely high affinity scFv against carcinoembryonic antigen was developed by Graff and co-workers [1]. We proposed to use this scFv, called sm3E, as the cancer-specific half of an optimal bispecific reagent for PRIT. It was then necessary to select a hapten for use in PRIT, and develop the anti-hapten half of the bispecific reagent.

Our first choice for an optimal hapten was the metal chelate DOTA (1,4,7,10-tetraazacyclododecane-1,4,7,10-tetraacetic acid), which binds many metal ions with +2

and +3 net charges with extremely high affinity [2, 3]. Metal chelates such as DOTA and DPTA are commonly used for conjugating radioisotopes to antibodies [4, 5]. The methods used for conjugating DOTA to proteins [6, 7] can be easily adapted to conjugate DOTA to biotin (which is necessary for fluorescent labeling of DOTA-binding yeast cells in FACS). Small metal chelates such as DOTA make ideal hapten molecules due to their very short pharmacokinetic clearance times [8]. Antibodies against metal-loaded DOTA-derivates had been developed previously [9] and were characterized during the course of this research [10, 11].

Yeast surface display has been used to isolate and engineer extremely high-affinity antibodies that bind to both small molecules [12] and protein targets [1, 13, 14]. The main advantage of yeast surface display is that because it uses flow cytometry as its selection method, selection can be performed in a quantitative manner, making possible very fine discrimination between mutants with similar properties [15]. In protein engineering contexts, yeast surface display has proven to be extremely powerful – for example, it was used to isolate a monovalent antibody fragment against fluorescein with sub-picomolar affinity [12]. Yeast surface display has also been used to display linear peptide libraries and select short peptides that bind to patterned surfaces [16, 17]. Finally, high-affinity peptides against small molecule targets have been isolated using phage display [12]. Based on these encouraging results in the literature, we expected that it would be possible to use yeast surface display to engineer a high affinity metal chelate binder. We attempted to isolate a high affinity antibody fragment or peptide that bound to Ga-DOTA to be used as the hapten-binding part of a PRIT targeting agent.

3.2 Methods

3.2.1 Loading DOTA with metal ions

DOTA (Macrocyclics) and DOTA loaded with Ga^{3+} by the addition of gallium nitrate (Sigma) were analyzed using NMR. Metal-free conditions were used throughout sample preparation and analysis. NMR experiments on 1-2 mM solutions of DOTA and Ga-DOTA were performed in 90% H_2O/10% D_2O, on a Varian Unity 300 MHz spectrometer, in order to determine if metal loading was successful.

3.2.2 Synthesis, purification and characterization of Ga-DOTA-biotin

DOTA was conjugated to biotin-XX based on the conjugation protocol used by Keire and co-workers [7]. Biotin-XX, a biotin-derivative with a long linker attached, was selected so that if the metal-DOTA part of the conjugate was bound deep in the cleft of an antibody fragment, the biotin moiety would still be accessible for binding by streptavidin-PE during fluorescent labeling. Synthesis of DOTA-biotin began with the addition of a solution of 3.6 mg of DOTA and 3 mg of sulfo-NHS in 0.1 mL of H_2O to 0.05 mL of a freshly prepared solution of EDC (50 mg/mL). After 30 min, 5 mg of biotin-XX (Molecular Probes) was added to the reaction mixture, the pH adjusted to 8 w/ 11 μL of 1M NaOH, and the solution was left overnight. The next morning, the reaction was quenched by lowering the pH of the reaction mixture to 2 with the addition of 33 μL of 1 N HCl. The final mixture contained both doubly and singled modified forms of DOTA-biotin and unmodified DOTA that were separated by reversed-phase chromatography.

The products of the reaction were purified using a Pharmacia Biotech FPLC chromatography system equipped with a Source 15RPC stationary phase column

(Amersham Pharmacia Biotech). The purification method used a flow rate of 0.3 mL/min throughout and used a linear gradient from 0 to 100% solvent B over 80 min (solvent A, 0.1% TFA in H_2O; solvent B, 0.1% TFA, 10% H_2O, 90% CH_3CN), beginning 28 min after injection. 1.2 mL samples were collected and the absorbance of each was measured at 214 nm. Peak samples were collected, lyophilized and identified by their mass-to-charge ratio using mass spectrometry.

Singly-conjugated DOTA-biotin was loaded with Ga^{3+} in the form of gallium nitrate according to published protocols for rapidly loading gallium into DOTA [18].

3.2.3 Screening of a yeast-displayed human nonimmune scFv library against Ga-DOTA-biotin

A nonimmune scFv library displayed on the surface of yeast [14] was screened for binders against Ga-DOTA-biotin using 1 round of magnetic cell sorting (MACS) and 3 rounds of flow activated cell sorting (FACS). In MACS, 3 x 10^9 induced cells from the nonimmune library were resuspended in 10 ml phosphate buffered saline (PBS) supplemented with 0.1% bovine serum albumin (BSA). Ga-DOTA-biotin as added to the resuspended cells at 1 μM final concentration, and the cells were incubated at 4°C for 60 minutes with constant mixing. The cells were then pelleted by centrifugation (3000*g* for 3 minutes) and washed twice with 10 mL PBS/BSA buffer. The cells were pelleted again, resuspended in 5 mL PBS/BSA buffer with 100 μL MACS streptavidin-coated beads (Miltenyi), and incubated at 4°C for 30 minutes with constant mixing.

45 ml of cold PBS/BSA buffer was added to the cell/bead mixture, and the cells were pelleted by centrifugation as above and washed in 50 m L PBS/BSA buffer. The suspension was vortexed thoroughly to ensure a single cell suspension, and incubated on

ice for 5 minutes. A Miltenyi LS column was loaded onto its magnetic stand and pretreated with 7 mL of cold PBS/BSA buffer. 7 mL of cell/bead suspension were added to the column at a time. After 7 mL of the mixture had entered the column and flow had stopped, the column was removed from the magnet and then put back in place immediately, but as gently as possible. The intent of this step is to rearrange the magnetic beads in the column and allow cells that are physically trapped in the column to pass through. With the column back in the magnet, an additional 7 mL of cells was added to the column, and the procedure was repeated until all 50 mL of cells had been added.

After all cells had been added, the column was washed with 3 mL PBS/BSA buffer, making sure that the upper loading column was washed of all residual cells. This wash removes the cells in the void volume of the column. The column was removed from the magnet, gently replaced, and another 3 ml of cold PBS/BSA buffer was added.

To elute Ga-DOTA-biotin binding cells, the column was removed from the magnet, 7 ml of SD-CAA media was added to the column, and the plunger was used to push all remaining cells into a 15 mL conical tube. Regardless of antigen concentration, 2-3 x 10^7 cells are typically eluted [19]. Eluted cells were grown overnight in 100 mL of SD-CAA supplemented with a 1:50 dilution of stock penicillin-streptomycin (10,000 units/mL penicillin, 10,000 μg/mL of streptomycin) to prevent bacterial contamination. Cells were grown overnight and induced for subsequent FACS.

Three rounds of FACS were performed on the cell population isolated using MACS. For all FACS screens, cells were labeled at a concentration of 5 μM Ga-DOTA-biotin. FACS was performed as previously documented [1, 12, 14, 15, 20], using anti-c-

myc antibodies to normalize for expression, and using three different secondary detection reagents – neutravidin-PE, streptavidin-PE, and streptavidin-APC – to prevent the isolation of scFvs that bind secondary reagents.

A population of Ga-DOTA-biotin binding yeast cells was isolated and characterized for binding to Ga-DOTA-biotin and unloaded DOTA-biotin. 20 single clones were cultured and screened using flow cytometry at 2 μM to determine which bound most strongly to Ga-DOTA-biotin. The three best clones – 9, 11 and 17 were characterized in more detail via flow cytometry.

3.2.4 Affinity maturation of Ga-DOTA-biotin-binding scFvs

In order for a bispecific molecule to function successfully in PRIT, it must be able to retain hapten for long enough so that the antigen-diabody-hapten complex can be internalized into the cell. Based on typical antigen turnover half-lives of 15-60 minutes, the hapten-binding part of the targeting agent needs to bind hapten with at least low nanomolar affinity. Therefore, the affinity of Ga-DOTA-biotin-binding scFvs needed to be improved by approximately 1,000-fold. Our philosophy in attempting to affinity mature anti-Ga-DOTA-biotin scFvs was to make larger, domain-level changes early in the process, followed by smaller, single-residue-level changes later. Consistent with that philosophy, two libraries were constructed and screened in an attempt to isolate high-affinity anti-Ga-DOTA-biotin scFvs.

First, a V_H-shuffled library was constructed. In this library, the V_L domains of a large pool of binders (population pMF3N) were held constant, and V_H domains from the nonimmune scFv library [14] were swapped in via homologous recombination [21] in an attempt to find an improved V_L/V_H pairing. The decision to swap out the V_H domains of

binding antibodies, rather than the V_L domains, was informed by the fact that a V_L-only mutant of the best Ga-DOTA-biotin-binding scFv maintained its Ga-DOTA-biotin-binding activity. This is counter to the observation that the V_H domain (and in particular the V_H CDR3) is usually most responsible for antibody binding function [22].

To create a V_H-shuffled library, plasmid DNA from the population pMF3N was collected using the Zymoprep method (Zymo Research) and amplified in *E. coli*. This DNA was then cut with restriction enzymes *Pst I* and *BamH I* to remove the V_H region from the plasmid. The construction and domain-level structure of nonimmune library-derived plasmids is described by Feldhaus et al [14]. The V_H region of the nonimmune scFv library was amplified from library plasmid by PCR, and the vector (cut plasmid) and insert (library PCR) were combined by homologous recombination in yeast [21]. The library of yeast-displayed proteins was labeled and sorted as previously described [14, 15], and the best binders were isolated, sequenced and characterized.

Following the screening of the V_H-shuffled library, a library was constructed using random mutagenesis as previously described [1, 12, 13]. In this library, promising anti-Ga-DOTA-biotin binding clones were subjected to error-prone PCR in order to introduce mutations in the genetic code of the antibody fragments. The library was based on the following material: 35% DNA from pMF3N clones, 5% each from clones 9, 11, and 17 (the best clones from population pMF3N), 10% of the unsorted V_H-shuffled library discussed above, and 10% each of the V_H-shuffled library after 1, 2, 3 and 4 rounds of sorting. The library was constructed by performing error-prone PCR on the entire scFv gene as previously described, and then transforming that insert and cut pCTCON2 backbone into yeast using homologous recombination [21]. The library of

yeast-displayed proteins was labeled with Ga-DOTA-biotin and sorted as previously described [14, 15], and the best binders were isolated, sequenced and characterized.

3.2.5 Screening of a yeast-displayed linear peptide library

Faced with the failure to isolate or engineer high-affinity scFvs that bound to Ga-DOTA-biotin, we explored to possibility of using a peptide as the hapten-binding part of the bispecific targeting agent. Peptides with affinities in the low nanomolar range have been reported [23], so it was possible that a high-affinity Ga-DOTA-biotin binding peptide could be isolated and engineered. In addition, attempts to isolate anti-Ga-DOTA-biotin scFvs had led to the isolation of peptide-like molecules, so we hypothesized that a peptide might potentially be better suited for binding this metal chelate.

A pre-existing linear peptide library composed of amino acid 10-mers [16, 17] was labeled with 1 μM Ga-DOTA-biotin and sorted via FACS. The diversity of the starting library was estimated to be 1-5 x 10^7 transformants. The peptides were displayed on the surface of yeast in the following format: HA epitope tag-$(gly_4ser)_3$-peptide. Four rounds of FACS were successfully completed, and specifically binding clones were isolated, sequenced and characterized. Alanine scanning, in which amino acid residues in the peptides were changed to alanine residues, were performed on the best binding clones. The intent of alanine scanning was to determine which residues in the peptide, if any, were crucial or most important for binding to Ga-DOTA-biotin.

3.3 Results

3.3.1 Characterizing the loading of DOTA with Ga^{3+} using NMR

NMR experiments showed that the presence of bound Ga^{3+} in the DOTA molecule significantly changed the chemical environment of the hydrogen atoms in the

DOTA chelate, as expected. NMR spectra for unloaded and Ga-loaded DOTA are shown in Fig. 3.1.

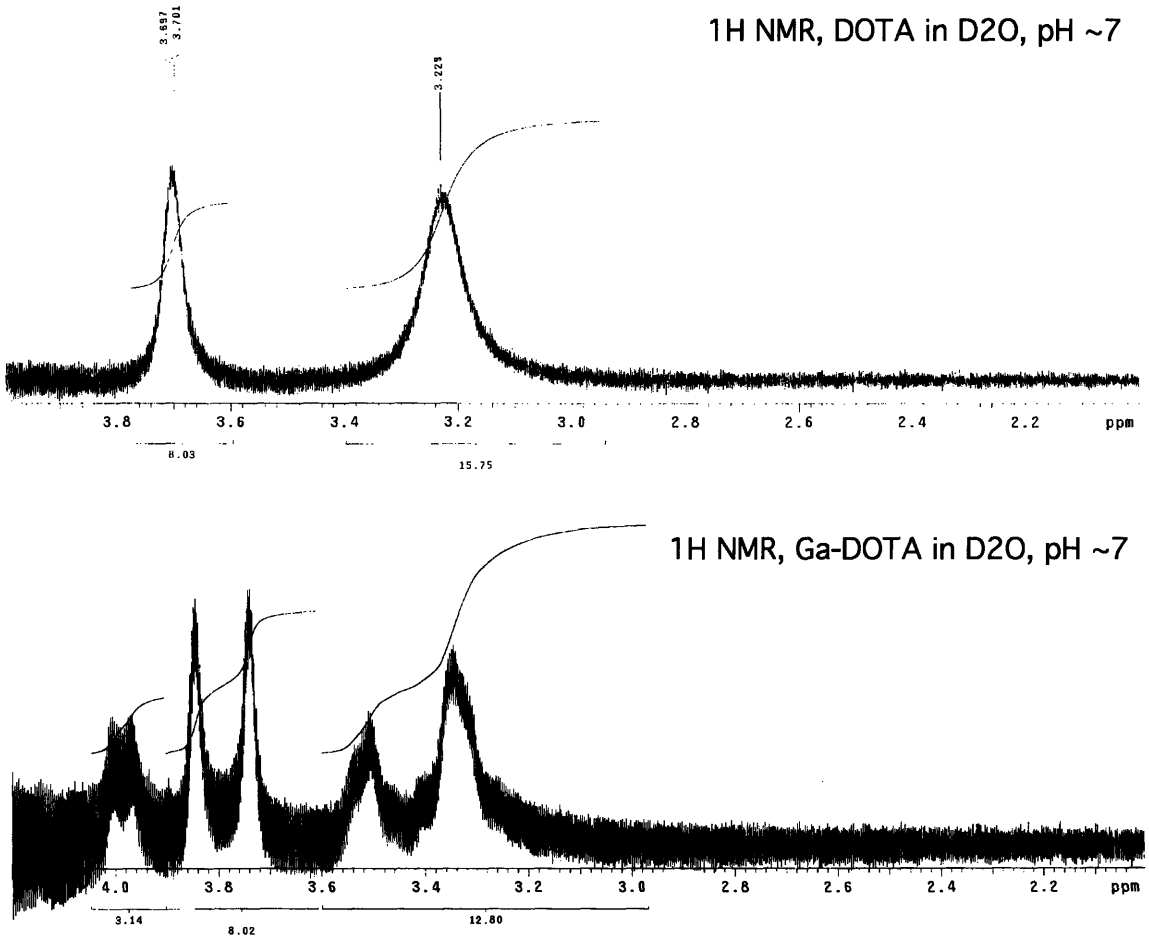

Fig. 3.1. NMR spectra of unloaded and Ga-loaded DOTA in 10% D_2O/90% H_2O, as measured on a Varian Unity 300 MHz NMR spectrometer.

These results confirmed that the Ga^{3+} ion could be successfully loaded into DOTA. In addition, they indicate that the environments of the hydrogen atoms in Ga-loaded DOTA are different than those of Y-DOTA [7], indicating that the two complexes may have different structures. This is in agreement with the finding that Ga-DOTA and Y-DOTA analogues do have substantially different structures; Ga-DOTA analogues bind to the metal ion in a six-coordinate fashion, while Y-DOTA analogues are 8-coordinate in their binding of the metal ion [24].

3.3.2 Synthesis, purification and characterization of Ga-DOTA-biotin

Singly and doubly conjugated DOTA-biotin were separated via reverse-phase chromatography. DOTA was detected by measuring the absorbance of each 1.2 ml sample at 214 nm, and peaks were submitted for analysis by mass spectrometry. The elution profile and mass spectrometry results are presented in Fig. 3.2.

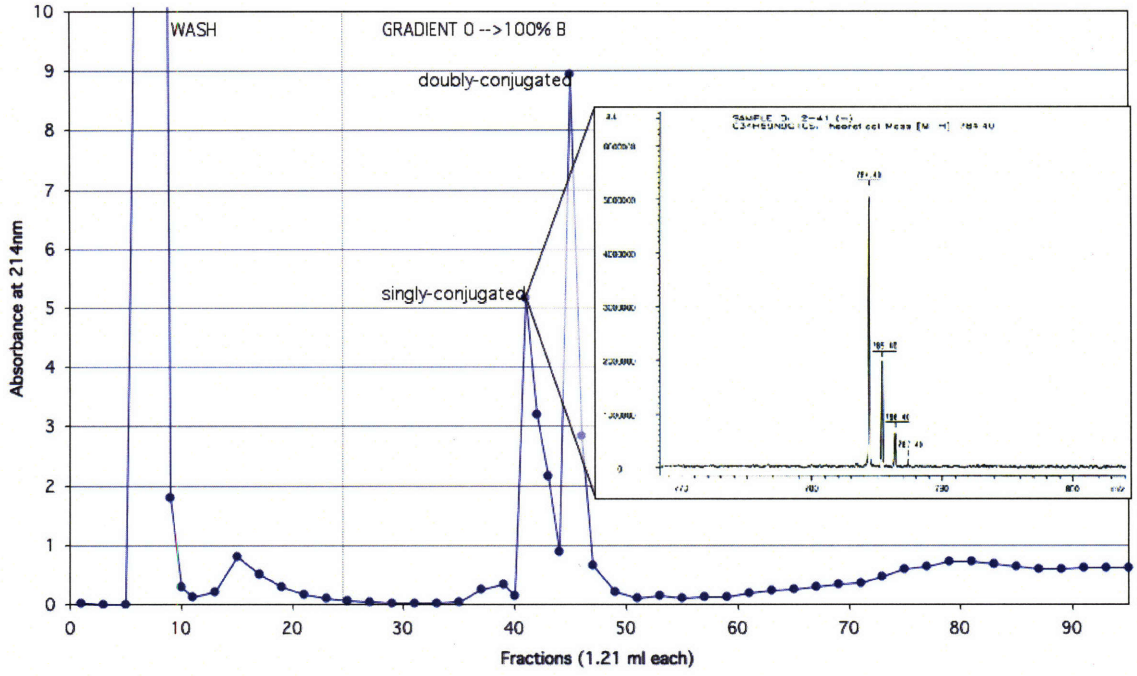

Figure 3.2. Elution profiles of unreacted DOTA, and singly and doubly conjugated DOTA-biotin, as separated by reverse phase chromatography. DOTA was detected by measuring the absorbances of samples at 214 nm.

Unreacted DOTA and other reactants eluted during the wash step, while singly and doubly conjugated DOTA-biotin were eluted during the gradient step. Singly-conjugated DOTA-biotin with the expected theoretical mass-to-charge ratio of 784.4 was eluted first, followed by doubly-conjugated DOTA-biotin. Singly-conjugated DOTA-biotin was lyophilized, resuspended in H_2O, loaded with gallium and then used in subsequent screening experiments. Ga-DOTA-biotin was stored at 4°C.

3.3.3 Screening of a yeast-displayed human nonimmune scFv library against Ga-DOTA-biotin

After MACS screening of the nonimmune library, eluted cells were grown overnight in SD-CAA supplemented with penicillin-streptomycin. The next morning, the absorbance at 600 nm was measured, and the maximum number of eluted cells (and thus the maximum diversity of the population) was calculated to be 3.3×10^7, based on a 3-hr doubling time for yeast. In the first round of sorting, 1.5×10^8 induced cells that had been labeled with 1 μM Ga-DOTA-biotin were sorted. Neutravidin-PE was used to detect antigen binding. 189,000 cells were collected (population pMF), grown up and induced for sorting. In the second round of sorting, 4.5×10^7 cells that had been labeled with 1 μM Ga-DOTA-biotin were sorted, and streptavidin-APC was used for secondary detection. 200,000 cells were collected (population pMF2A), grown up and induced for sorting. In the third and final round of sorting, 3×10^7 cells that had been labeled with 1 μM Ga-DOTA-biotin were sorted, and neutravidin-PE was used for secondary detection. 30,000 cells were collected (population pMF3N). Note that in each round of sorting, both the biotin-binding protein and the dye used for secondary detection were changed from what had been used in the previous round, in order to prevent the isolation of clones that bound to the secondary reagents, rather than Ga-DOTA-biotin. Dot-plots from each round of sorting are shown in Fig. 3.3.

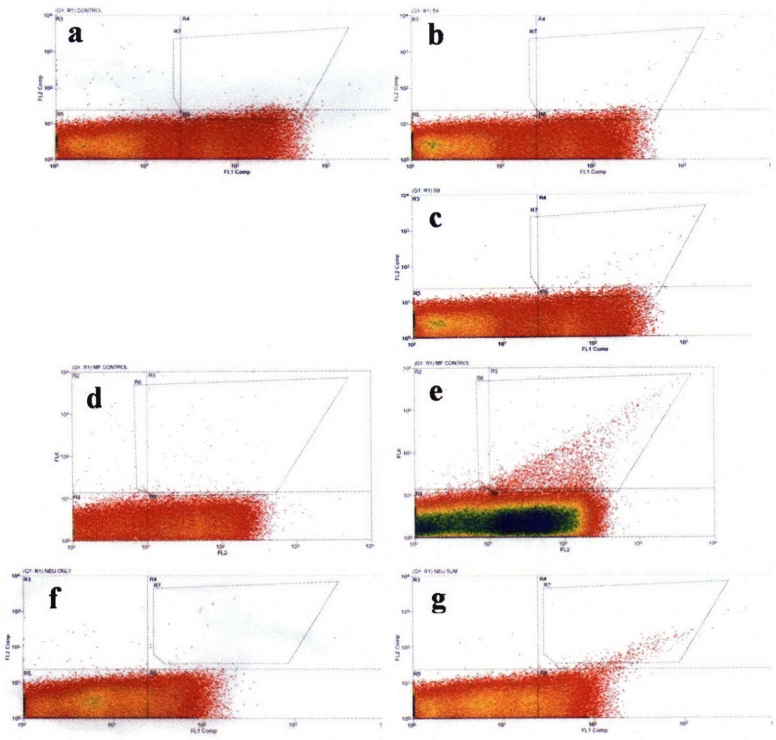

Figure 3.3. Dot-plots from three FACS sorts against Ga-DOTA biotin. (a) Post-MACS population, negative control (all labeling reagents added except for Ga-DOTA-biotin). (b) Post-MACS population labeled with 1 μM Ga-DOTA-biotin, first tube of cells. (c) Post-MACS population labeled with 1 μM Ga-DOTA-biotin, second tube of cells. (d) Population pMF, negative control. (e) Population pMF, labeled with 1 μM Ga-DOTA-biotin. (f) Population pMF2A, negative control. (g) Population pMF2A, labeled with 1 μM Ga-DOTA-biotin. The 30,000 cells collected in this sort comprise population pMF3N.

In each round of sorting, the lack of double-positive cells in the negative control indicates that the fluorescence of the labeled cells is Ga-DOTA-biotin-specific.

The binding of the population pMF3N was titrated against varying concentrations of Ga-DOTA-biotin. As shown in Figure 3.4, it was not possible to reach the upper limit of fluorescence with this population by increasing the concentration of Ga-DOTA biotin, making it difficult to estimate a K_d for the population.

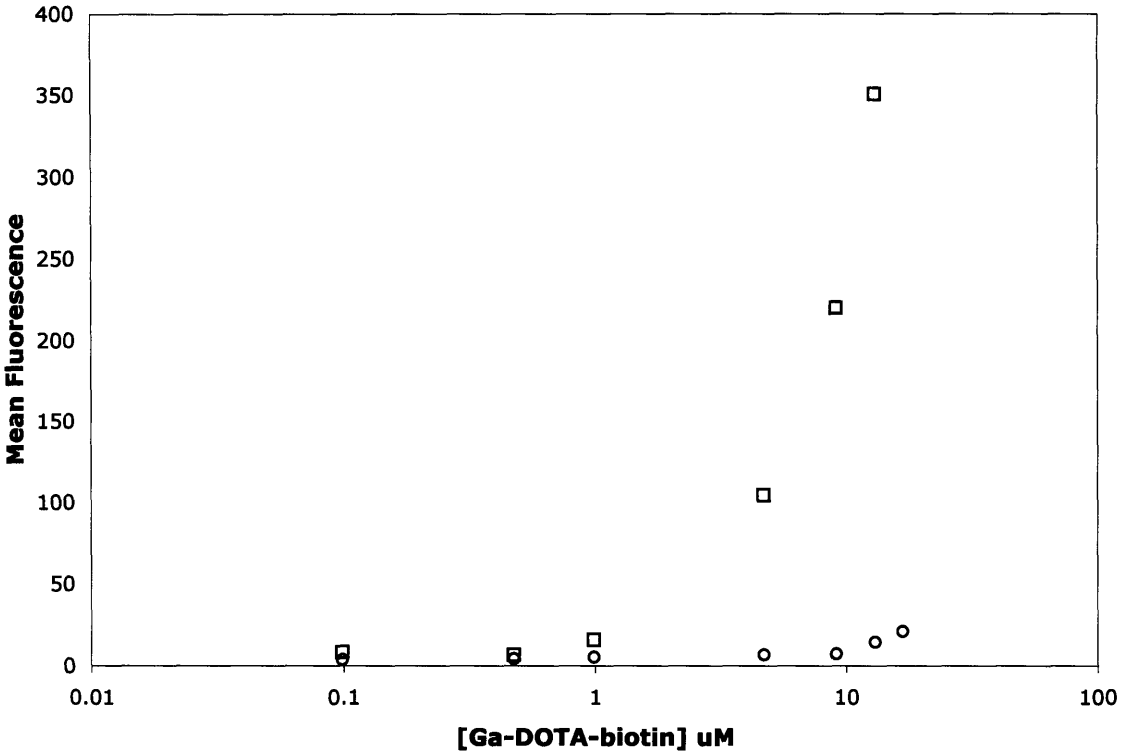

Figure 3.4 Titration of binding of population pMF3N displayed on the surface of yeast to Ga-DOTA-biotin. Mean fluorescence of displaying cells (as gated by c-myc labeling) is reported (squares). Negative control is an irrelevant yeast surface-displayed protein fusion (circles).

However, it was possible to show that the binding of the clones in population pMF3N to Ga-DOTA-biotin was dependent on the presence of gallium. As shown in Fig. 3.5, population pMF3N does not bind to unloaded DOTA-biotin. Also note that at high concentrations of Ga-DOTA-biotin, almost all of the displaying cells in the population exhibit some level of binding.

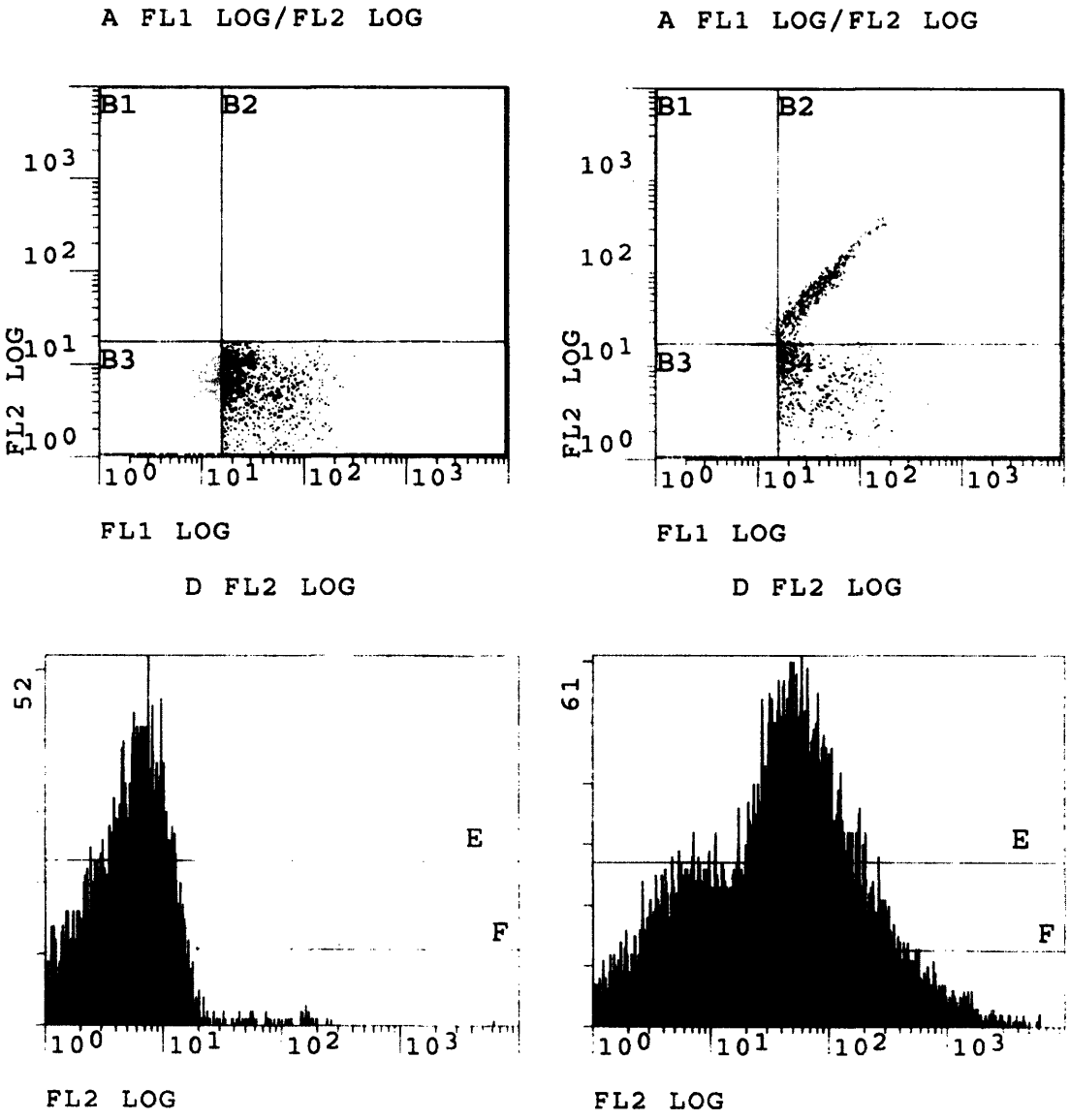

Figure 3.5. Binding of population pMF3N to Ga-DOTA-biotin is dependent on the presence of gallium. On the left, population pMF3N is labeled with 5 μM unloaded DOTA-biotin, and on the right, pMF3N is labeled with 5 μM Ga-DOTA-biotin. In the absence of gallium, the population does not bind to the metal chelate. Dot-plots are shown at the top, and histogram plots of binding-associated fluorescence are shown at the bottom. Labeling for display was performed using 12CA5, an antibody which binds to the HA tag.

Twenty single clones were isolated from population pMF3N for further characterization and analysis. Each of these clones was grown up, induced and labeled with 2 μM Ga-DOTA-biotin, in order to determine which clones bound Ga-DOTA-biotin with the highest affinity. The results of that cytometry experiment are shown in Fig. 3.6.

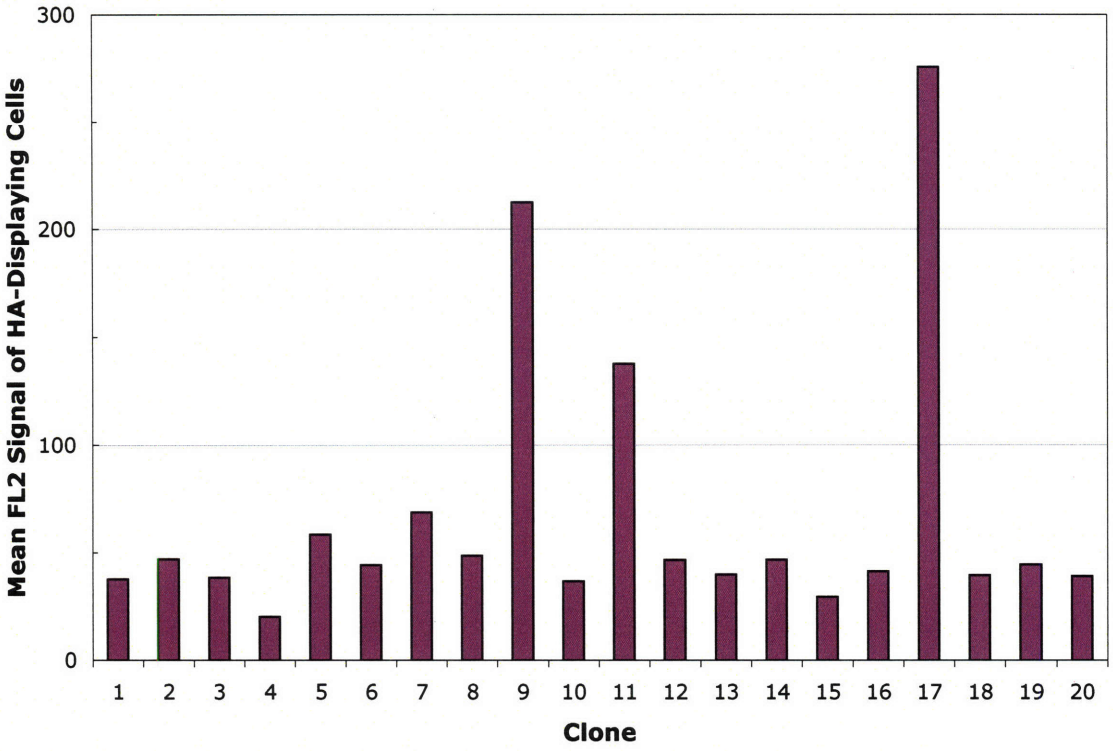

Figure 3.6. Single clone analysis. Twenty clones from population pMF3N were labeled with 2 μM Ga-DOTA-biotin to assess their binding ability. The HA tag was used to normalize for expression.

Titrations were performed on clones 9, 11 and 17 in an attempt to determine the dissociation constants of these scFvs for Ga-DOTA-biotin. Unfortunately, as was the case for the population as a whole, it was not possible to determine the K_d of these clones for Ga-DOTA-biotin, because the fluorescent signal of the labeled cells increased without end as more Ga-DOTA-biotin was added. However, it was estimated that the binding was approximately single-digit micromolar. These titrations are shown in Figure 3.7, and Figure 3.8 presents further labeling data for the best binding clone, 17.

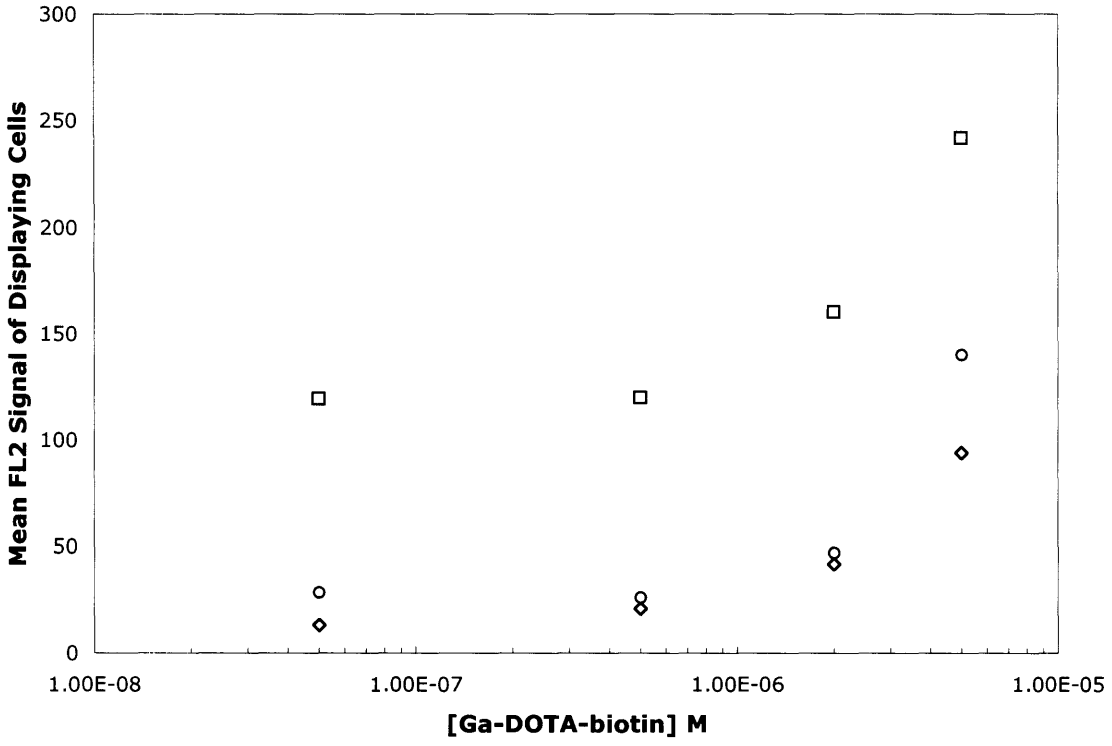

Figure 3.7. Titration of Ga-DOTA-biotin binding of clones 9 (diamonds), 11 (circles) and 17 (squares) from population pMF3N.

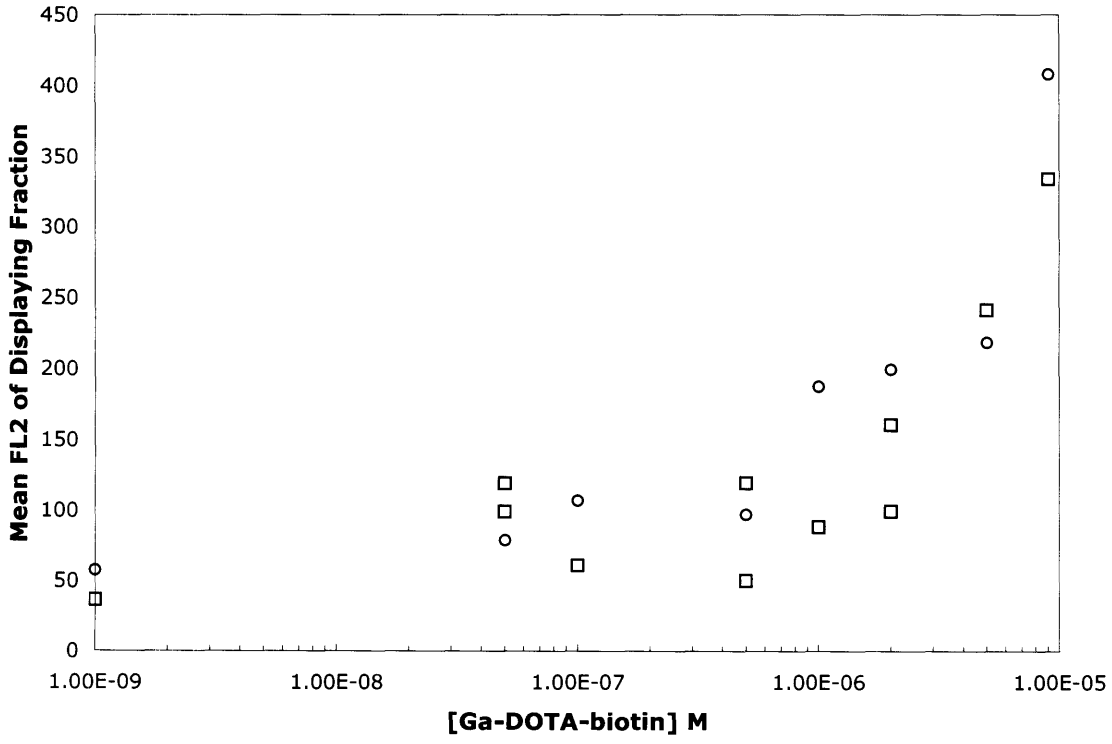

Figure 3.8. Mixed titration data for the binding of clone 17 to Ga-DOTA-biotin. Squares are circles are from experiments performed on different days but from the same induced yeast culture.

At this point, we decided to attempt to affinity mature these anti-Ga-DOTA-biotin-binding scFv clones in an effort to improve the affinity enough that it could be accurately measured using flow cytometry.

3.3.4 Affinity maturation of Ga-DOTA-biotin-binding scFvs

A V_H-shuffled library was constructed via *in vivo* homologous recombination [21] in yeast by combining the plasmid DNA of population pMF3N with the V_H domain removed with the amplified V_H domain of the nonimmune scFv library [14]. The diversity of the library as measured by the number of yeast transformed was 2 x 10^5. The library was labeled with Ga-DOTA-biotin and screened as described above, as shown in Fig. 3.9. After four rounds of sorting, single clones were isolated and characterized.

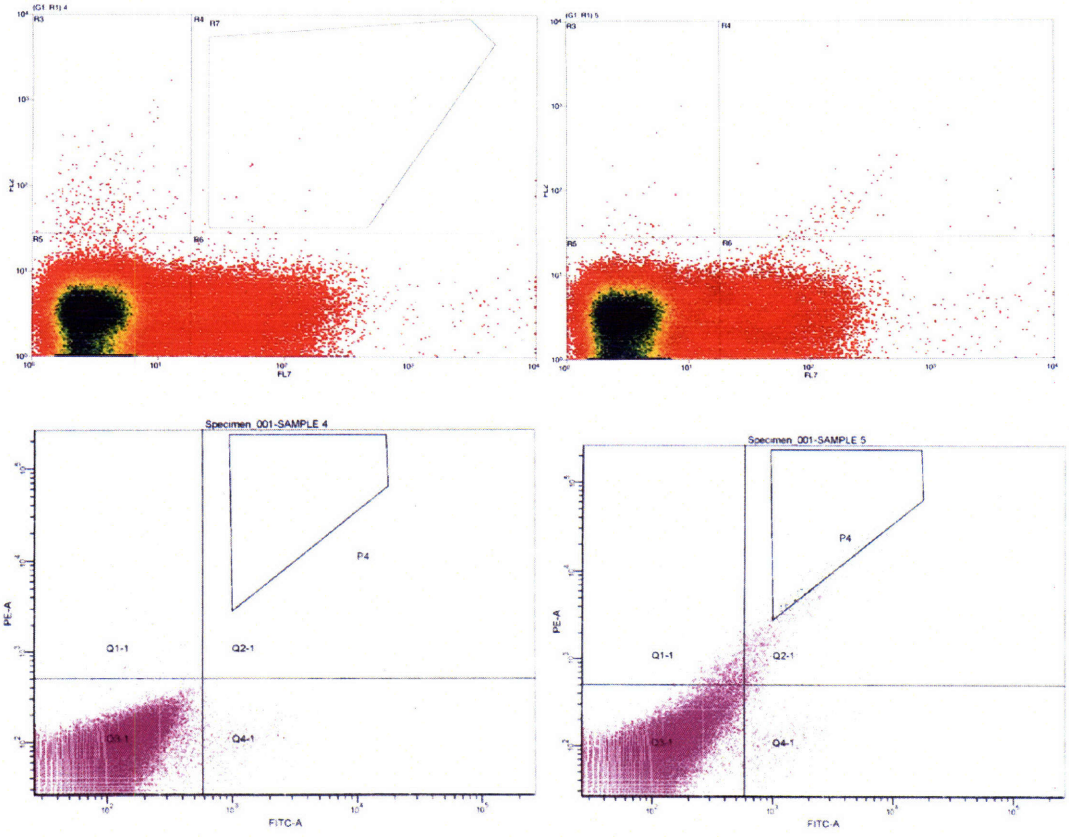

Figure 3.9. Screening a V_H-shuffled scFv library based on the V_L-regions of clones in population pMF3N for improved binders to Ga-DOTA-biotin. In each dot-plot, display of expressed proteins correlates with the x-axis, while binding of expressed proteins to Ga-DOTA-biotin or secondary reagents correlates with the y-axis. Top left, the unsorted V_H-shuffled library, labeled with all reagents except Ga-DOTA-biotin. Top right, the unsorted V_H-shuffled library, labeled with 1 μM Ga-DOTA-biotin in addition to other reagents. Clones binding to Ga-DOTA-biotin are double positive. Bottom left, the V_H-library after two rounds of sorting, labeled with all reagents except Ga-DOTA-biotin. Bottom right, the V_H-shuffled library after two rounds of sorting, labeled with 500 nM Ga-DOTA-biotin in addition to other reagents. Clones binding to Ga-DOTA-biotin are double positive. Note that by the third round of sorting, clones that bind to Ga-DOTA-biotin only label for display in the presence of Ga-DOTA-biotin.

Several individual clones were isolated from the screening of the V_H-shuffled library by FACS. These clones bound Ga-DOTA-biotin with affinities in the low micromolar range – in order words, the affinity of the clones had not been improved by performing the V_H domain shuffle. In addition, the isolated clones exhibited a peculiar behavior – as shown in the bottom panels of Fig. 3.9, the cells expressing Ga-DOTA-biotin-binding scFvs could only be labeled for display (fluorescence on the x-axis) when they were also labeled with Ga-DOTA-biotin (fluorescence on the y-axis). This strange phenotype indicated that the c-myc epitope tag being used to label the proteins for display might in some way be involved in the Ga-DOTA-biotin binding event. In any event, as the clones isolated from the V_H-shuffled library were not improved in affinity, and had developed a peculiar display phenotype, further affinity maturation was necessary.

A random mutagenesis library was constructed using error-prone PCR on the following DNA templates: 35% DNA from population pMF3N, 5% each from clones 9, 11 and 17 (the three best clones isolated from pMF3N), and 10% each from the V_H-shuffled library after 0, 1, 2, 3 and 4 rounds of sorting against Ga-DOTA-biotin. Five transformations via homologous recombination [21] were performed, and 4-5 x 10^5

transformants were obtained per shock, for a total starting diversity of 2.2 x 10^6. After three rounds of sorting at 250 nM Ga-DOTA-biotin, single clones were isolated and characterized.

The three best Ga-DOTA-biotin-binding clones isolated from the mutagenic library were clones m14, m18 and m20. Like previous clones isolated from both the nonimmune and V_H-shuffled libraries, they were only approximately micromolar in affinity for Ga-DOTA-biotin, indicating that their binding had not been improved, as shown in Fig. 3.10.

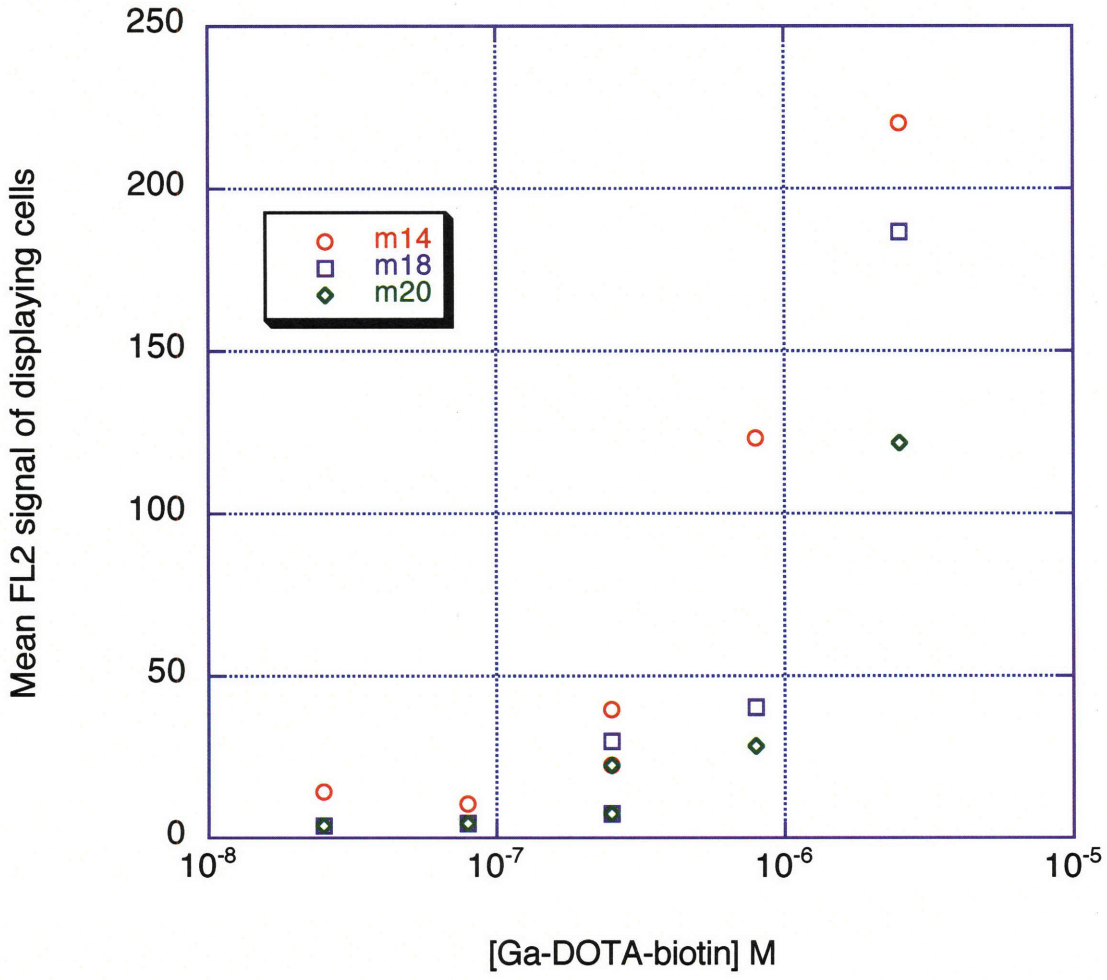

Fig 3.10. Binding of three best clones isolated after three rounds of sorting from a mutagenic scFv library based on Ga-DOTA-biotin-binding clones. The K_ds of the clones for Ga-DOTA-biotin could not be calculated, but they are estimated to be in the low micromolar range.

Worse yet, upon sequencing the clones it was discovered that rather than full-length scFvs, all three best clones were truncated antibody fragments that resulted from frameshift mutations. In each of the clones, a frameshift mutation in the V_L domain resulted in an overwhelming positively-charged peptide-like region at the C-terminal end of the protein. This group of positive charges was likely interacting in a weak, nonspecific way with the negatively-charged carboxyl groups on Ga-DOTA-biotin. At this point, we began to consider other options for obtaining Ga-DOTA-biotin binding molecules, as screenings of a nonimmune library and two subsequent affinity maturation libraries had not isolated or improved binders against the metal chelate.

3.3.5 Screening of a yeast-displayed linear peptide library

A library of linear peptides displayed on the surface of yeast underwent four rounds of FACS screening in an attempt to isolate high-affinity binders to Ga-DOTA-biotin. The diversity of the starting population was roughly 1-5 x 10^7, and its amino acid composition has been previously described [16, 17]. After four rounds of sorting with labeling at 1 μM Ga-DOTA-biotin, enriched populations of peptide binders were isolated, as shown in Fig. 3.11.

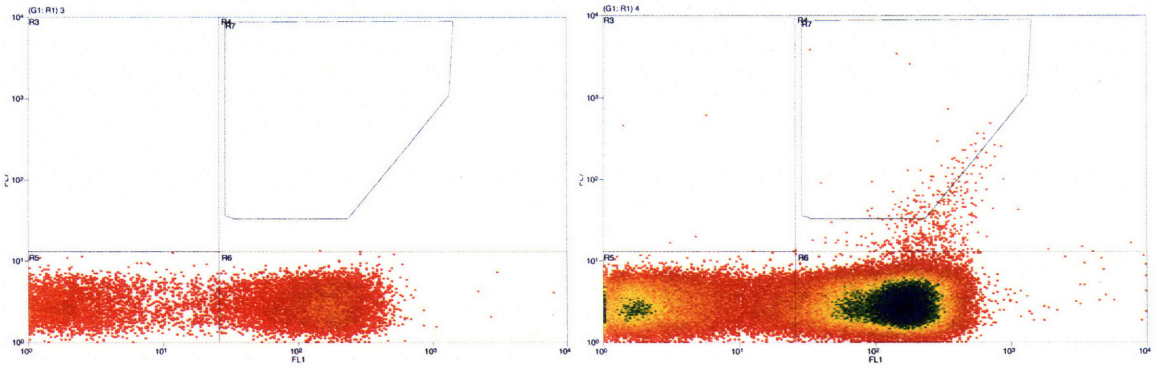

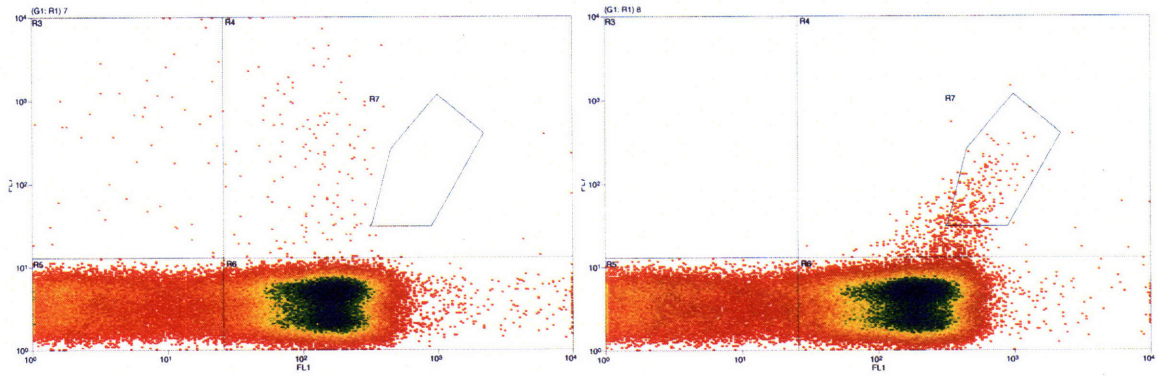

Figure 3.11. The isolation of anti-Ga-DOTA-biotin linear peptides via FACS. Top row, fourth round of FACS screening on population 3A. Left, all labeling reagents except for Ga-DOTA-biotin. Right, 1 μM Ga-DOTA-biotin and other labeling reagents. Bottom row, fourth round of FACS screening on population 3B. Left, all labeling reagents except for Ga-DOTA-biotin. Right, 1 μM Ga-DOTA-biotin and other labeling reagents.

13 individual clones that bound Ga-DOTA-biotin were sequenced, and 7 unique peptide sequences were determined, as shown below in Fig. 3.12. Almost all of the peptides isolated are overwhelming positive in charge at pH 7 (4 of the 7 peptides have net charges of +5 or greater).

5A-1	R R K C T K K Y V S N Y
5A-2	T V G L G R P C E Y P P
5A-4	R C R V M W G P R P S Q
5B-2	A R G R R G R R W S R C S
5B-3	R R G P R R G K R K P Y
5B-4	P V P C R K R K C R W G
5C-5	Q E A D G G V K T S F S

Figure 3.12. The sequences of seven unique Ga-DOTA-biotin-binding peptides. All sequences were preceded by ASQGGGGSG, where AS is the Nhe I restriction site and the rest of the leader sequence is a linker region.

To gain a greater understanding of how these peptides were interacting with Ga-DOTA-biotin, alanine scanning was performed. Site-directed mutagenesis was used to

change, individually, each amino acid residue of interest (R, W, C, P or K) to alanine in the two best binding peptides, 5B-2 and 5B-3. Each mutant was sequenced to verify the correct DNA sequence, and then labeled with Ga-DOTA-biotin to determine if the mutation had affected the ability of the peptide to bind Ga-DOTA-biotin. Remarkably, none of the alanine scanning mutants significantly affected Ga-DOTA-biotin binding, indicating that no single residue in either of the peptides in question was crucial for binding.

3.4 Conclusions & Discussion

Libraries of scFvs and linear peptides were screened on the surface of yeast in an attempt to isolate high affinity (nanomolar or better) binders of Ga-DOTA-biotin. Unfortunately, this effort was unsuccessful. Binders isolated from a nonimmune scFv library and subsequent V_H-shuffled and random mutagenesis affinity maturation libraries had at best low micromolar affinity for Ga-DOTA-biotin. These mutants seem resistant to affinity maturation, as several different approaches failed to improve binding. For one set of mutants, binding was depending on the presence of the epitope tag c-myc and anti-c-myc antibodies; for another set, binders initially thought to be scFvs turned out to be peptide-like truncations of full-length scFvs that ended in strongly positive polypeptide regions. In addition, screening of a linear peptide library against Ga-DOTA-biotin also led to a set of overwhelmingly positively-charged peptides.

Alanine scanning performed on the positively-charged peptides indicates that no single residue is important in the binding interaction with Ga-DOTA-biotin. It seems likely that the binding interaction is mediated by nonspecific electrostatic interactions

between the positively charged peptides and Ga-DOTA-biotin, which has regions of negative charge. Such interactions are not particularly amenable to improvement through random mutagenesis or other means of affinity maturation.

As discussed earlier in the chapter, when binding Ga^{3+} ion DOTA is though to be six-coordinate. Those six points of binding are the four cyclic nitrogens, and two of the carboxyl arms, leaving two carboxyl arms free and in solution. Even when DOTA is conjugated to biotin, one of the arms remains free. We hypothesize that this free arm rapidly exchanges with the carboxyl groups that are binding the metal ion. While this exchange does not result in the release of the metal ion from the chelate, it may result in a continually changing structure of Ga-DOTA-biotin in solution, which could make isolating binders against the conjugated metal chelate quite difficult. This is opposed to a molecule such as Y-DOTA-biotin, in which all of the carboxyl arms are directly involved in the 8-coordinate binding of the metal ion. We believe that it may be easier to isolate binders against 8-coordinate forms of metal-chelate complexes, as has been previously accomplished [10]. However, as discussed in Chapter 5, it may be more useful to design and use in PRIT studies a targeting agent that binds to a small molecule to which any given radioisotope of interest can be conjugated.

3.5 Works Cited

1. Graff, C.P., et al., *Directed evolution of an anti-carcinoembryonic antigen scFv with a 4-day monovalent dissociation half-time at 37 degrees C.* Protein Eng Des Sel, 2004. **17**(4): p. 293-304.
2. Clarke, E.T., Martell, A.E., *Stabilities of trivalent metal ion complexes of the tetraacetate derivatives of 12-, 13- and 12-membered tetraazamacrocycles.* Inorganica Chimica Acta, 1991. **190**: p. 37-46.

3. Clarke, E.T., Martell, A.E., *Stabilities of alkaline earth and divalent transition metal complexes of the tetraazamacrocyclic tetraacetic acid ligands.* Inorganica Chimica Acta, 1991(190): p. 27-36.
4. Zhang, M., et al., *Pretargeting radioimmunotherapy of a murine model of adult T-cell leukemia with the alpha-emitting radionuclide, bismuth 213.* Blood, 2002. **100**(1): p. 208-16.
5. Karacay, H., et al., *Pretargeting for cancer radioimmunotherapy with bispecific antibodies: role of the bispecific antibody's valency for the tumor target antigen.* Bioconjug Chem, 2002. **13**(5): p. 1054-70.
6. Lewis, M.R., et al., *An improved method for conjugating monoclonal antibodies with N-hydroxysulfosuccinimidyl DOTA.* Bioconjug Chem, 2001. **12**(2): p. 320-4.
7. Keire, D.A. and M. Kobayashi, *NMR studies of the metal-loading kinetics and acid-base chemistry of DOTA and butylamide-DOTA.* Bioconjug Chem, 1999. **10**(3): p. 454-63.
8. Tsai, S.W., et al., *Metabolism and renal clearance of 111In-labeled DOTA-conjugated antibody fragments.* Bioconjug Chem, 2001. **12**(2): p. 264-70.
9. Goodwin, D.A., et al., *Pharmacokinetics of pretargeted monoclonal antibody 2D12.5 and 88Y-Janus-2-(p-nitrobenzyl)-1,4,7,10-tetraazacyclododecanetetraacetic acid (DOTA) in BALB/c mice with KHJJ mouse adenocarcinoma: a model for 90Y radioimmunotherapy.* Cancer Res, 1994. **54**(22): p. 5937-46.
10. Corneillie, T.M., A.J. Fisher, and C.F. Meares, *Crystal structures of two complexes of the rare-earth-DOTA-binding antibody 2D12.5: ligand generality from a chiral system.* J Am Chem Soc, 2003. **125**(49): p. 15039-48.
11. Corneillie, T.M., et al., *A rare earth-DOTA-binding antibody: probe properties and binding affinity across the lanthanide series.* J Am Chem Soc, 2003. **125**(12): p. 3436-7.
12. Boder, E.T., K.S. Midelfort, and K.D. Wittrup, *Directed evolution of antibody fragments with monovalent femtomolar antigen-binding affinity.* Proc Natl Acad Sci U S A, 2000. **97**(20): p. 10701-5.
13. Colby, D.W., et al., *Development of a human light chain variable domain (V(L)) intracellular antibody specific for the amino terminus of huntingtin via yeast surface display.* J Mol Biol, 2004. **342**(3): p. 901-12.
14. Feldhaus, M.J., et al., *Flow-cytometric isolation of human antibodies from a nonimmune Saccharomyces cerevisiae surface display library.* Nat Biotechnol, 2003. **21**(2): p. 163-70.
15. Boder, E.T. and K.D. Wittrup, *Optimal screening of surface-displayed polypeptide libraries.* Biotechnol Prog, 1998. **14**(1): p. 55-62.
16. Peelle, B.R., et al., *Probing the interface between biomolecules and inorganic materials using yeast surface display and genetic engineering.* Acta Biomater, 2005. **1**(2): p. 145-54.
17. Peelle, B.R., et al., *Design criteria for engineering inorganic material-specific peptides.* Langmuir, 2005. **21**(15): p. 6929-33.
18. Ugur, O., et al., *Ga-66 labeled somatostatin analogue DOTA-DPhe1-Tyr3-octreotide as a potential agent for positron emission tomography imaging and*

receptor mediated internal radiotherapy of somatostatin receptor positive tumors. Nucl Med Biol, 2002. **29**(2): p. 147-57.

19. Siegel, R.W., et al., *High efficiency recovery and epitope-specific sorting of an scFv yeast display library.* J Immunol Methods, 2004. **286**(1-2): p. 141-53.
20. Boder, E.T. and K.D. Wittrup, *Yeast surface display for screening combinatorial polypeptide libraries.* Nat Biotechnol, 1997. **15**(6): p. 553-7.
21. Swers, J.S., B.A. Kellogg, and K.D. Wittrup, *Shuffled antibody libraries created by in vivo homologous recombination and yeast surface display.* Nucleic Acids Res, 2004. **32**(3): p. e36.
22. de Wildt, R.M., et al., *Heavy chain CDR3 optimization of a germline encoded recombinant antibody fragment predisposed to bind the U1A protein.* Protein Eng, 1997. **10**(7): p. 835-41.
23. Marks, K.M., M. Rosinov, and G.P. Nolan, *In vivo targeting of organic calcium sensors via genetically selected peptides.* Chem Biol, 2004. **11**(3): p. 347-56.
24. Heppeler, A., et al., *Radiometal-labelled macrocyclic chelator-derivatised somatostatin analogue with superb tumour-targeting properties and potential for receptor-mediated internal radiotherapy.* Chemistry-a European Journal, 1999. **5**(7): p. 1974-1981.

Chapter 4: The application of asymptotically optimal probability estimation to protein engineering

In protein engineering, it is very desirable for a researcher to be able to estimate the number of clones in an enriched population of protein clones with specific desirable properties, and to be able to determine how many clones must be characterized in order to discover all unique clones within the population. Asymptotically optimal probability estimation provides us with a tool that can be used to accurately estimate the total number of unique elements (including unseen elements) from a small sample of data. We have combined asymptotically optimal probability estimation with numerical bootstrapping and non-linear curve fitting to make accurate predictions of the actual diversity of populations with different types of underlying probability distributions. The advantages and limitations of this method are discussed with a focus on practical, protein engineering applications.

4.1 Introduction

In display-based protein engineering, proteins are interest are physically linked to their genotypes. This is typically accomplished by expressing the protein on the surface of an organism (such as phage [1] or yeast [2]) containing the gene coding for the protein, but it can also be accomplished by physically linking the mRNA that codes for the protein to the expressed protein itself [3]. Typically, large libraries of proteins are designed and constructed with the goal of selecting a particular clone with desirable properties from the library. These libraries can either be based upon an existing wild-type protein that needs to be improved in some way, or the library can be nonimmune,

meaning that it is not derived from any particular clone, nor is it biased towards a particular sequence or family of sequences.

Once a library of candidate proteins has been assembled, constructed and displayed – no small task in and of itself [4] – it is necessary to screen the library to identify clones with desirable properties such as improved affinity, stability, or catalytic activity. For yeast surface-displayed libraries, this is accomplished by flow activated cell sorting (FACS); for phage and ribosome/RNA display, physical panning is used. In a typical screening process, several rounds of enrichment for desirable clones are performed. After the first round (in which the unscreened library is screened), selected clones are amplified and subjected to further rounds of screening, often under increasingly stringent conditions. The goal of these further rounds of screening is to amplify and isolate the most desirable clones within the library.

After multiple rounds of screening, a successful screening process will yield a highly enriched population of improved protein clones. From a starting library size of 10^6-10^{12}, a small number (perhaps 10-1000) of the very best clones will have been isolated. Given the time, effort and financial resources that have been invested into the library creation and selection process, it is in the best interest of the researcher to know as much as possible about this pool of improved proteins. In addition, it is useful to isolate as many of the clones within the pool as possible, as individual clones may possess desirable properties other than the one screened for that might make them more or less favorable for whatever final application they are intended. For example, antibodies that bind with very high affinity to a particular target might have different association and dissociation rates, thermostabilities, or isoelectric points. Some might have more

potentially immunogenic amino acid changes from germline, and some might be easier to produce in large quantities. For all of these reasons, it is very desirable for a protein engineer to be able to both estimate the number of clones in an enriched population, and then isolate as many of those clones as possible.

The current method for estimating the total underlying diversity of an enriched population has been used for thousands of years in a wide range of human pursuits: it is guessing. A protein engineer knows that there cannot be more clones in the population that the number of phage or yeast collected in the last round of enrichment, but this upper bound is typically in the tens of thousands, if not higher. Some basic deduction can be performed: for example, if 20 clones are sequenced and all are unique, then the diversity of the enriched population is likely "high". Similarly, if 20 clones are sequenced and only 2 unique clones are identified, the underlying diversity is probably "low". However, more complicated intermediate situations will defy even the most ingenious researcher's intuition. This is not surprising – estimating the probability distribution, including unseen elements, from an incomplete sample set of data is a difficult task. Fortunately, mathematical tools called asymptotically optimal probability estimators have been developed to address precisely such a problem.

Probability estimators, which estimate a probability distribution – including unseen elements – from a sample of data, were first studied by Laplace [5], and improved upon substantially by Good [6] and Turing, who used probability estimation to crack German cryptography codes during World War II. Any probability estimator takes as input a sample of data from a population, and associates with that sample a probability over the set of unique elements in the sample, plus "new" (as yet unseen elements).

Recently, Orlitsky and co-workers developed a metric (called attenuation) to mathematically assess the performance of different probability estimators [7]. This advance allowed them to devise new asymptotically optimal estimators. In this context, asymptotically optimal means that as more data is sampled, the estimators do not underestimate the probability of any particular sequence of selected elements. This is a property that the best previous estimator, developed by Good and Turing, does not possess.

We propose to apply the mathematical tool of asymptotically optimal probability estimation to the problem of diversity estimation that is constantly encountered in protein engineering. Asymptotically optimal probability estimation is ideal for situations in which the number of possible elements in large in relation to the sample size, and this is often the case in protein engineering. Orlitsky and co-workers developed two different asymptotically optimal estimators, referred to as the 2/3 and 1/2 estimators. While the 1/2 estimator is mathematically more optimal, it is more complex to implement and requires a rapidly increasing number of mathematical operations as the number of elements in a sample increases, to the extent that running an estimator program based on the 1/2 estimator would very likely overwhelm the processor and memory capacities of modern personal computers. For this reason, the 2/3 estimator, which is computationally more efficient and requires only a constant number of operations per unique element, is used throughout. For comparison's sake, we have also employed the Good-Turing estimator and a modified add-one estimator as they are defined by Orlitsky and co-workers.

4.2 Modeling Methods

The modified add-one, Good-Turing and Orlitsky 2/3 estimators as defined by Orlitsky and co-workers [7] were implemented in MATLAB. In this work, we will adopt terminology used by Orlitsky and co-workers. A sample drawn from a population is a pattern. Each item drawn to form the pattern is an element. Each unique element in a pattern or population is a symbol. The multiplicity of a symbol is the number of times it appears in a pattern. For the example, the sequence *abacaca* is a pattern with seven elements and three symbols, and the multiplicities of a, b and c are 4, 1 and 2, respectively. Finally, we add the following term: the diversity of a population is the number (actual or predicted) of symbols in the population.

All populations used for these simulations have an actual diversity of 100. Three different probability distributions were used to generate patterns: uniform, normal with a variance of 10, and dominant. In the dominant distribution, one symbol occurs 40% of the time, and the remaining 60% of the probability is uniformly distributed among the remaining 99 symbols. The dominant distribution is considered because it is a situation which sometimes arises in protein engineering contexts.

4.2.1 Numerical bootstrapping of estimates

Numerical bootstrapping is a method for estimating distribution properties (such as mean, standard deviation or confidence intervals) of the result of an algorithm applied to a set of data [8]. In our case, for each pattern selected, an estimator will generate a single estimate of the underlying diversity of the population from which the pattern was sampled. Numerical bootstrapping assumes that the data in the pattern approximately

represents the actual population, and then resamples the data in the pattern to estimate the mean (and other statistics) of the diversity estimate for that particular pattern.

The mean bootstrapped diversity estimate for a particular pattern and estimator combination was calculated as follows: the pattern was resampled with replacement to generate 250 resampled patterns. From each of these patterns, the diversity was estimated using the estimator of interest. The mean and other statistical measures were calculated for this distribution of diversity estimates.

To determine the ideal resampling number (that is, the number of elements r selected with replacement from the n elements in the pattern; r can be less than, equal to, or greater than n), we calculated the mean bootstrapped diversity for a range of r/n ratios, while varying n as a proportion of the underlying diversity d. The analysis was performed for each of the three different types of probability distributions used.

4.3 Results

4.3.1 Evaluating accuracy of estimators

To test the accuracy of the three estimators considered, patterns of size n were drawn from populations with uniform, normal and dominant distributions. For each pattern, each estimator was used to estimate the underlying diversity of the population being sampled. The mean diversity predicted averaged over 500 patterns was plotted against the varying pattern size n for each estimator/distribution combination, as shown in Figs. 4.1, 4.2 and 4.3.

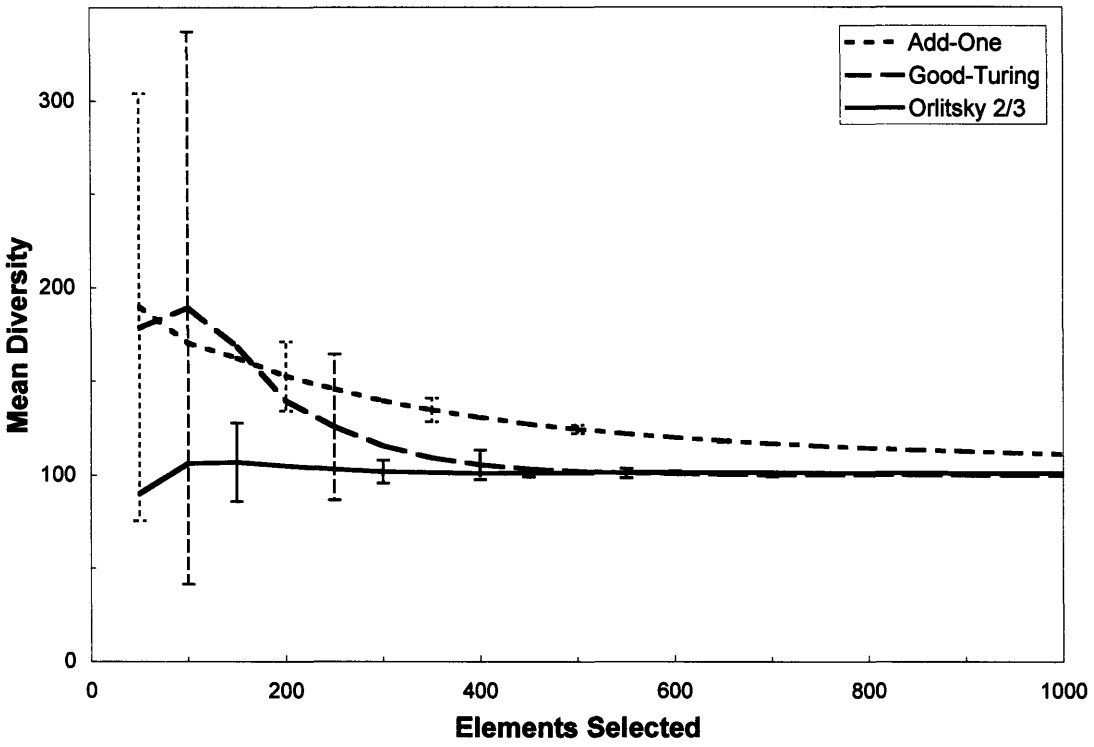

Figure 4.1. Mean diversity vs. number of elements in pattern, uniform distribution. Underlying diversity = 100. Number of unique elements drawn after 1000 = 100. Each point is the average of 500 runs. Error bars are 2 σ, and are shown for every third point in each curve for clarity.

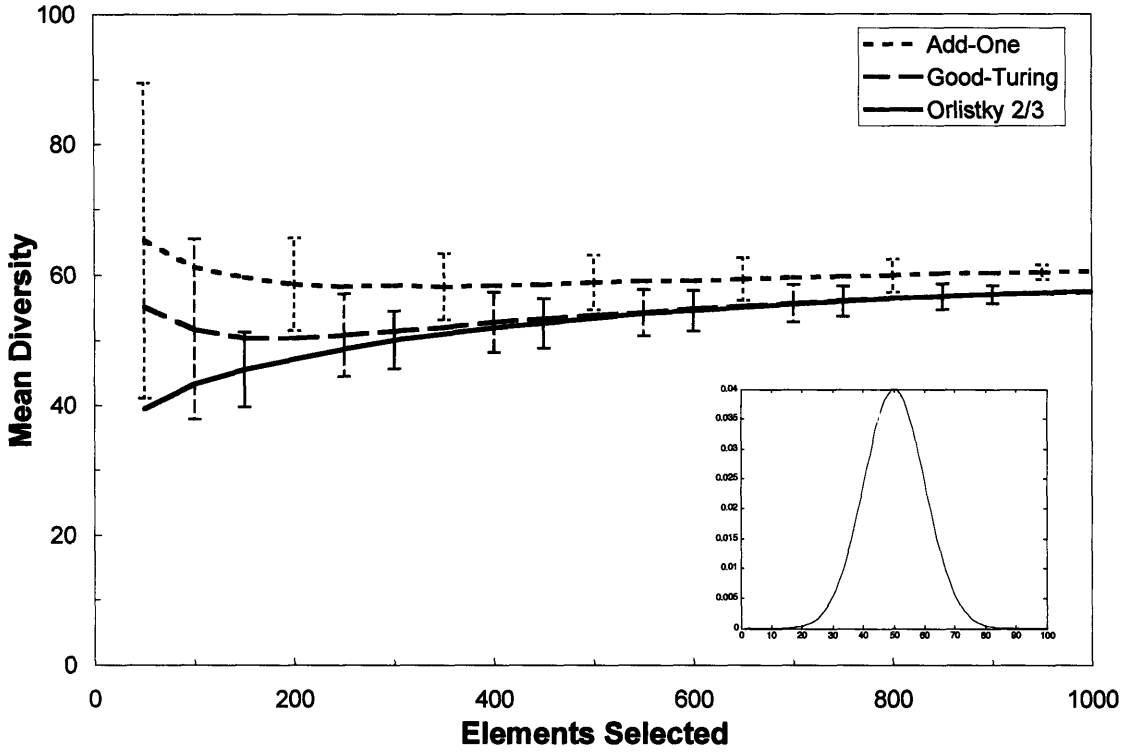

Figure 4.2. Mean diversity vs. number of elements in pattern, normal distribution, variance = 10 (as shown in the inset). Underlying diversity = 100. Number of unique elements drawn after 1000 = 57. Each point is the average of 500 runs. Error bars are 2σ, and are shown for every third point in each curve for clarity.

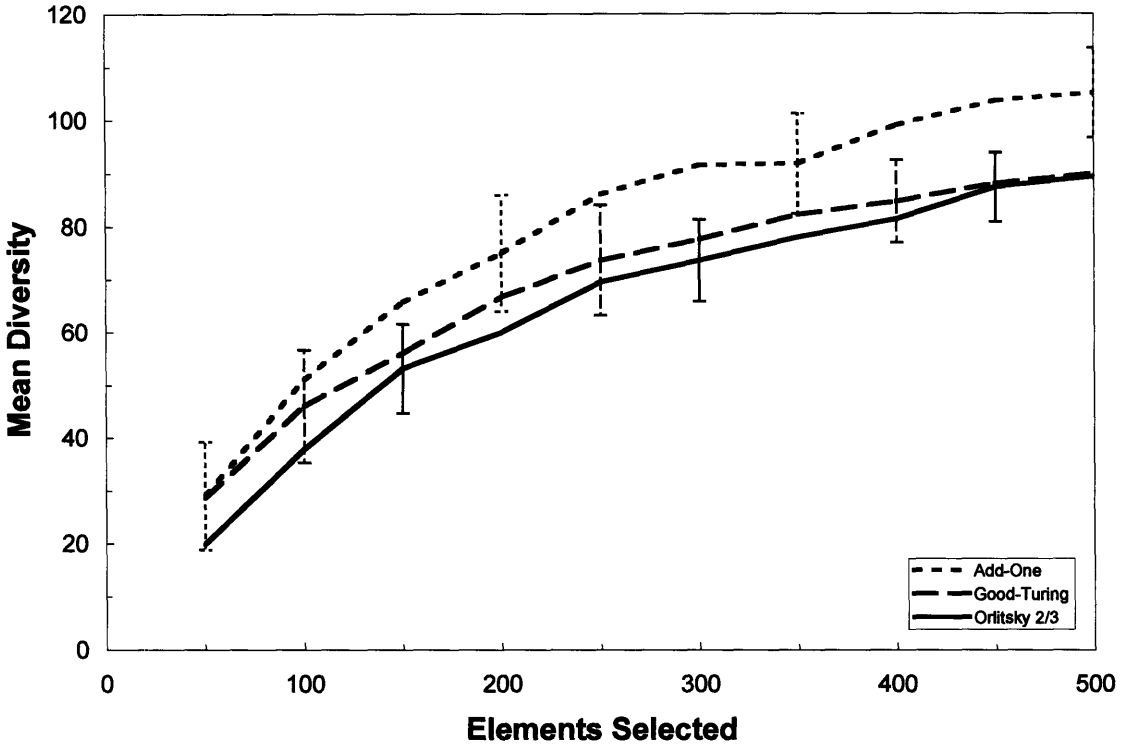

Figure 4.3. Mean diversity vs. number of elements in pattern, dominant distribution. Underlying diversity = 100. Each point is the average of 500 runs. Error bars are 2σ, and are shown for every third point in each curve for clarity.

As shown in Fig. 4.1, though both the Orlitsky 2/3 and Good-Turing estimators eventually hone in on the actual underlying diversity, the Orlitsky estimator approaches it much more quickly, and with a smaller variance. In Fig. 4.2, the results are quantitatively different. An underlying normal distribution with a variance of 10 means that an extremely large number of elements will need to be sampled to discover all 100 unique elements in the underlying population. The estimators reflect this reality, and converge on the number of elements that are accessible to them in patterns of reasonable size. Note that after 1000 elements have been sampled, on average only 57 unique elements have been discovered. In Fig. 4.3, the accuracy of the estimators in estimating the diversity of dominant distributions is demonstrated. For the dominant situation, the

diversity predicted by the estimators rises in conjunction with the number of unique elements discovered.

4.3.2 Numerical bootstrapping of estimates

To determine an ideal resampling ratio r/n for numerical bootstrapping, we calculated the mean bootstrapped diversity (averaged over three randomly selected patterns) for a range of r/n ratios, while varying n in proportion to the underlying diversity d. This analysis was performed for the Orlitsky 2/3 and Good-Turing estimators each of the three different types of probability distributions used and is presented below in Fig. 4.4.

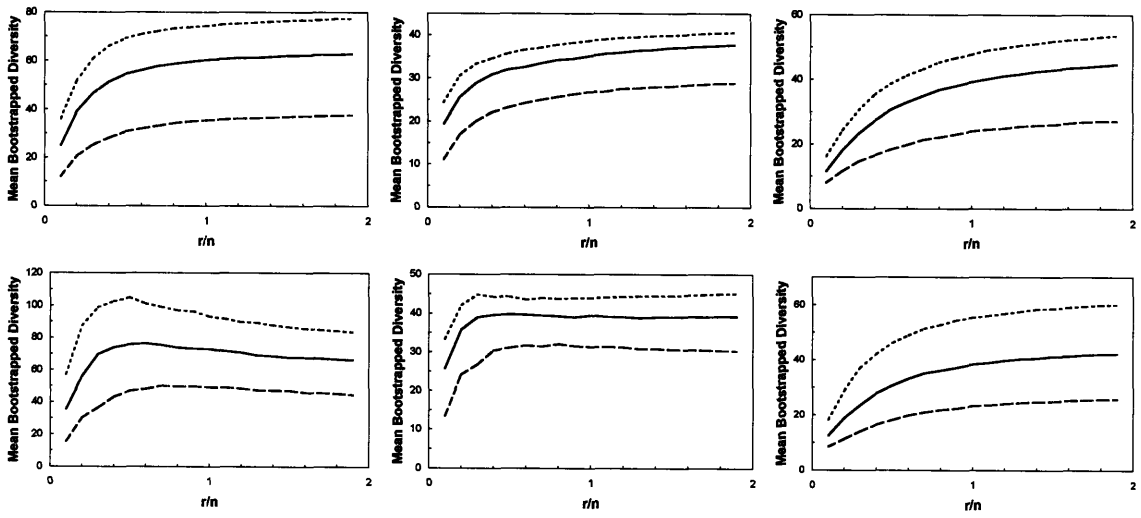

Figure 4.4. Determining the optimal resampling number for the Orlitsky 2/3 and Good-Turing estimators. The mean bootstrapped diversity is plotted as a function of r/n, where r is the number of elements selected with replacement from the n elements in the pattern for bootstrapping calculations. Top row, Orlitsky 2/3 estimator. Bottom row, Good-Turing estimator. Left column, uniform distribution. Center column, normal distribution (variance 10). Right column, dominant distribution. Dashed line, $n = 0.5d$ (where d is the actual underlying diversity); solid line, $n = d$; dotted line, $n = 1.5d$.

Based on the results in Fig. 4.4, a r/n ratio of 1 was selected for all bootstrapping calculations. This makes sense on an intuitive level, as well – the estimators will perform

most accurately when provided with all of the data in a pattern, but without artificially over-representing the selected elements during bootstrapping calculations (as would be the case if $r/n > 1$).

4.3.3 Making estimates from a single set of data

In order to be useful for research, asymptotically optimal probability estimation must be able to make good predictions of the underlying diversity of a population from a single, particular pattern. We calculated the bootstrapped diversity estimate, non-bootstrapped diversity estimate, and the number of symbols discovered for a particular pattern of increasing n, using each of the three different estimators. The results of these calculations for uniform underlying distributions are shown in Figs. 4.5, 4.6 and 4.7.

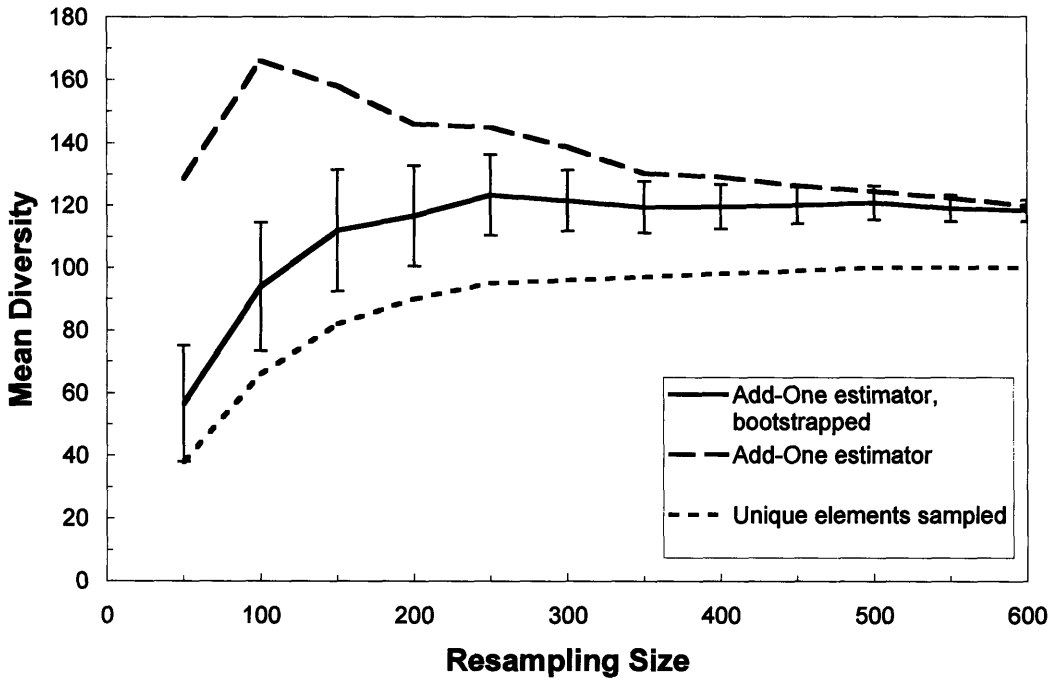

Fig 4.5. Convergence of bootstrapped diversity estimates using Add-One estimator. Resampling size = number of elements sampled. Uniform distribution, underlying diversity = 100. Error bars = 2σ.

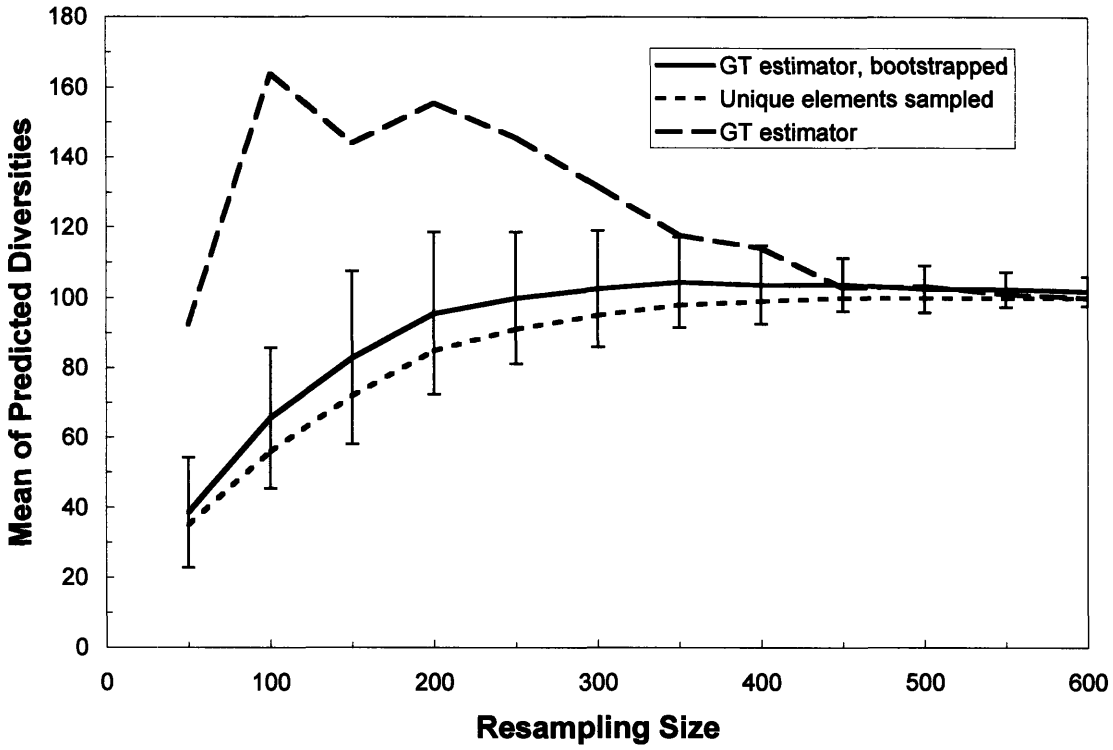

Fig 4.6. Convergence of bootstrapped diversity estimates using Good-Turing estimator. Resampling size = number of elements sampled. Uniform distribution, underlying diversity = 100. Error bars = 2σ.

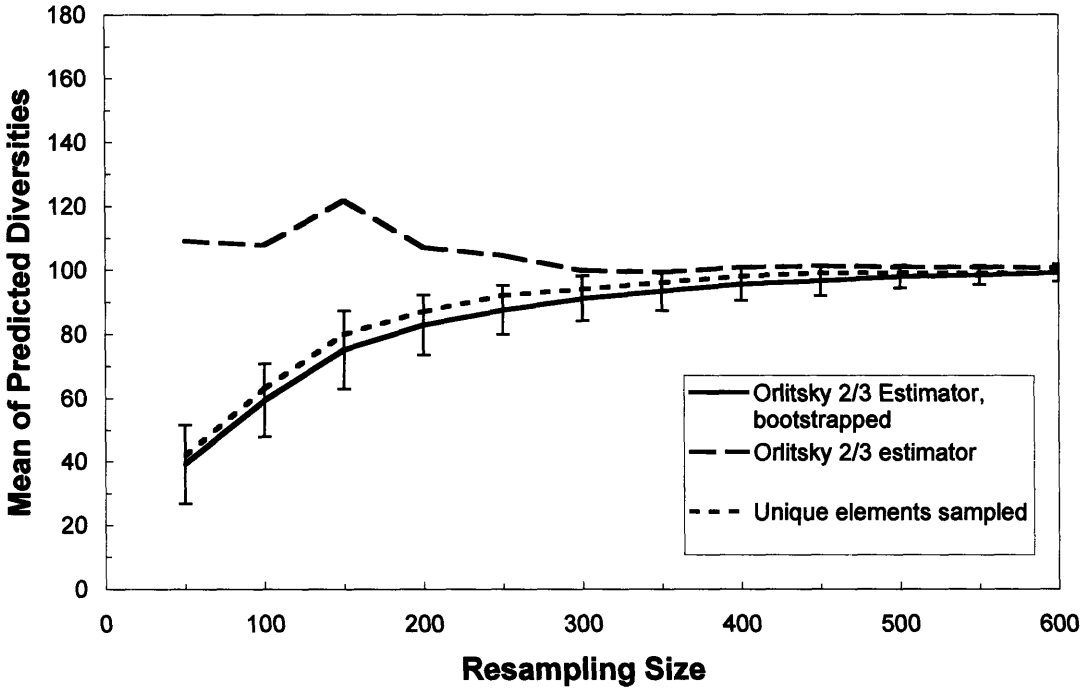

Fig 4.7. Convergence of bootstrapped diversity estimates using Orlitsky 2/3 estimator. Resampling size = number of elements sampled. Uniform distribution, underlying diversity = 100. Error bars = 2σ.

As shown in Fig. 4.5, while the modified Add-One estimator rapidly approaches the actual diversity of the population (100), it overshoots that value and converges on a mean diversity of roughly 120. The bootstrapped mean diversities predicted by the Good-Turing and Orlitsky 2/3 estimators, on the other hand, asymptotically approach the actual underlying diversity of the sampled population. Thus, numerical bootstrapping provides a means of transforming the somewhat erratic (but, as shown in Figs. 4.1, 4.2 and 4.3, on average accurate) predictions of the estimators into smooth, predictable curves that asymptotically approach the true diversity.

4.3.4 Estimating the underlying diversity by fitting estimator data

The data presented in Figs. 4.5, 4.6 and 4.7 shows the asymptotic progression of probability estimates as more elements are sampled in a particular pattern. Can we estimate the asymptotic value (the underlying actual diversity) before actually discovering all of the unique elements in the population? To accomplish this, a pattern of size n was selected from a uniform distribution, and the mean bootstrapped diversity was predicted, as indicated by the X on Fig. 4.8. Next, the preceding part of the asymptotic curve was calculated by drawing subsets of the selected pattern without replacement, and calculating the mean bootstrapped diversity at each fraction of n, as indicated by the empty squares. Finally, this data was fitted using a non-linear least squares method to an equation of the form $f(n) = A(1-e^{-mn})$, where A is the asymptotic value of the mean bootstrapped diversity and m is a coefficient related to how quickly the curve is approaching the asymptote. The coefficient m can be used to calculate how many additional elements must be drawn in order to discover all (or, some arbitrary percentage thereof) of the unique elements in the population.

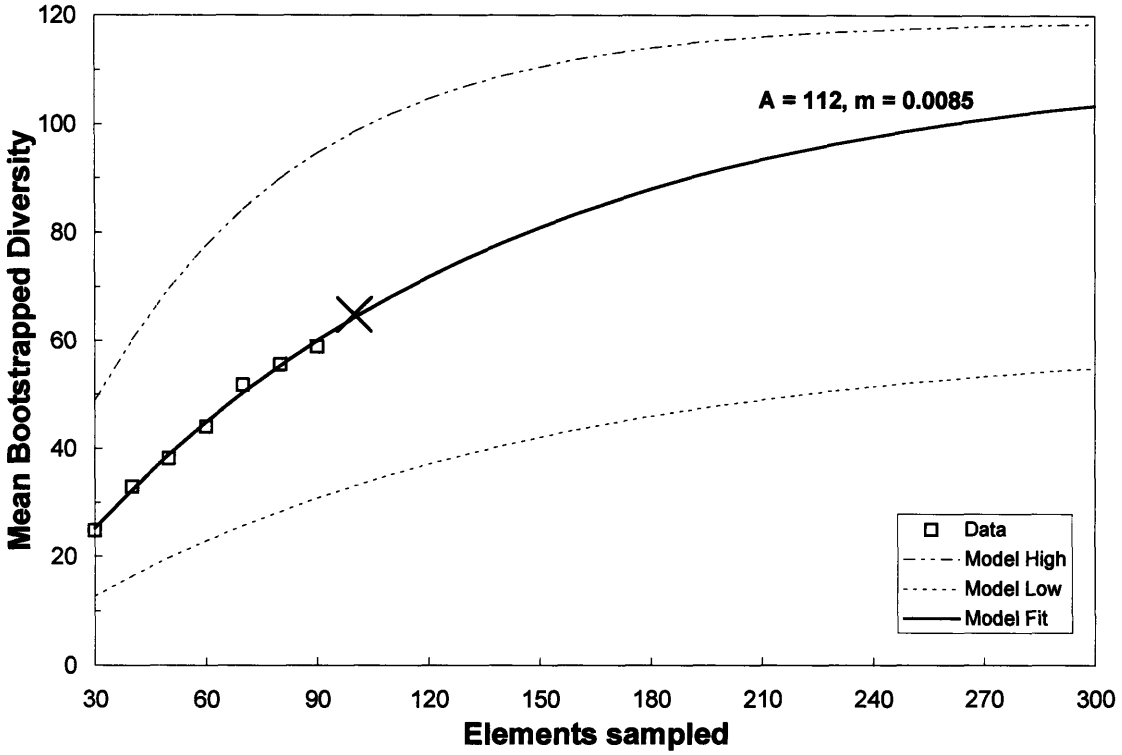

Figure 4.8. Estimating underlying diversity from a single sample by fitting estimator data. A pattern of 100 elements containing 70 unique elements was randomly selected from a uniformly distributed population with underlying diversity of 100. The mean bootstrapped diversity estimate was calculated using the Orlitsky 2/3 estimator for 30, 40, ... 90, and 100 elements from the pattern (drawn without replacement and averaged over three selections), and that data was fitted to an equation of the form $f(n) = A(1-e^{-mn})$. Highest possible and lowest possible curves are also plotted based on 95% confidence interval values for A and m.

In Fig. 4.8, while only 70 unique elements from the actual 100 have been selected, this method predicts a diversity of 112, which is reasonably close to the actual value. Furthermore, this method is generalizable to other underlying distributions, and the predicted diversity improves as more elements are sampled. A summary of the results from other probability distributions is presented in Table 4.1.

Uniform	Unique elements in pattern	Predicted diversity
$n = 100$	70	112
$n = 200$	87	94
$n = 300$	96	95
Normal		
$n = 100$	35	35
$n = 200$	40	38
$n = 300$	45	43
Dominant		
$n = 100$	50	82
$n = 200$	76	91
$n = 300$	87	94

Table 4.1. Performance of Orlitsky 2/3-based diversity estimation for different underlying probability distributions. *n* is the number of elements selected.

As shown in Table 4.1, the diversity estimation algorithm employed here – in which bootstrapped mean diversity estimates are fitted to an exponential function to estimate the actual underlying diversity – gets closer to the actual underlying diversity (which, here, is always 100) with the addition of additional data. The attentive observer will note that in some situations, such as for $n = 300$, uniform distribution and $n = 200$ or 300, normal distribution, the estimated diversity is less than the actual number of unique elements in the pattern. Obviously, the actual diversity must be at least equal to the number of unique elements in the selected pattern, so these results are artifacts of the fitting function. However, for uniform and dominant distributions, they are useful artifacts – when the predicted diversity is approximately equal to (or even slightly less than) the unique number of elements in the pattern, nearly all of the elements in the population have been sampled.

Populations with normal distributions present a different situation, however. For normal distributions with tight variances (such as used here), a very large number of elements will have to be drawn before all of the unique elements in the population are

discovered. As a result, the diversity estimation method employed here significantly underestimates the underlying diversity of the population, simply because it (and the researchers selecting the elements) cannot gain access to the majority of the necessary information without drawing extremely large numbers of elements. It is in the interest of any user of this algorithm to perform a statistical analysis on their selected data to determine if the underlying probability distribution is uniform, normal, dominant, or some intermediate distribution, as this will aid in interpreting the diversity estimation results.

4.4 Conclusions & Discussion

We have developed a method for estimating the underlying diversity of a population based on an incomplete sample set of data from that population. The method combines the numerical methods of asymptotic probability estimation, numerical bootstrapping and non-linear least squares fitting to predict the diversity of a population with reasonable accuracy. While the method at times returns artifactual results, it is far more accurate and informative than guessing, the method currently used to tackle this problem. We expect that this method will be useful for protein engineers in interpreting their own screening results, and the code and executable programs associated with this algorithm will be posted online so that they can be used by other researchers.

The diversity estimation method employed here performs best (that is, it correctly estimates the underlying diversity of a population with the smallest amount of data) for populations that have uniform distributions of symbols. It also performs quite well for dominant distributions, in which one symbol represents a large fraction of the elements in

the population, but the other symbols are uniformly distributed. However, this method does not perform very well for normal distributions with narrow variances, since in this situation some symbols are so overrepresented in selected patterns that it is very difficult to ever see most of the symbols in the population. For these reasons, it will be very useful for researchers using the algorithm to determine the expected or actual type of probability distribution in the population, as this will aid significantly in interpreting the results of this method.

Future work on this method will aim to incorporate additional statistical analysis of the pattern submitted (for example, to determine if it is roughly uniform or normal, as discussed above), and to alter the algorithms used so that the method does not return nonsensical results (such as predicting a diversity less than the unique number of elements already discovered under certain circumstances). Even in its present form, however, this diversity estimation method should be of substantial practical use to working protein scientists.

4.5 Works Cited

1. Paschke, M., *Phage display systems and their applications*. Appl Microbiol Biotechnol, 2006. **70**(1): p. 2-11.
2. Boder, E.T. and K.D. Wittrup, *Yeast surface display for screening combinatorial polypeptide libraries*. Nat Biotechnol, 1997. **15**(6): p. 553-7.
3. Rothe, A., R.J. Hosse, and B.E. Power, *Ribosome display for improved biotherapeutic molecules*. Expert Opin Biol Ther, 2006. **6**(2): p. 177-87.
4. Feldhaus, M.J., et al., *Flow-cytometric isolation of human antibodies from a nonimmune Saccharomyces cerevisiae surface display library*. Nat Biotechnol, 2003. **21**(2): p. 163-70.
5. Laplace, P., *Philosophical Essays on Probabilities (A. I. Dale, transl. from ed. 5, 1825)*. 1995, New York: Springer-Verlag.
6. Good, I., *The population frequencies of species and the estimation of population parameters*. Biometrika, 1953. **40**: p. 237.

7. Orlitsky, A., N.P. Santhanam, and J. Zhang, *Always Good Turing: asymptotically optimal probability estimation.* Science, 2003. **302**(5644): p. 427-31.
8. Efron, B.a.T., *An Introduction to the Bootstrap.* 1993, New York: Chapman and Hall.

Chapter 5: Construction, production and characterization of an anti-CEA, anti-fluorescein single-chain bispecific diabody

An anti-CEA, anti-fluorescein single-chain bispecific diabody was designed based on the variable domains of anti-CEA scFv sm3E and anti-fluorescein scFv 4M5.3. The diabody was secreted in *S. cerevisiae*, and purified using anti-FLAG affinity chromatography and size exclusion chromatography, for a final yield of 80 μg / L. The full-length diabody (55 kDa) binds CEA expressed on the surface of colorectal cancer-derived SW1222 cells with an a K_d of 4.3 ± 2.5 nM, and also binds fluorescein while bound to CEA on the cell surface. This novel reagent should be useful for future PRIT preclinical studies, and as a framework for even better PRIT targeting agents.

5.1 Introduction

Faced with the inability to isolate high-affinity Ga-DOTA-biotin binders that could be used as the hapten-specific part of a bispecific targeting agent for PRIT, we considered alternative approaches. We proposed to take advantage of an existing extremely high-affinity scFv (4M5.3) against fluorescein [1, 2] to construct a bispecific target agent that could be used to deliver any radioisotope desired in a PRIT setting. In this approach, the hapten-specific part of the bispecific target agent binds fluorescein with very high affinity, and the radioisotope of choice is conjugated to the fluorescein molecule.

While this approach was conceived as an alternative to a hapten-binding part of the targeting agent that binds directly to the metal chelate, it actually has several advantages over the direct-binding approach. First, the method is generic with respect to

metal chelate conjugated and radioisotope loaded. It appears from other researchers' work [3, 4] and our own results (see Chapter 4) that the binding of anti-metal-chelate antibodies is dependent on the metal loaded into the chelate. While this specificity is impressive and scientifically interesting, it is not necessarily advantageous – it potentially requires that a new antibody be isolated, engineered, charaterized and approved for each different radioisotope proposed for use in PRIT or pretargeted imaging. By using a fluorescein-binding antibody as the hapten-binding half of the targeting agent, a single targeting agent can be used to deliver many different radioisotopes, and conceivably other types of cytotoxic payloads.

The second advantage of using fluorescein binding to link bispecific and hapten is that fluorescein-tetramethylrhodamine (TMR) bifluorophores have been developed that have altered fluorescent properties in the presence of fluorescein-binding proteins [5]. Fluorescein and TMR are structurally similar, and when conjugated to each other a ring-stacking interaction leads to a substantial decrease in the fluorescence of both dyes. However, in the presence of fluorescein-binding proteins this interaction is disrupted, and TMR recovers its normal fluorescent properties. As a result, these bifluorophores can be used as molecular reporters for the presence of fluorescein-binding proteins. We anticipate that these molecules may be extremely useful in *in vitro* cell spheroid imaging studies, since they can be used to pinpoint the location of not just hapten, but of hapten-bispecific complexes.

After deciding to pursue an anti-CEA, anti-fluorescein bispecific targeting agent, it was necessary to decide on a molecular format for protein. A wide variety of antibody-fragment based molecular formats are available for the synthesis of a bispecific agent,

including conjugated scFvs [6], non-covalent diabodies [7, 8], single-chain diabodies [8], and more exotic constructions such as triabodies and larger fusion proteins [9]. A targeting agent with molecule weight just higher that the 50 kD molecular weight cutoff was considered ideal, since such a targeting agent would avoid very rapid clearance from the plasma, but would not be hindered in tumor penetration by the low diffusivity of a higher molecular weight protein such as a full IgG. This molecular weight requirement ruled out larger fusion proteins and non-covalent combinations such as triabodies and tetrabodies. Single-chain diabodies were selected as an ideal diabody format, as post-expression conjugation of scFvs and covalently-formed diabodies between co-secreted molecules both suffer from heterogeneity in protein formulations, which is a problem both in pre-clinical development and a potential problem further down the drug development pipeline. Single-chain diabodies had previously only been secreted in *E. coli*, but the ability of *S. cerevisiae* to secrete complex, multi-domain heterologous proteins [10, 11] suggested that it would be possible to secrete single-chain diabodies from yeast.

5.2 Methods

5.2.1 Single-chain bispecific diabody gene synthesis

Single-chain diabodies are composed of four variable domains in the following order: V_H^1-L10-V_L^2-LL-V_H^2-L10-V_L^1, where V_H^1 and V_L^1 are the variable domains of a particular scFv, V_H^2 and V_L^2 are the variable domains of another, and L10 and LL are linker regions with the amino acid sequences AKTTPKLGGL and

RADAAAAGGGGSGGGGSGGGG, respectively. Initially, we had intended for the diabody to bind directly to the metal chelate hapten Ga-DOTA-biotin and the cancer-specific protein antigen CEA. The diabody was therefore designed with V_H^1 and V_L^1 regions taken from the best available anti-Ga-DOTA-biotin clone at the time, clone 17. V_H^2 and V_L^2 were taken from sm3E, a high-affinity scFv previously developed against CEA [12].

The variable domains from clone 17 and sm3E were amplified via PCR, and then assembled in two steps. First, overlap extension PCR was used to construct V_H^1-L10-V_L^2-LL and LL-V_H^2-L10-V_L^1 fragments [13], and then those two fragments were combined into the desired gene by utilizing homologous recombination in yeast [14]. The initial annotated sequence of the single-chain diabody gene is shown below as Figure 5.1.

```
Nhe I 17 VH
A  S  Q  V  Q  L  Q  E  S  G  P  G  L  V  K  P  S  E  T  L  S  L  T  C  T  V
GCTAGCCAGGTGCAGCTGCAGGAGTCCGGCCCAGGACTGGTGAAGCCTTCGGAGACCCTGTCCCTCACGTGCACTGTC
S  G  H  S  I  N  D  Y  Y  W  S  W  I  R  Q  P  P  G  K  G  L  E  W  I  G  Y
TCTGGTCACTCCATCAATGACTACTACTGGAGTTGGATTCGGCAGCCCCCAGGGAAGGGACTGGAGTGGATTGGGTAT
I  K  N  S  G  S  R  N  Y  N  P  S  L  K  S  R  V  T  I  S  V  D  P  S  K  N
ATCAAAAACAGTGGGAGCAGAAACTACAATCCCTCCCTCAAGAGTCGAGTCACCATATCTGTTGACCCGTCCAAGAAC
Q  F  S  L  K  L  T  S  G  T  A  A  D  T  A  V  Y  Y  C  A  R  G  I  A  A  S
CAGTTCTCCCTGAAACTGACCTCTGGGACCGCTGCGGACACGGCCGTGTATTACTGTGCGAGGGGTATAGCAGCATCT
                                                                L10
G  T  E  N  P  W  G  Q  G  T  L  V  T  V  S  S  G  I  L  G  L  S  A  K  T  T
GGTACCGAAAACCCCTGGGGCCAGGGAACCCTGGTCACCGTCTCCTCAGGAATTCTAGGGTTAAGTGCTAAAACTACT
              Avr II sm3E VL
P  K  L  G  G  L  G  E  N  V  L  T  Q  S  P  S  S  M  S  V  S  V  G  D  R  V
CCAAAATTAGGTGGCCTAGGTGAAAATGTGCTGACCCAATCTCCAAGCTCCATGTCTGTTTCTGTTGGCGATAGAGTA
T  I  A  C  S  A  S  S  S  V  P  Y  M  H  W  L  Q  Q  K  P  G  K  S  P  K  L
ACCATCGCTTGTAGCGCATCCTCTAGTGTCCCATATATGCACTGGCTTCAACAGAAGCCAGGTAAAAGCCCAAAGTTG
L  I  Y  L  T  S  N  L  A  S  G  V  P  S  R  F  S  G  S  G  S  G  T  D  Y  S
TTGATTTATTTGACATCCAACTTGGCTTCTGGAGTGCCTTCAAGGTTTTCTGGTTCCGGCTCAGGAACCGATTATAGT
L  T  I  S  S  V  Q  P  E  D  A  A  T  Y  Y  C  Q  Q  R  S  S  Y  P  L  T  F
TTGACTATTAGCTCAGTGCAGCCAGAGGATGCTGCAACCTACTATTGCCAGCAAAGGTCCTCATATCCACTGACTTTC
                                        Aat II LL
G  G  G  T  K  L  E  I  K  A  A  A  G  S  T  S  R  A  D  A  A  A  A  G  G  G
```

```
GGGGGTGGAACGAAGTTGGAAATCAAGGCTGCAGCCGGATCGACGTCAAGAGCTGATGCTGCTGCTGCTGGTGGTGGT
                                  Mlu I  sm3E VH
G  S  G  G  G  G  S  G  G  G  G  S  R  V  Q  V  K  L  E  Q  S  G  A  E  V  V
GGTTCTGGTGGTGGTGGTTCTGGTGGTGGTGGTTCACGCGTTCAAGTTAAACTGGAACAGTCCGGTGCTGAAGTTGTC

K  P  G  A  S  V  K  L  S  C  K  A  S  G  F  N  I  K  D  S  Y  M  H  W  L  R
AAACCAGGTGCTTCCGTGAAGTTGTCCTGTAAAGCCTCTGGTTTTAACATCAAGGATTCGTATATGCATTGGTTGAGA
Q  G  P  G  Q  R  L  E  W  I  G  W  I  D  P  E  N  G  D  T  E  Y  A  P  K  F
CAAGGGCCAGGACAAAGATTGGAATGGATTGGCTGGATTGATCCAGAGAATGGTGATACCGAGTACGCTCCTAAATTT
Q  G  K  A  T  F  T  T  D  T  S  A  N  T  A  Y  L  G  L  S  S  L  R  P  E  D
CAGGGAAAGGCTACTTTTACTACCGACACTTCCGCTAATACCGCATACTTGGGCTTATCTTCCTTGAGACCAGAGGAC
T  A  V  Y  Y  C  N  E  G  T  P  T  G  P  Y  Y  F  D  Y  W  G  Q  G  T  L  V
ACTGCCGTATACTACTGCAACGAAGGGACACCAACTGGTCCTTACTATTTCGACTACTGGGGACAAGGTACCTTAGTT
            Nar I L10                          Sph I   17 VL
T  V  S  S  G  A  S  A  K  T  T  P  K  L  G  G  M  L  E  I  V  L  T  Q  S  P
ACTGTCTCTAGCGGCGCCTCTGCTAAAACTACTCCAAAATTAGGTGGCATGCTAGAAATTGTGTTGACACAGTCTCCA
A  T  L  S  V  S  P  G  E  R  A  T  L  S  C  R  A  S  Q  S  V  S  S  N  L  A
GCCACCCTGTCTGTGTCTCCAGGGGAAAGAGCCACCCTCTCCTGCAGGGCCAGTCAGAGTGTTAGCAGTAACTTAGCC
W  Y  Q  H  K  P  G  Q  A  P  R  L  L  I  S  G  S  S  S  R  A  T  G  I  P  D
TGGTACCAGCACAAACCTGGCCAGGCTCCCAGGCTCCTCATCTCTGGTTCATCCAGTAGGGCCACTGGCATCCCAGAC
R  F  S  G  S  G  S  G  T  D  F  T  L  T  I  S  R  L  E  P  E  D  F  A  V  Y
AGGTTCAGTGGCAGTGGGTCTGGGACAGACTTCACTCTCACCATCAGCAGACTGGAGCCTGAAGATTTTGCAGTGTAT
Y  C  Q  Q  Y  D  T  S  P  I  T  F  G  P  G  T  K  V  D  I  K  S  G  I  L  E
TACTGTCAGCAGTATGATACGTCACCGATCACTTTCGGCCCTGGGACCAAAGTGGATATCAAATCCGGAATTCTAGAA
      BamH I
Q  K  G  S
CAAAAGGGATCC
```

Figure 5.1 Annotated DNA and amino acid sequence of 3A-1C, a single-chain diabody composed of the variable regions of the anti-Ga-DOTA-biotin scFv 17 and the anti-CEA scFv CEA.

Because of difficulties in isolating high-affinity Ga-DOTA-biotin binders and the advantages of an alternative approach, we decided to design a bispecific molecule to bind to a fluorescein-based hapten, rather than directly to a radiometal chelate. This approach has the advantage of being generic – the same bispecific molecule can be used to deliver any radioisotope in almost any metal chelate without modification.

To implement this approach, we amplified the V_H and V_L regions of the anti-fluorescein scFv 4M5.3 [1] from an existing plasmid in the lab, and subcloned these

regions into the diabody construct shown in Fig. 5.1, in place of the anti-Ga-DOTA-biotin scFv 17. The resulting annotated DNA and amino acid sequence (referred to as 4sdb-1) is shown below as Fig. 5.2.

```
Nhe I   start 4M5.3 VH
A   S   G   G   V   K   L   D   E   T   G   G   G   L   V   Q   P   G   G   A
GCT AGC GGT GGC GTC AAA CTG GAT GAG ACT GGA GGA GGC TTG GTG CAA CCT GGG GGG GCC
M   K   L   S   C   V   T   S   G   F   T   F   G   H   Y   W   M   N   W   V
ATG AAA CTC TCC TGT GTT ACC TCT GGA TTC ACT TTT GGT CAC TAC TGG ATG AAC TGG GTC
R   Q   S   P   E   K   G   L   E   W   V   A   Q   F   R   N   K   P   Y   N
CGC CAG TCT CCA GAG AAA GGA CTG GAG TGG GTA GCA CAA TTT AGA AAC AAA CCT TAT AAT
Y   E   T   Y   Y   S   D   S   V   K   G   R   F   T   I   S   R   D   D   S
TAT GAA ACA TAT TAT TCA GAT TCT GTG AAA GGC AGA TTC ACC ATC TCA AGA GAT GAT TCC
K   S   S   V   Y   L   Q   M   N   N   L   R   V   E   D   T   G   I   Y   Y
AAA AGT AGT GTC TAT CTG CAA ATG AAC AAT TTA AGA GTT GAA GAC ACG GGT ATC TAT TAC
C   T   G   A   S   Y   G   M   E   Y   L   G   Q   G   T   S   V   T   V   S
TGT ACG GGT GCT TCC TAT GGT ATG GAA TAC TTG GGT CAA GGA ACC TCA GTC ACC GTC TCC
  Afl II    start L10                             Avr II    start sm3E VL
G   L   S   A   K   T   T   P   K   L   G   G   L   G   E   N   V   L   T   Q
GGC TTA AGT GCT AAA ACT ACT CCA AAA TTA GGT GGC CTA GGT GAA AAT GTG CTG ACC CAA
S   P   S   S   M   S   V   S   V   G   D   R   V   T   I   A   C   S   A   S
TCT CCA AGC TCC ATG TCT GTT TCT GTT GGC GAT AGA GTA ACC ATC GCT TGT AGC GCA TCC
S   S   V   P   Y   M   H   W   L   Q   Q   K   P   G   K   S   P   K   L   L
TCT AGT GTC CCA TAT ATG CAC TGG CTT CAA CAG AAG CCA GGT AAA AGC CCA AAG TTG TTG
I   Y   L   T   S   N   L   A   S   G   V   P   S   R   F   S   G   S   G   S
ATT TAT TTG ACA TCC AAC TTG GCT TCT GGA GTG CCT TCA AGG TTT TCT GGT TCC GGC TCA
G   T   D   Y   S   L   T   I   S   S   V   Q   P   E   D   A   A   T   Y   Y
GGA ACC GAT TAT AGT TTG ACT ATT AGC TCA GTG CAG CCA GAG GAT GCT GCA ACC TAC TAT
C   Q   Q   R   S   S   Y   P   L   T   F   G   G   G   T   K   L   E   I   K
TGC CAG CAA AGG TCC TCA TAT CCA CTG ACT TTC GGG GGT GGA ACG AAG TTG GAA ATC AAG
                  Aat II    start LL
A   A   A   G   S   T   S   R   A   D   A   A   A   A   G   G   G   G   S   G
GCT GCA GCC GGA TCG ACG TCT AGA GCT GAT GCT GCT GCT GCT GGT GGT GGT GGT TCT GGT
                                    Mlu I     start sm3E VH
G   G   G   S   G   G   G   G   S   R   V   Q   V   K   L   E   Q   S   G   A
GGT GGT GGT TCT GGT GGT GGT GGT TCA CGC GTT CAA GTT AAA CTG GAA CAG TCC GGT GCT
E   V   V   K   P   G   A   S   V   K   L   S   C   K   A   S   G   F   N   I
GAA GTT GTC AAA CCA GGT GCT TCC GTG AAG TTG TCC TGT AAA GCC TCT GGT TTT AAC ATC
K   D   S   Y   M   H   W   L   R   Q   G   P   G   Q   R   L   E   W   I   G
AAG GAT TCG TAT ATG CAT TGG TTG AGA CAA GGG CCA GGA CAA AGA TTG GAA TGG ATT GGC
W   I   D   P   E   N   G   D   T   E   Y   A   P   K   F   Q   G   K   A   T
TGG ATT GAT CCA GAG AAT GGT GAT ACC GAG TAC GCT CCT AAA TTT CAG GGA AAG GCT ACT
```

```
F   T   T   D   T   S   A   N   T   A   Y   L   G   L   S   S   L   R   P   E
TTT ACT ACC GAC ACT TCC GCT AAT ACC GCA TAC TTG GGC TTA TCT TCC TTG AGA CCA GAG
D   T   A   V   Y   Y   C   N   E   G   T   P   T   G   P   Y   Y   F   D   Y
GAC ACT GCC GTA TAC TAC TGC AAC GAA GGG ACA CCA ACT GGT CCT TAC TAT TTC GAC TAC
                                            Nar I       start L10
W   G   Q   G   T   L   V   T   V   S   S   G   A   S   A   K   T   T   P   K
TGG GGA CAA GGT ACC TTA GTT ACT GTC TCT AGC GGC GCC TCT GCT AAA ACT ACT CCA AAA
        Sph I       start 4M5.3 VL
L   G   G   M   L   D   V   V   M   T   Q   T   P   L   S   L   P   V   S   L
TTA GGT GGC ATG CTA GAC GTC GTT ATG ACT CAA ACA CCA CTA TCA CTT CCT GTT AGT CTA
G   D   Q   A   S   I   S   C   R   S   S   Q   S   L   V   H   S   N   G   N
GGT GAT CAA GCC TCC ATC TCT TGC AGA TCT AGT CAG AGC CTC GTA CAC AGT AAT GGA AAC
T   Y   L   R   W   Y   L   Q   K   P   G   Q   S   P   K   V   L   I   Y   K
ACC TAT TTA CGT TGG TAC CTG CAG AAG CCA GGC CAG TCT CCA AAG GTC CTG ATC TAC AAA
V   S   N   R   V   S   G   V   P   D   R   F   S   G   S   G   S   G   T   D
GTT TCC AAC CGA GTT TCT GGG GTC CCA GAC AGG TTC AGT GGC AGT GGA TCA GGG ACA GAT
F   T   L   K   I   N   R   V   E   A   E   D   L   G   V   Y   F   C   S   Q
TTC ACA CTC AAG ATC AAC AGA GTG GAG GCT GAG GAT CTG GGA GTT TAT TTC TGC TCT CAA
                                                                        BamH
S   T   H   V   P   W   T   F   G   G   G   T   K   L   E   I   K   S   S   G
AGT ACA CAT GTT CCG TGG ACG TTC GGT GGA GGC ACC AAG CTT GAA ATT AAG TCC TCT GGA
S
TCC
```

Figure 5.2. The annotated DNA and protein sequence of 4sdb-1, a single-chain bispecific diabody composed of the variable regions of the anti-fluorescein scFv 4M5.3 and the anti-CEA scFv sm3E.

As noted in Figs. 5.1 and 5.2, each variable region in the diabody is flanked with restriction sites, so that subcloning new variable regions of interest into the diabody is straightforward.

5.2.2 Single-chain bispecific expression in *S. cerivisiae* and purification

The anti-sm3E, anti-fluorescein single-chain bispecific diabody referred to as 4sdb-1 was secreted from *S. cerivisiae* (strain YVH10 [15]). After sequencing to confirm the correct DNA sequence, the plasmid was subcloned into a secretion vector containing the optimized alpha prepreo leader sequence S4 [16]. In this vector, 4sdb-1 is fused to a N-terminal FLAG epitope tag and a C-terminal his6 epitope tag, to provide different

options for purification and characterization. This plasmid was transformed into YVH10 cells, and grown at 30°C to an optical density/ml (OD/ml; absorbance at 600 nm per mL culture) of 10 in a 5 mL culture of SD-CAA supplemented with uracil (0.04 mg/mL). The fully-grown culture (50 OD, or approximately 5 x 10^8 cells total) was innoculated into 1L of SD-CAA with uracil and a 1:100 dilution of penicillin-streptomycin (stock concentration 10,000 units/mL penicillin, 10,000 μg/mL streptomycin). The liter culture was grown at 30°C until a cell density of 5 OD/ml was obtained. The cells were harvested via centrifugation (5 minutes at 3000*g* in bottles), the supernatant was removed, and the cells were resuspended in 1 L of YPG with penicillin-streptomycin. Induction took place at 20°C in unbaffled glass flasks with constant shaking. After two days of induction, the supernatant was collected via centrifugation as above and filtered using a 0.2 μm bottle-top filter to remove any remaining cells from the supernatant.

The supernatant was concentrated from a volume of 1 L to 50 mL using an Amicon stirred-cell concentrator (Millipore) at room temperature. 250 mL of TBS (pH 7.5) was added to the concentrated supernatant, and the pH of the buffered supernatant was adjusted to 7.5 with the addition of 12M NaOH. The buffered supernatant was concentrated from a volume of 300 mL to 50 mL using a stirred cell concentrator at room temperature. The concentrated, buffered supernatant was sterilized by filtration, and stored in a 50 mL conical tube until purification.

The concentrated, buffered supernatant was added to 1 mL of anti-FLAG M2 agarose resin (Sigma) that had been pre-equilibrated with TBS, pH 7.5. The supernatant and resin were allowed to equilibrate for 1 hour at room temperature, after which the resin was washed once with 10 mL TBS. The resin was applied to a chromatography

column, and the diabody was eluted with the addition of 5 1 mL fractions of 0.1M glycine HCL, pH 3.5.

The presence of diabody in the eluted fractions was determined by SDS-PAGE with a NuPAGE 4-12% Bis-Tris minigel (Invitrogen) followed by Coomassie staining. Elution fractions that appeared to contain the diabody were collected, concentrated using a Centricon device (Millipore) and purified using size exclusion chromatography on a Superdex 75 column (GE Healthcare) using TBS as a running buffer. The final concentration of purified, full-length diabody was estimated by measuring the absorbance at 280 nm of the fractions eluted from the size exclusion column.

5.2.3 Characterization of anti-CEA, anti-fluorescein single-chain bispecific diabody on the surface of CEA-expressing mammalian cells

Purified anti-CEA, anti-fluorescein single-chain bispecific diabody was concentrated from fractions eluted during size exclusion chromatography to approximately 150 μL. A fraction of the purified diabody was labeled with the Alexa-488 dye using the Alexa-488 Microscale Labeling Kit (Invitrogen). Separation of the dye-labeled protein from the unreacted fluorophore was verified using thin-layer chromatography.

SW1222 cells conservatively estimated to be expressing CEA at approximately 500,000 copies / cell [17, 18] were grown in advanced MEM cell culture media supplemented with fetal bovine serum and L-glutamine in stationary cell culture at 37°C in 5% CO_2/95% air. Cells were lifted from cell tissue culture plates using trypsin and Versene, collected and counted with a hemacytometer. Between 6 and 30 million cells were collected per lifting from 75 cm^2 tissue culture plates.

Cells were labeled with unlabeled bispecific that had been purified using the anti-FLAG resin, but had not yet been purified via size exclusion chromatography. Based on subsequent quantification of the concentration of full-length protein, the concentration of full-length bispecific used to label cells was 40 nM. Cells labeled with bispecific were incubated with anti-FLAG and anti-his6 antibodies to demonstrate the presence of the bispecific on the surface of the cells. Cells were also labled with fluorescein-biotin, followed by streptavidin-PE, to demonstrate the ability of the cell-bound bispecific to bind a fluorescein-conjugated hapten. All binding was measured using flow cytometry on a Coulter Epics® XL flow cytometer. In all cases, negative controls were performed in which the bispecific was not included in the cell labeling mixture, to ensure that the binding of secondary reagents was not nonspecific.

After demonstrating the presence of bispecific on the surface of CEA-expressing SW1222 cells, and demonstrating the ability of cell-bound bispecific to bind fluorescein, the affinity of the bispecific diabody for cell-expressed CEA was measured. Alexa-488-labeled diabody was incubated with SW1222 cells (4×10^5 per labeling) at concentrations varying from 60 pM to 30 nM. In all labeling experiments, the diabody was in excess compared to the number of CEA molecules, ensuring that depletion of soluble diabody would not affect the equilibrium measurement. Cells and diabody were incubated for 4 hours at 37°C, after which the mean fluorescence of cells was measured by flow cytometry. As a control, three tubes were labeled exactly the same as the tubes with the highest concentrations of bispecific (7.5 nM, 15 nM and 30 nM), except that the cells were pre-blocked for 30 minutes at 37°C with 10 μL of 10 μM disulfide-stabilized sm3E dimer. Since the high affinity sm3E dimer would bind all of the CEA on the cells, this

allowed the measurement of background concentration-dependent binding of Alexa-488-labeled diabody to the SW1222 cells. The K_d of 488-labeled bispecific diabody was determined by a non-linear least-squares fit to the data.

5.3 Results

5.3.1 Single-chain bispecific expression in *S. cerivisiae* and purification

Single-chain bispecific diabody 4sdb-1 was secreted in *S. cerevisiae* and purified using an anti-FLAG M2 agarose resin. The diabody was eluted in 5 1 mL fractions of 0.1M glycine HCL, pH 3.5. Each fraction was collected in a 1.5 mL Eppendorf microfuge tube containing 25 μL of 1M Tris-Hcl, pH 7.0. 12 μL of each collected fraction was analyzed using reducing SDS-PAGE and stained using SimplyBlue™ Safestain (Invitrogen), as shown in Fig. 5.3 below.

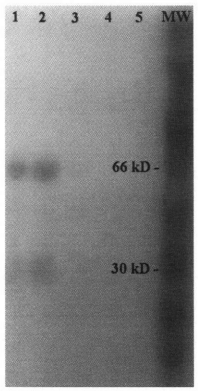

Figure 5.3. Coomassie stain of SDS-PAGE gel loaded with fractions eluted from anti-FLAG purification resin. Molecular weight ladder is Full Range Rainbow Ladder (GE Healthcare).

As shown in Fig. 5.3, the full length protein (expected size ~ 55 kDa) was present in eluted fractions 1, 2 and 3. In addition, a smaller protein fragment approximately 30 kDa in size was also present. Fractions 1, 2 and 3 were collected, concentrated and further purified via FPLC on a Superdex 75 size exclusion column. The absorbance at 280 nm of each fraction eluted from the Superdex 75 size exclusion column was

measured, and the resulting chromatagraph is shown in Fig. 5.4, along with BSA (66 kDa) and lysozyme (14 kDa) standards.

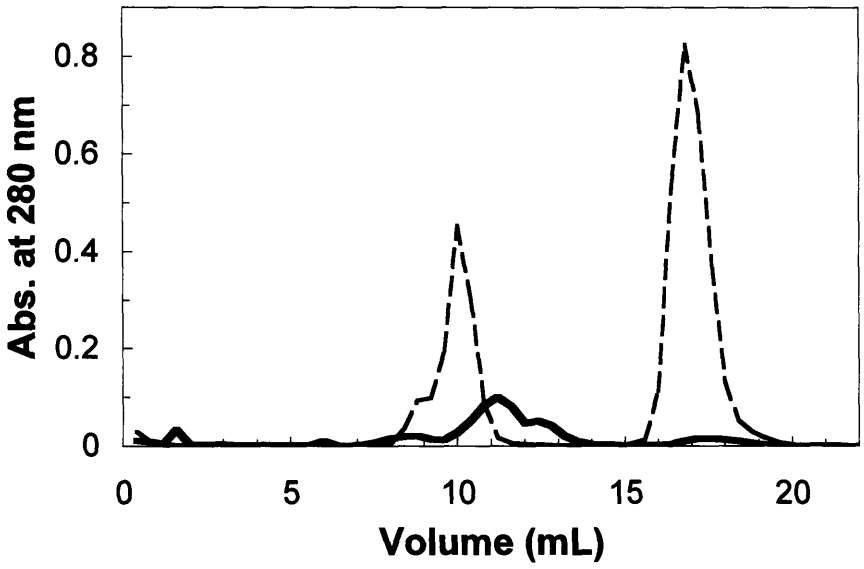

Figure 5.4. Elution of FLAG-purified bispecific diabody from a Superdex 75 size exclusion chromatography column. Solid line, diabody; dashed line, BSA and lysozyme standards.

As shown in Fig. 5.4, the major peak in the size exclusion chromatography fractions occurs just after the standards peak correpsonding to 66 kDa BSA, where a protein approximately 55 kDa in size would be expected to elute. Smaller peaks before and after the major peak are likely composed of noncovalent dimers and truncated versions of the full-length protein. The fractions corresponding to the major peak were collected and concentrated. Based on absorbance measurements at 280 nm, approximately 80 μg of purified, full-length diabody was present. These fractions were concentrated to a final volume of 150 μL, and the buffer was changed from TBS to PBS via dialysis using an ElutaTube (Invitrogen).

5.3.2 Characterization of anti-CEA, anti-fluorescein single-chain bispecific diabody on the surface of CEA-expressing mammalian cells

A fraction of the purified diabody was labeled with the Alexa-488 dye using the Alexa-488 Microscale Labeling Kit (Invitrogen). Separation of the dye-labeled protein from the unreacted fluorophore was verified using thin-layer chromatography, as shown in Fig. 5.5.

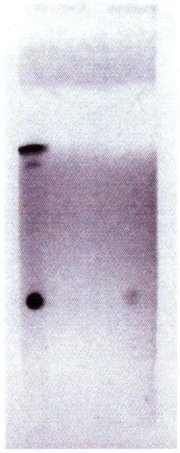

Figure 5.5. Thin layer chromatography of Alexa-488 labeled bispecific diabody. On the left, a control sample containing both labeled protein (black dot) and unreacted fluorophore (two bands). On the right, sample of Alexa-488 labeled bispecific diabody contains no unreacted fluorophore.

SW1222 cells expressing CEA at approximately 500,000 copies / cell were labeled with unlabeled bispecific that had been purified using the anti-FLAG resin, but had not yet been purified via size exclusion chromatography. Based on subsequent quantification of the concentration of full-length protein, the concentration of full-length bispecific used to label cells was 40 nM. Cells labeled with bispecific were incubated with anti-FLAG and anti-his6 antibodies to demonstrate the presence of the bispecific on the surface of the cells. As shown in Fig. 5.6 and 5.7, the binding of anti-FLAG and anti-his6 antibodies to SW1222 cells was dependent on the presence of bispecific, indicating that epitope-tagged bispecific was present on the surface of the cells. The binding of

anti-his antibody to bispecific localized to the surface of SW1222 cells also indicates that the bispecific diabody is full-length, as the his tag is a C-terminal tag in this construct.

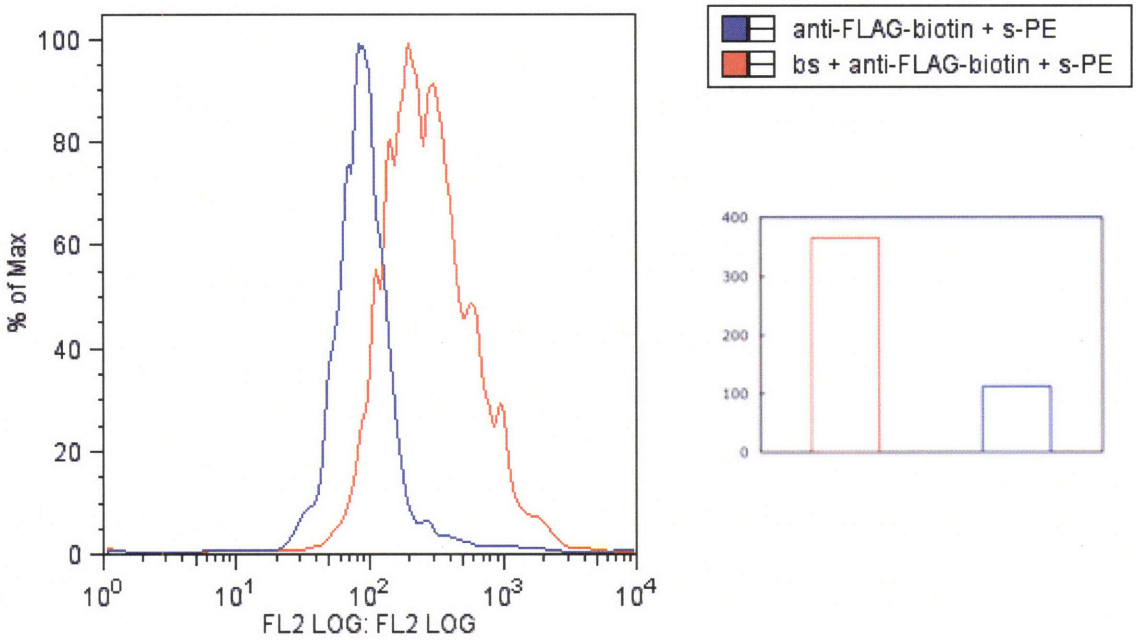

Figure 5.6. The binding of anti-FLAG antibody to SW1222 cells. SW1222 cells were incubated with 1 μL of 0.21 mg/mL bispecific diabody (bs), 1 μL of 1.2 mg/mL biotinylated anti-FLAG M2 antibody (anti-FLAG-biotin), and 1 μL of 1 mg/mL streptavidin-phycoerithryn (s-PE) in 100 μL of PBS/BSA on ice. Bispecific was incubated with the cells for 60 minutes, while anti-FLAG antibody and streptavidin-PE were incubated with cells for 15 minutes. Cell fluorescence was measured via flow cytometry; PE fluorescence was measured with the FL2 channel. The cells were washed with 0.5 ml cold PBS/BSA before each label was added. Histogram is shown on the left, while the average fluorescence of each cell labeling is shown on the right.

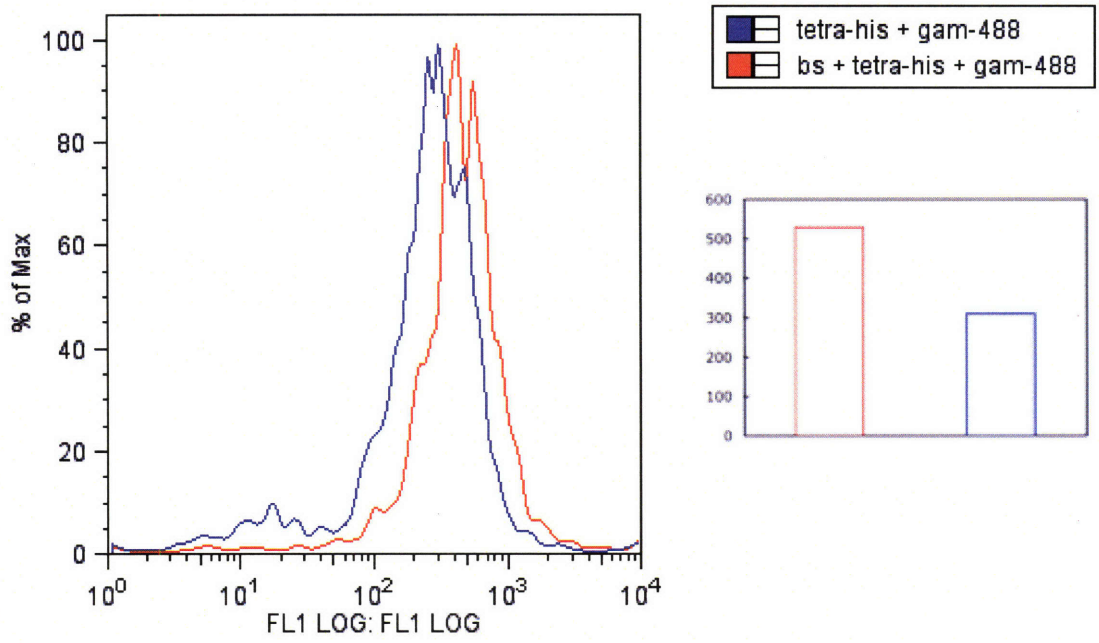

Figure 5.7. The binding of anti-his antibody to SW1222 cells. SW1222 cells were incubated with 1 µL of 0.21 mg/mL bispecific diabody (bs), 1 µL of 0.5 mg/mL tetra-his anti-his6 antibody (tetra-his), and 1 µL of 1 mg/mL Alexa-488 labled goat anti-mouse antibody (gam-488) in 100 µL of PBS/BSA on ice. Bispecific was incubated with the cells for 60 minutes, while anti-his antibody and goat anti-mouse antibody were incubated with cells for 15 minutes. Cell fluorescence was measured via flow cytometry; PE fluorescence was measured with the FL1 channel. The cells were washed with 0.5 ml cold PBS/BSA after each label was added. Histogram is shown on the left, while the average fluorescence of each cell labeling is shown on the right.

Cells labled with bispecific diabody were also labeled with fluorescein-biotin, followed by streptavidin-PE, to demonstrate the ability of the cell-bound bispecific to bind a fluorescein-conjugated hapten. As shown in Figure 5.8, the binding of fluorescein-biotin to SW1222 cells is dependent on the presence of bispecific, indicating that the fluorescein biotin is being bound by the bispecific molecule on the surface of the cell.

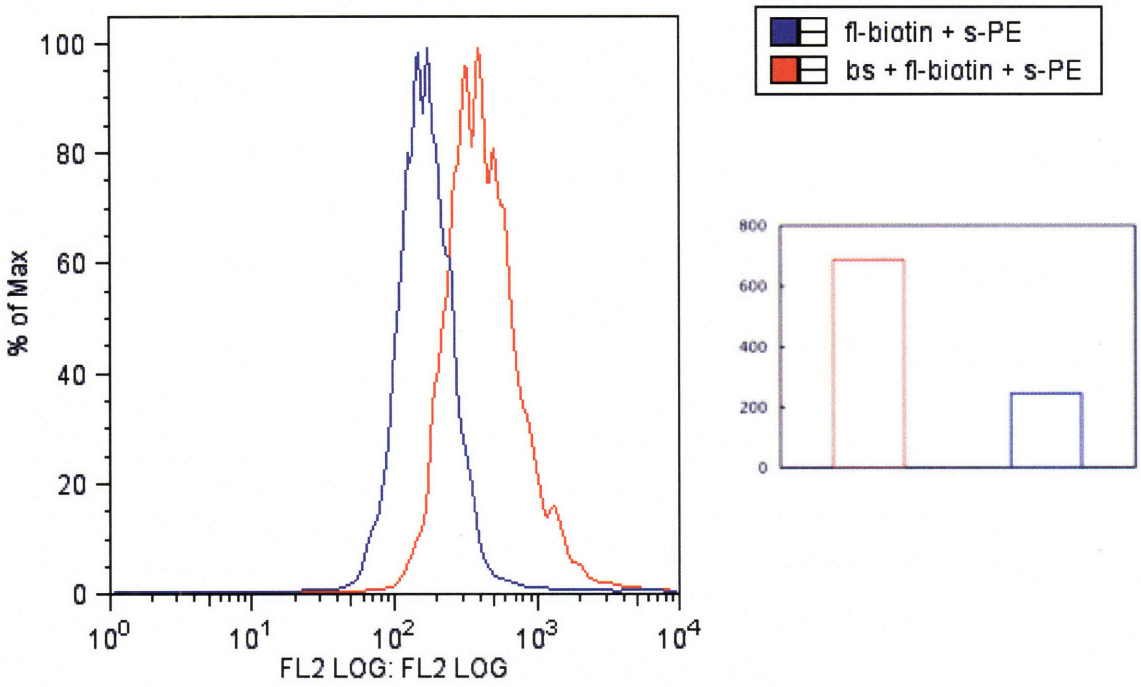

Figure 5.8. The binding of fluorescein-biotin to SW1222 cells. SW1222 cells were incubated with 1 µL of 0.21 mg/mL bispecific diabody (bs), 1 µL of 6 mM fluorescein-biotin (fl-biotin), and 1 µL of 1 mg/mL streptavidin-PE (strep-PE) in 100 µL of PBS/BSA on ice. Bispecific was incubated with the cells for 60 minutes, while fluorescein-biotin and streptavidin-PE were incubated with cells for 15 minutes. Cell fluorescence was measured via flow cytometry; PE fluorescence was measured with the FL2 channel. The cells were washed with 0.5 ml cold PBS/BSA before each label was added. Histogram is shown on the left, while the average fluorescence of each cell labeling is shown on the right.

After demonstrating the presence of bispecific on the surface of CEA-expressing SW1222 cells, and demonstrating the ability of cell-bound bispecific to bind fluorescein, the affinity of the bispecific diabody for cell-expressed CEA was measured. Alexa-488-labeled diabody was incubated with SW1222 cells (4×10^5 per labeling) at concentrations varying from 60 pM to 30 nM. Cells and diabody were incubated for 4 hours at 37°C, after which the mean fluorescence of cells was measured by flow cytometry. Control cells pre-blocked with high-affinity disulfide-stabilized sm3E dimer indicated no concentration-dependent nonspecific binding of diabody at the concentrations measured.

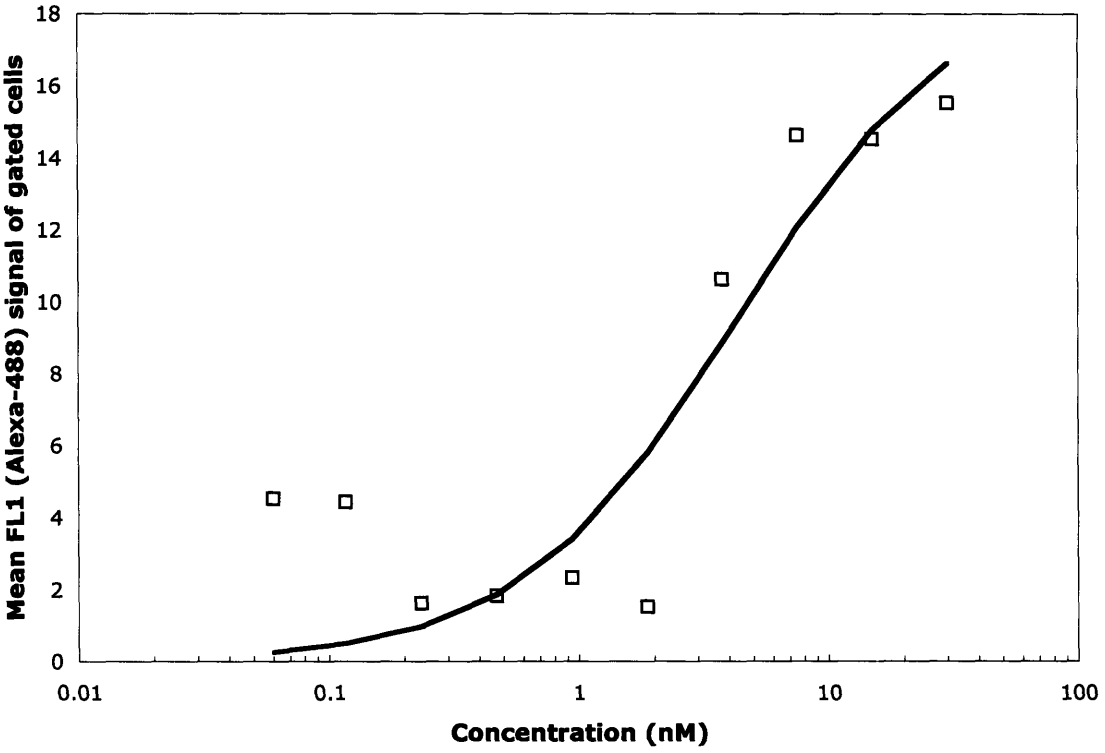

Figure 5.8. Binding of Alexa-488 bispecific diabody to CEA-expressing SW1222 cells. Cells were incubated with varying concentrations of fluorescently-labeled diabody for 4 hours, and then fluorescence was measured via flow cytometry. Background fluorescence (as measured by three tubes of cells pre-blocked with disulfide-stabilized sm3E dimer) was concentration independent at the concentrations tested, and was subtracted from each data point. Squares are data points, and the line is a non-linear least squares fit for a measured K_d of 4.3 ± 2.5 nM.

As shown in Fig. 5.8, the K_d of bispecific diabody for CEA expressed on the surface of SW1222 cells at 37°C is 4.3 ± 2.5 nM. This is significantly lower than the affinity of sm3E, the scFv which the CEA-binding part of the bispecific is based on, for CEA, which has been measured to be 30 pM at 25°C [12]. The decrease in affinity is likely due to altered orientation of the variable domains as a result of the scFv being reformated into a single-chain bispecific diabody.

5.4 Conclusions & Discussion

A novel bispecific targeting agent for PRIT has been designed, produced, purified and characterized. Rather than binding directly to a radioisotope-carrying metal chelate, this single-chain bispecific diabody binds to fluorescein, which can be conjugated to almost any metal chelate/radioisotope pairing of therapeutic interest. As a result, this targeting agent can be used to deliver a wide variety of radioisotopes to CEA-expressing cancer cells. In addition, the targeting agent can be easily modified to target any particular cancer-specific marker molecule that is desired.

The diabody is secreted from yeast as a full-length, 55 kDa protein that can be cleanly purified by anti-epitope-tag affinity chromatography and size exlusion chromatography. A truncated version of the approximately 30 kDA is size is also present in the unpurified supernatant. This variant may be a mixture of proteolysis products resulting from linkage cleavage, or it may be a truncated version of the diabody that arises in the yeast secretory system due to unknown causes. The total yield of full-length protein was low (80 μg/L), possibly due to the difficulty of secreting a four-variable-domain protein fusion, but subsequent optimization of the secretion conditions should result in improved yields. This was the first known single-chain bispecific diabody expressed in *S. cervisiae.*

The bispecific diabody binds CEA expressed on the surface of SW1222 cells with a K_d of 4.3 ± 2.5 nM. This affinity is intermediate between anti-CEA scFvs sm3E and shMFE, which have K_ds of 30 pM and 8 nM, respectively. The bispecific diabody contains the variable regions of sm3E, and the lower affinity is likely a result of an altered orientation of the variable domains as a result of being expressed in a single-chain diabody. Both the physical constraints upon the protein and the linker regions used to

connect the variable domains are different in the diabody format than in the scFv format, so it is not suprising to see that the affinity has decreased. In addition, it has also been demonstrated that the diabody binds fluorescein-biotin, a model fluorescein-based hapten molecule, while binding CEA on the surface of SW1222 cells.

This anti-CEA, anti-fluorescein single-chain bispecific diabody can be used in the future preclinical PRIT studies. Future work should include experiments to follow the diffusion, binding and catabolism of diabody in cancer cell-spheroids. Additionally, it should be possible to use fluorescein-tetramethylrhodamine bifluorophores as molecular reporters of diabody-fluorescein binding, allowing for a far clear picture of PRIT on a cellular level than has been achievable to date. It may also be desirable to further engineer this bispecific diabody, in order to either increase its affinity for CEA and fluorescein, or to modulate those interactions. For example, it might be desirable to engineer the anti-fluorescein portion of diabody so that it binds fluorescein with high affinity at pH 7, but at a much lower affinity at pH 5. This modified diabody, if internalized upon binding at the cell surface and recycled back to the cell surface, could then potentially be used to deliver multiple payloads of radioactive hapten. In summary, this anti-CEA, anti-fluorescein single-chain bispecific diabody provides a tool for improved understanding of PRIT at the cellular and micrometastasic levels, and provides a framework for designing future antibody-based targeting agents for PRIT treatments.

5.5 Works Cited

1. Boder, E.T., K.S. Midelfort, and K.D. Wittrup, *Directed evolution of antibody fragments with monovalent femtomolar antigen-binding affinity*. Proc Natl Acad Sci U S A, 2000. **97**(20): p. 10701-5.

2. Midelfort, K.S., et al., *Substantial energetic improvement with minimal structural perturbation in a high affinity mutant antibody.* J Mol Biol, 2004. **343**(3): p. 685-701.
3. Corneillie, T.M., A.J. Fisher, and C.F. Meares, *Crystal structures of two complexes of the rare-earth-DOTA-binding antibody 2D12.5: ligand generality from a chiral system.* J Am Chem Soc, 2003. **125**(49): p. 15039-48.
4. Corneillie, T.M., et al., *A rare earth-DOTA-binding antibody: probe properties and binding affinity across the lanthanide series.* J Am Chem Soc, 2003. **125**(12): p. 3436-7.
5. Wei, A.-P., Herron, J.N., *Bifluorophoric molecules as fluorescent beacons for antibody-antigen binding.* J. Mol. Recognit., 2002. **15**: p. 311-320.
6. Albrecht, H., G.L. Denardo, and S.J. Denardo, *Monospecific bivalent scFv-SH: effects of linker length and location of an engineered cysteine on production, antigen binding activity and free SH accessibility.* J Immunol Methods, 2006. **310**(1-2): p. 100-16.
7. Sundaresan, G., et al., *124I-labeled engineered anti-CEA minibodies and diabodies allow high-contrast, antigen-specific small-animal PET imaging of xenografts in athymic mice.* J Nucl Med, 2003. **44**(12): p. 1962-9.
8. Kipriyanov, S.M., et al., *Effect of domain order on the activity of bacterially produced bispecific single-chain Fv antibodies.* J Mol Biol, 2003. **330**(1): p. 99-111.
9. Todorovska, A., et al., *Design and application of diabodies, triabodies and tetrabodies for cancer targeting.* J Immunol Methods, 2001. **248**(1-2): p. 47-66.
10. Piatesi, A., et al., *Directed evolution for improved secretion of cancer-testis antigen NY-ESO-1 from yeast.* Protein Expr Purif, 2006. **48**(2): p. 232-42.
11. Rakestraw, A. and K.D. Wittrup, *Contrasting secretory processing of simultaneously expressed heterologous proteins in Saccharomyces cerevisiae.* Biotechnol Bioeng, 2006. **93**(5): p. 896-905.
12. Graff, C.P., et al., *Directed evolution of an anti-carcinoembryonic antigen scFv with a 4-day monovalent dissociation half-time at 37 degrees C.* Protein Eng Des Sel, 2004. **17**(4): p. 293-304.
13. Higuchi, R., B. Krummel, and R.K. Saiki, *A general method of in vitro preparation and specific mutagenesis of DNA fragments: study of protein and DNA interactions.* Nucleic Acids Res, 1988. **16**(15): p. 7351-67.
14. Swers, J.S., B.A. Kellogg, and K.D. Wittrup, *Shuffled antibody libraries created by in vivo homologous recombination and yeast surface display.* Nucleic Acids Res, 2004. **32**(3): p. e36.
15. Shusta, E.V., et al., *Increasing the secretory capacity of Saccharomyces cerevisiae for production of single-chain antibody fragments.* Nat Biotechnol, 1998. **16**(8): p. 773-7.
16. Rakestraw, A., *in press.* 2006.
17. Lee, F.T., et al., *Immuno-PET of human colon xenograft- bearing BALB/c nude mice using 124I-CDR-grafted humanized A33 monoclonal antibody.* J Nucl Med, 2001. **42**(5): p. 764-9.
18. Leibovitz, A., et al., *Classification of human colorectal adenocarcinoma cell lines.* Cancer Res, 1976. **36**(12): p. 4562-9.

Curriculum Vitae

Stefan C. Zajic
scz@mit.edu

CURRENT RESEARCH EXPERIENCE 2001-2006

Massachusetts Inst. of Technology, Cambridge, MA
Graduate Research Assistant, Lab of Prof. K. Dane Wittrup
Department of Chemical Engineering
Research Summary: Optimized pretargeted radioimmunotherapy (PRIT) of cancer, with the goal of completely killing avascular, pre-clinical micrometastases in an adjuvant setting. To optimize PRIT protocols, we have comprehensively modeled the pharmacokinetics, transport, and dosimetry that determine the efficacy of PRIT treatments. To optimize PRIT reagents, we have engineered a functional bispecific protein based on the anti-CEA scFv sm3E and the anti-fluorescein scFv 4M5.3.

EDUCATION

Massachusetts Inst.of Technology, Cambridge, MA
Department of Chemical Engineering
Ph.D.: October, 2006, GPA: 4.5/5.0
Major: Chemical Engineering Minor: Biology
Thesis Advisor: Prof. K. Dane Wittrup
Thesis Title: Improved Methods and Reagents for Pretargeted Radioimmunotherapy of Cancer

University of Pennsylvania, Philadelphia, PA
B.S.E.: *Summa Cum Laude*, May, 2001, GPA: 3.75/4.0
Major: Chemical Engineering
Minors: Chemistry, English and Mathematics

PREVIOUS RESEARCH EXPERIENCE

Spring 2004

MedImmune, Inc., Gaithersburg, MD
Antibody Discovery & Protein Engineering Division
Research Assistant (Internship)
Research Supervisors: Dr. Changshou Gao, Dr. Herren Wu
Isolated antibodies against novel human protein targets from a phage-displayed library. Developed assays for testing the specificity of antibodies using phage-ELISAs, and determined cross-species-reactivity of selected antibodies.

2000-2001

University of Pennsylvania, Philadelphia, PA
Department of Biochemistry and Biophysics
Undergraduate Research Assistant
Research Supervisor: Prof. P. Leslie Dutton
Quantitatively predicted electron transfer rates in metabolic proteins by using computer modeling. Designed and

produced charged self-assembling monolayers on gold-plated electrodes; used electrochemical methods to study electron transfer in proteins selectively adsorbed to monolayers.

Summer 2000 **Rohm and Haas Company**, Croydon, PA
Croydon Engineering Division
Assistant Process Engineer
Project Leader: Jim Staudt
Diagnosed and solved design problems for planned adhesives plant. Assessed hazards associated with charging vessels with powdered, solid acids. Solved storage problems for bulk raw materials.

1999-2000 **University of Pennsylvania**, Philadelphia, PA
Department of Chemical Engineering
Undergraduate Research Assistant
Research Supervisor: Prof. Raymond Gorte
Worked towards a quantitative understanding of the unusual catalytic properties of acid sites formed by the substitution of iron for aluminum in H-ZSM-5 zeolite.

Summer 1999 **University of Michigan**, Ann Arbor, MI
Department of Chemical Engineering
Undergraduate Research Assistant
Research Supervisor: Prof. Ralph Yang
Synthesized lithium and lithium-silver X-type zeolites. Determined the effect of trace amounts of water on the adsorption of N_2, O_2 and Ar onto X-type zeolites.

PUBLICATIONS & PRESENTATIONS

Zajic SC and Wittrup KD, "Asymptotically optimal probability estimation to predict diversity in protein populations," in preparation.

Zajic SC, Thurber GT and Wittrup KD, "Theoretical limitations for two-step pretargeted radioimmunotherapy of cancer," in preparation.

Thurber GT, **Zajic SC** and Wittrup KD, "Theoretical criteria for antibody saturation of tumors and micrometastases," submitted.

Zajic SC, Thurber GT and Wittrup KD, "Optimal Reagents and Dosing for Pretargeted Radioimmunotherapy of Cancer", poster at the CHI Protein Engineering Summit in Boston, MA, April 24-28, 2006.

Zajic SC and Wittrup KD, "Optimizing Pretargeted Radioimmunotherapy of Cancer: Classical Transport Concepts Applied to Cancer Treatment," presentation at the American Institute of Chemical Engineering Annual Meeting in Austin, TX, November 7, 2004.

Zajic SC and Wittrup KD, "Pretargeted Radioimmunotherapy of Cancer," poster at the IBC Antibody Engineering Conference in San Diego, CA, Nov. 30-

Dec. 3, 2003.

Churchill SW and **Zajic SC**, "Prediction of fully developed turbulent convection with minimal explicit empiricism," *AIChE J.* **48**(5): 927-940 (2002).

Hutson ND, **Zajic SC** and Yang RT, "Influence of Residual Water on the Adsorption of Atmospheric Gases in Li-X Zeolite: Experiment and Simulation," *Ind. Eng. Chem. Res.*, **39**: 1775-1780 (2000).

HONORS AND AWARDS

2001 Honorable Mention, NSF Graduate Research Fellowship Program
2001 American Chemical Society, Philadelphia Section, Annual Award, Philadelphia, PA
2000 American Institute of Chemical Engineers, Delaware Valley Section, Outstanding Chemical Engineering Student at the University of Pennsylvania, Philadelphia, PA

SKILLS

MOLECULAR

PCR (standard, mutagenic, overlap-extension, touchdown, phage), DNA library construction (random mutagenesis, chain shuffling, homologous recombination in *S. cerevisiae*), site-directed mutagenesis, subcloning (restriction digestion, ligation), DNA electrophoresis, DNA sequencing, DNA fingerprinting, protein purification (FPLC, ion-exchange, gel filtration, hydrophobicity and affinity chromatography), SDS-PAGE, western blotting, ELISAs, biotinylation.

CELLULAR

Directed evolution of peptides and proteins via yeast surface display and phage display, magnetic cell sorting (MACS), flow cytometry, fluorescent-activated cell sorting (FACS), phage panning, phage-ELISAs, protein expression in *S. cerevisiae*, microscopy (light, fluorescent, and confocal).

LEADERSHIP EXPERIENCE

2006	Served as part of a team of teaching assistants administering a chemical & biological engineering projects laboratory. Interacted with professors and students to plan meetings, prepare materials, and resolve interpersonal conflicts.
2003-2005	Supervised three undergraduate research assistants who assisted with laboratory work and computer programming.
2003	Program Director at WMBR-88.1 FM (MIT's college radio station) for three seasons. Responsible for all broadcast content; appointed programming boards, and with those boards determined the program schedule for each season.

OTHER INTERESTS

The repair and maintenance of vintage and modern motorscooters, amateur audio electronics, homebrewing beer, and sailing.

REFERENCES

Prof. K. Dane Wittrup
Massachusetts Institute of Technology
Department of Chemical Engineering
77 Massachusetts Ave., Rm. E19-563
Cambridge, MA 02139
Phone: (617) 253-4578
E-mail: wittrup@mit.edu

Dr. Herren Wu
MedImmune, Inc.
Senior Director, Antibody Discovery & Protein Engineering
One MedImmune Way
Gaithersburg, MD 20878
E-mail: wuh@medimmune.com